Fermi National Accelerator Laboratory

FERMILAB-Pub-81/82-EXP
7160.118
(Submitted to Phys. Rev. D)

EXPERIMENTAL STUDY OF SINGLE PARTICLE INCLUSIVE HADRON SCATTERING AND ASSOCIATED MULTIPLICITIES

A. E. Brenner, D. C. Carey, J. E. Elias, P. H. Garbincius,
G. Mikenberg, and V. A. Polychronakos
Fermi National Accelerator Laboratory, Batavia, IL 60510 USA

and

W. Aitkenhead, D. S. Barton, G. W. Brandenburg, W. Busza,
T. Dobrowolski, J. I. Friedman, H. W. Kendall, T. Lyons,
B. Nelson, L. Rosenson, W. Toy, R. Verdier, and L. Votta
Massachusetts Institute of Technology, Cambridge, MA 02139 USA

and

M. T. Chiaradia, C. DeMarzo, C. Favuzzi, G. Germinario,
L. Guerriero, P. LaVopa, G. Maggi, F. Posa, G. Selvaggi,
P. Spinelli and F. Waldner
Istituto di Fisica and Istituto Nazionale di Fisica Nucleare
Bari, Italy

and

R. Meunier
CERN, Geneva, Switzerland

and

D. Cutts, R. S. Dulude, R. E. Lanou, Jr., and J. T. Massimo
Brown University, Providence, RI 02912 USA

December 30, 1981

Operated by Universities Research Association Inc. under contract with the United States Department of Energy

Experimental Study of Single Particle Inclusive Hadron Scattering and Associated Multiplicities

A. E. Brenner, D. C. Carey, J. E. Elias, P. H. Garbincius,

G. Mikenberg,[a] and V. A. Polychronakos[b]
Fermi National Accelerator Laboratory, Batavia, Illinois 60510 USA

and

W. Aitkenhead,[c] D. S. Barton,[b] G. W. Brandenburg,[d] W. Busza,

T. Dobrowolski, J. I. Friedman, H. W. Kendall, T. Lyons,

B. Nelson, L. Rosenson, W. Toy,[e] R. Verdier, and L. Votta[f]
Massachusetts Institute of Technology, Cambridge, Massachusetts 02139 USA

and

M. T. Chiaradia, C. DeMarzo, C. Favuzzi, G. Germinaric,
L. Guerriero, P. LaVopa, G. Maggi, F. Posa,
G. Selvaggi, P. Spinelli, and F. Waldner
Istituto di Fisica and Istituto Nazionale di Fisica Nucleare, Bari, Italy

and

R. Meunier
CERN, Geneva, Switzerland

and

D. Cutts, R. S. Dulude,[g] R. E. Lanou, Jr., and J. T. Massimo
Brown University, Providence, Rhode Island 02912 USA

ABSTRACT

An experiment using the Fermilab Single Arm Spectrometer (SAS) facility and an associated non-magnetic vertex detector studied the reactions a + p → c + X where a and c were $\pi^{\pm}$, $K^{\pm}$, p or $\bar{p}$. Extensive measurements were made at 100 and 175 GeV/c beam momenta, with the outgoing hadrons detected in the SAS covering a kinematic range $0.12 < x < 1.0$ and a $p_T < 1.25$ GeV/c. Additional data covering a more restricted range in x were also gathered at 70 GeV/c incident momentum. In this high statistics experiment, the identification of both the incoming and outgoing charged hadrons were made with a total of eight Cerenkov counters. New and extensive single particle inclusive data for charged particle production in low p_T hadronic fragmentation are presented. The average associated charged particle multiplicity and pseudo-rapidity distributions are also given.

I. INTRODUCTION

Inclusive scattering results from hadronic interactions have yielded a great deal of information on the basic physical processes involved. In a manner which is complementary to the study of complete hadron jets by calorimetry, models which describe inclusive scattering within the quark-parton framework have provided information about the substructure of hadrons. In such models of inclusive scattering the identification of the produced particles provides indirect information on the flavor of the participating quarks.

This paper is a summary report of a high statistics inclusive scattering experiment with complete particle identification of the incoming and outgoing charged hadrons. This experiment, designated E118, was performed using the Single Arm Spectrometer facility[1] at Fermilab. The associated charge particle multiplicities and angular distributions were measured simultaneously using a non-magnetic vertex detector. The reactions studied were a + p → c + X where a and c were charged pions, kaons, protons or antiprotons. Most of the data were taken at two beam momenta, 100 and 175 GeV/c. The kinematic range covered by the outgoing hadrons in Feynman x was $0.12 < x < 1.0$ and in transverse momentum was $p_T < 1.25$ GeV/c. A small amount of additional data was taken with a positive 70 GeV/c

beam spanning an x range $0.75 < x < 0.97$, with the same p_T limit. Within these ranges, data were taken at more than three hundred separate kinematic settings. Results of analyses of subsets of this data reporting on the importance of resonance production[2] via one pion exchange in reactions yielding π^- for large values of Feynman x, on the power law behavior in (1-x) for the cross sections[3], on the determination of the pion and kaon structure functions[4], on triple Regge parameterizations[5], and on the associated charged hadron multiplicity[6,7] in hadron reactions, have appeared earlier.

The apparatus used for this experiment is described in Section II and the analysis procedures are described in Sections III and IV of this paper. The spectrometer data are presented in Section V together with fitted parameterizations of the x and p_T dependence and triple-Regge representations. In Section VI, the vertex detector data are presented giving the associated charge multiplicities and their angular distributions. Finally, a summary of results and conclusions presented here and earlier appear in Section VII.

II. THE APPARATUS

The apparatus for this experiment, much of it previously described in detail[1], consisted of the M6E beam line in the Meson Lab together with the Fermilab Single Arm Spectrometer (SAS) augmented by a non-magnetic vertex detector. In this section, the major features will be outlined with special emphasis on modifications made for this experiment.

A. The Beam

The M6E beam line had a production angle of 2.7 mrad relative to the primary proton beam and could transport up to 6×10^6 hadrons/pulse into the experimental area. The momentum could be centered in the range from 20 to 175 GeV/c with a 1% momentum bite. With 400 GeV primary protons incident upon the 8" long beryllium production target, the observed pion, kaon and proton ratios at the hydrogen target are listed in Table 1.

A schematic drawing of the beam is shown in Figure 1. See Reference 1 for detailed phase space and optics contours. Scintillation counter hodoscopes were placed at the appropriate positions in the beam to determine the momenta, angles, and positions of the transmitted particles. The properties and element sizes of the hodoscopes are given in Table 2. In all cases, the elements were overlapped by 1/3 counter widths to give finer position resolution.

The beam trigger counters BT1, BT2, B3J and BT0 were plastic scintillation counters located in the last stage of the beam line. BT1 and BT2 spanned the usable beam phase space, and a coincidence between them formed the primary beam trigger. B3J and BT0 were adjustable hole counters that were used to veto halo around the incident beam. The beam trigger for data taking was

$$BT = BT1.BT2.\overline{B3J}.\overline{BT0}.$$

The beam dimensions at the hydrogen target are given in Table 3.

Elements BGAS0, BGAS, BDIF, and BDISC were pressurized gas Cerenkov counters in the beam.[8,9,10,11] Their properties are summarized in Table 4. BGAS0 and BGAS were the beam pion threshold detectors, while BDIF and BDISC were differential counters pressurized to detect protons and kaons respectively. With this system of counters, the beam particle type could be determined on an event-by-event basis for $\geq$ 95% of the incident particles at normal operating intensity. This allowed data to be taken simultaneously for incident π's, K's and protons. Unidentified or ambiguous beam particles were discarded from the incident flux samples. The lepton content of the beam was always less than 0.5%.

The scattering angle between the beam and spectrometer axes was varied by changing the vertical pitch of the beam as it passed through the target.[1] This was accomplished by a set of three angle-varying bend (AVB) magnets. This is shown in Fig. 2, which also defines the coordinate systems used. Several targets were located on a rotating turntable, shown in Fig. 3, which could also be tilted to match the beam angle. The target was rotated and tilted by remote control between data runs. The data reported on here were taken with the 20" long liquid hydrogen filled target cell and a complementary 20" empty cell. A typical data point had contributions from target full and empty runs each with the beam pitched alternatively up and down to minimize systematic offsets.

B. The Spectrometer

The Single Arm Spectrometer as shown in Fig. 4 was a separate magnetic transport system which was used to analyze fast forward particles scattered from the target. Measurements were made of the momentum, angle, position, and identity of one particle resulting from each interaction in the target. ST1 and ST2 were the spectrometer trigger counters located respectively at the momentum focus and at the end of the spectrometer. A coincidence was required between these counters to indicate the presence of a charged particle within the spectrometer aperture. A spectrometer event (SEV) was then defined as

$$ST = ST1.ST2.BT.$$

On each trigger, the coordinates of the scattered particle were measured using multiwire proportional counters which were positioned at four locations along the spectrometer. The properties of these chambers are given in Table 5. Momentum and spatial coordinates at the target were decoded from the x, y position information measured by these detectors. The resolution of these measurements and the aperture of the spectrometer are given in Table 6. Here the fractional momentum, $(\Delta p/p)$, is the fractional deviation of a particle's momentum from the spectrometer setting.

The spectrometer optics were slightly modified with respect to those described in Reference 1 to increase further the angular acceptance. To reduce point-to-point systematic errors, a single spectrometer tune was employed over the entire range of momentum from 20 to 175 GeV/c.

The determination of the fractional momentum deviation from the central spectrometer setting, ($\Delta p/p$), was independent of the position and angle of the scattered particle at the target. The first wire planes H11 and H12 were used to measure the particle position in front of the spectrometer bends, and wire planes H21, H22, H3, and H4 to measure the angle and position of the particle after it left the bend magnets (see Fig. 4). The momentum of the particle could then be determined from the change in trajectory angle caused by the bending magnets.

As in the beam line, the spectrometer had several gas Cerenkov counters[9,11] for identifying particle type. These were SDIF, SGAS1, SGAS2, and SGAS3 (see Table 4). SDIF was a dual channel differential counter and the three SGAS counters were threshold counters. At momenta above 100 GeV/c, the SGAS counters were used to identify pions. Light falling on the coincidence ring mirror of SDIF differential Cerenkov counter signalled the presence of a proton. In the absence of a pion signature, a signal in the veto mirror of SDIF defined a kaon. For increased efficiency at spectrometer momenta below 100 GeV/c, SGAS2 was pressurized to count kaons as well as pions.

Appendix I contains a discussion of the spectrometer Cerenkov counter particle identification strategy.

Electromagnetic and hadronic shower counters and a 15 foot long steel-loaded counter telescope at the end of the spectrometer, were used to tag events with lepton-like triggers. This information was helpful in determining corrections for pion and kaon decays in flight in which daughter particles were emitted within the spectrometer trigger aperture.

Periodically, the spectrometer was set at zero degrees and tuned to the beam momentum. The incident beam then passed through the spectrometer providing verification of spectrometer tune, alignment, and transformation coefficients as well as a calibration of the detectors.

C. Vertex Detector

The 20" liquid hydrogen (0.06 absorption length) target was surrounded by a non-magnetic vertex detector. The primary purpose of this detector system was to measure the associated charged particle multiplicities and pseudo-rapidity distributions for single particle inclusive events triggered by the Single Arm Spectrometer. The vertex detector and liquid hydrogen target were mounted on a tilt frame to maintain alignment along the incident beam while the beam was pitched vertically to vary the p_T of the trigger reaction. A schematic layout showing the relative positions of the vertex detector

components is shown in Fig. 5.

Three separate detector systems, all with hexagonal geometry were used to cover the full angular range: the forward multiplicity Cerenkov counters (MC), the mid-range multiwire proportional chambers (PC), and the wide angle target recoil hodoscopes (MT and MB). Two adjacent detector regions allowed substantial overlap for tracks originating from any vertex within the hydrogen target. Table 7 lists the detector properties.

The multiplicity Cerenkov counters [12], MC, composed of six 1/2" thick (0.02 absorbtion length) Pilot 425 lucite wedge shaped members, detected charged particles within 1.8^{o} of the incident beam. The incident beam and spectrometer trigger particle also passed through the MC counters. This required short resolving times and high rate capability. The Cerenkov light output was independent of the velocity for particles with $\beta > 0.9$ allowing detection of multiple particles in a single MC counter by pulse height analysis.

Multi-wire proportional chambers[13] (PC) covered the angular range 1.5^{o} to 24^{o}. In addition to track counting, the PC array was used to reconstruct the interaction vertex position for each event, since knowledge of the vertex position is necessary for studying angular distributions for an extended target. The nine sense planes were arranged in three packages providing three wire hits for each track in each of three

projections rotated 120^{o} between views. There were 2600 sense wires of 0.080" spacing in the entire vertex detector. Hexagonal kapton plugs of 0.002" thickness were used to deaden the beam region of the PC's, which corresponded to the active region of the MC counters.

The hexagonal target hodoscope (MT and MB) counters covered the region beyond 22^{o}. The double layer of scintillators discriminated against delta rays while maintaining sensitivity to stopping protons. A coincidence between the inner (MT) and outer (MB) counters signaled a penetrating particle. Stopping recoil protons were detected by requiring a 6 times minimum energy deposition in the inner MT layer without requiring a MT.MB coincidence. The MT counters formed three hexagonal barrels along the beam. Each set of three MT counters was backed up by a single MB counter for a total of eighteen MT and six MB counters.

The overall resolving time of the vertex detector was determined by the 40 nsec charge collection time of the multi-wire proportional chambers. Accidental rates and MWPC wire currents limited the luminosity to 1.5×10^{5} interactions/second or 3×10^{6} incident hadrons/second.

The performance of the vertex detector components was monitored by the on-line analysis of frequent runs with an interaction trigger which was decoupled from the SAS. The trigger for these runs was BT.IT, where IT was a ring shaped scintillation counter with a hole for the beam which was located immediately downstream of the MC array.

D. Electronics

To trigger an event it was required that a charged particle be observed in both the beam and spectrometer. When a spectrometer event (SEV) trigger occurred, the status of all the detectors was latched in a CAMAC system and read into a PDP-11 computer. The complete event buffer was written onto magnetic tape; part of the information was saved for on-line analysis and monitoring.

In addition to forming the trigger, the fast electronics provided extensive scaler information on the flux of each beam and spectrometer particle type, along with the various trigger rates. These scalers were gated on only when the computer was ready to take data, thus doing away with dead time corrections.

A prescaled sample of beam particles without spectrometer trigger was also selected during each beam pulse. These beam events (BEV) gave the phase space, detection efficiencies and resolutions for beam particles, whether or not they scattered into the spectrometer. The mixture of π's, K's, and p's could

also be independently checked using this beam event sample.

III. SPECTROMETER DATA ANALYSIS

The first step in the analysis of the spectrometer data was a selection of those spectrometer events that could be decoded without error and also occurred in the region of uniform spectrometer acceptance. Next, the yield of good spectrometer events and the corresponding incident beam flux were used to calculate and store run-by-run cross sections. Finally, the various runs were combined, full minus empty target subtractions were made and AVB up and down averages were taken over similar runs. The procedures used in carrying out the analysis are described here.

A. Event Selection

For spectrometer events, the coordinates of the beam and spectrometer particles were calculated and the particle types in the beam and spectrometer were determined from the recorded Cerenkov patterns. The event was discarded if the requirements for a good particle track in the spectrometer wire chambers, an unambiguous beam Cerenkov pattern, and a good beam hodoscope pattern were not all met. All spectrometer Cerenkov patterns were given particle assignments; corrections were later made to resolve ambiguities. If the spectrometer particle coordinates

were within the good acceptance region, the event was binned in spectrometer production coordinates θ, ϕ, $(\Delta p/p)$ as shown in Fig. 2, and stored for the cross section calculation.

The yields of two different classes of events were saved. The acceptance regions for these classes are illustrated in Fig. 6. The first class of events came from the central uniform spectrometer acceptance region with aperture $\Delta\Omega.(\Delta p/p) = 14.1$ μsterad-%. The second acceptance class took advantage of the full spectrometer size. For this class, events were accepted from a parallelpiped in the θ, ϕ, $(\Delta p/p)$ space whose size was 25 μsterad-%. Comparisons between these classes for high statistics processes validated the second acceptance class. These results agreed with a second independent analysis using a Monte Carlo calculation[14] of the larger spectrometer acceptance.

Final cross sections were determined using the data from each spectrometer kinematic setting as a single bin. Finer grained information was used for acceptance cuts and for resolution corrections, which compensated for non-linear variation of the cross section over the spectrometer acceptance. In this case, the event yields were integrated over θ and ϕ in Fig. 6, but were separated into seven $\Delta p/p$ bins. This allowed systematic study of overlapping data between adjacent x bins in the region $x > 0.8$. The fine binning procedure was also used in triple Regge fits to leading particle channels $a + p \to a + X$ where there would be rapid variation of the cross section across

a single coarse data bin.

For beam events (BEV), coordinate and particle type information was decoded using the same Cerenkov and hodoscope criteria employed for the SEV sample. This determined the respective fraction of good beam triggers for pions, kaons, and protons. The beam phase space distributions were checked to verify that all acceptable beam particles of one type had nearly equal probability to scatter into the spectrometer.

Finally, the beam fluxes of pions, kaons, protons, and total beam triggers were accumulated. These fluxes were saved along with the event yields for the calculation of cross sections.

B. Cross Section Calculation

Using the stored yields and fluxes the cross sections were calculated for the 3 (beam particles) x 3 (spectrometer particles) = 9 (different reaction channels) simultaneously for each run. The invariant cross section for the reaction $ap \to cX$ is given by

$$E\frac{d^3\sigma(a,c)}{dp^3} = \frac{E}{p^2}\frac{d^3\sigma(a,c)}{dpd\Omega} = \frac{\text{Yield}(a\to c)}{\text{Flux}(a)}\frac{E}{p^3}\frac{A}{\Delta\Omega(\Delta p/p)N_o\rho\ell} \qquad (1)$$

where $\Delta\Omega.(\Delta p/p)$ is the acceptance of the spectrometer

N_o is Avogadro's number

ρ is the density of hydrogen in the target

ℓ is the length of the target

A is the atomic number of hydrogen.

E,p are the energy and momentum of the scattered particle c in the Laboratory frame.

Normalized empty target subtractions were made. Next, data with opposite scattering angles (AVB polarity) were averaged, producing cross sections indexed by reaction type, beam momentum, Feynman x, and transverse momentum p_T, representing the uncorrected cross sections.

To calibrate the aperture, it was first established through a set of studies that the physical aperture stops (magnet pole faces, etc.) were not shadowing the good acceptance region. Then it was necessary to find the transformation between the true scattering coordinates θ, ϕ, and $(\Delta p/p)$ (two angles and fractional momentum) and the spectrometer exit coordinates measured by the spectrometer wire planes. For this purpose, the program TRANSPORT[14] was used. This program provided a second order description of the transformation between x, y, θ, ϕ, $(\Delta p/p)$ (production coordinates at the target) and x_o, y_o, θ_o, ϕ_o, $(\Delta p/p)_o$ (coordinates measured in the spectrometer) with $(\Delta p/p)_o = (\Delta p/p)$. Using this transformation, the systematic uncertainties in alignment, magnetic excitations, and resolutions were combined to yield an estimated 7% total systematic uncertainty in the spectrometer acceptance. This is the largest source of systematic error for the cross sections.

As an independent check of the acceptance, both elastic and inelastic cross sections were measured where experimental data from other groups existed. The elastic differential cross section data for incident beam momenta 70 GeV/c positive polarity, 100 GeV/c both polarities, and 175 GeV/c negative polarity agreed in both slope and intercept to within 10% of the Ayres et al.[1] data. This is consistent within the combined error of these two experiments. Inelastic data at 100 GeV/c in the channel pp → pX were compared with data from Johnson et al.[15] and Sannes et al.[16]. The data agreed within the estimated 7% systematic normalization uncertainty.

C. Systematic Corrections

There were several important corrections applied during the analysis. They are listed here in decreasing order of importance. The residual uncertainties in these systematic corrections are listed in Table 8.

1. Transmission and decay loss in the spectrometer

Over the 500 foot length of the spectrometer, there was a significant probability for particle decay, absorption or scattering out of the acceptance. The fractions of particles transmitted at various energies were determined experimentally to ±2% accuracy from special runs in which an incident beam was run directly into the spectrometer at various energies. The results are shown in Fig. 7. The transmitted fraction was lowest for kaons, ranging from 36% at 30 GeV/c to 90% at 170 GeV/c. Pion and proton transmissions were comparable and were near 70% and 95%, respectively, for these momenta. Decays into either muons or electrons within the spectrometer aperture could be tagged and vetoed on an event-by-event basis using the calorimeter and transmission counters downstream of ST2.

2. Particle misidentification in the spectrometer.

The four gas Cerenkov counters in the spectrometer gave five independent signals, thus, there were $2^5 = 32$ Cerenkov patterns. However, some of the Cerenkov patterns were ambiguous and could be produced by more than one particle type. Nevertheless, each spectrometer event was initially classified as π, K or proton on the basis of its Cerenkov pattern. The particle misidentification correction (Appendix I) rectified cross section errors due to these ambiguities. The probabilities of misidentifying pions or protons in the spectrometer were typically less than 1%, whereas the misidentification probabilities for kaons were typically 7% above 100 GeV and 11% below 100 GeV.

3. Spectrometer wire chamber tracking loss.

A few percent of the spectrometer events could not be properly tracked because of inefficiencies in the wire chambers and because of ambiguities arising from interactions in the spectrometer. These interactions led to the detection of more than one particle in some of the wire chambers. This tracking loss was measured

using runs in which the unscattered beam passed directly through the spectrometer, and was found to be 2% at 20 GeV/c spectrometer momentum, gradually increasing to 3% at 175 GeV/c.

4. Double scattering.

The hydrogen target was 20 inches long, corresponding to about 6% of an absorbtion length. The probability that a particle that scattered more than once in the hydrogen target and would be detected was calculated[17] and the resulting small correction was parameterized as a function of x and $p_{\perp}$. The average magnitude of this double scattering correction was less than 2% over most of the kinematic range studied. At low spectrometer momenta, the correction increased to as much as 6% while the uncertainty in this correction was estimated to be less than 2%.

5. Radiative Corrections.

During the scattering, either the incident or scattered particle may radiate photons in the bremsstrahlung process. The photon emission will affect the kinematics of the emitting particle and, therefore, the

cross section as a function of the kinematics. The radiative correction[17] to leading particle reactions due to the elastic radiative tail averaged 2%. The inelastic radiative corrections also averaged 2%.

6. Other Effects

Several other effects that might affect the cross section results have been considered. In each case, these effects were shown to be small. They are:

a. Simultaneous presence of two beam particles.

These events were effectively rejected by their ambiguous signature in a beam hodoscope or the beam Cerenkov counters or large pulse heights in the beam trigger counters. The residual error was less than 0.5%.

b. Electron contamination in the beam.

Direct lepton production from the meson target was small, so that most electrons that entered the beam line came from π^0 gamma conversions. The electron flux in the primary beam was measured with a shower counter at the end of the spectrometer and was found to be less than 0.5% of the hadron flux at 100 GeV/c.

c. Muon contamination in the beam.

Few muons were produced directly at the production target. Muons were produced quite copiously from decays of pions in the primary beam line. However, due to the 1% momentum acceptance of the beam line, most decay muons were swept from the beam by the bend magnets. The measured muon contamination at the hydrogen target was less than 0.5%.

IV. VERTEX DETECTOR DATA ANALYSIS

A. Event Selection

For those spectrometer event triggers which were completely reconstructed, were within all aperture and software cuts, and had unambiguous Cerenkov particle identification, the vertex detector data analysis processing was invoked. It was further required that there be no other beam particle incident within ± 3 RF bunches (± 55 nsec) of the spectrometer trigger to minimize backgrounds due to out of time tracks from events in nearby RF bunches. Events were discarded if there were more than one beam particle in an RF bunch as detected by ambiguous beam Cerenkov patterns or large pulse heights in beam trigger counters. The standard scattering up/scattering down, target full, and target empty data cycles were followed to minimize scattering angle offsets and to perform empty target subtractions.

In addition to normal spectrometer triggers, the vertex detector data were also analyzed for non-interacting beam triggers (BEV, for beam events) and special total cross section, or minimum bias, triggers described below. These subsidiary triggers were primarily used for monitoring and calibrating the vertex detector.

B. Analysis

The tracking algorithm for the multiwire proportional chambers first found a vertex by extrapolating hits in each projection back to the target. A fit combining all three projections determined the x,y,z coordinates of the interaction vertex. Tracks were discarded until an acceptable χ^2 was attained, and the discarded tracks were examined for a second vertex. Using thin nuclear targets, the PC vertex resolution was measured to be $\sigma_z = 1.9$ cm. For low multiplicity events, if no vertex was found, the center of the target was used to compute the track coordinates. The three PC packages were analyzed beginning with the downstream one. The most probable set of unique points was found, each point having a hit in all three projections. Lines were drawn from these points to the vertex, including those hits in other packages within a 4mm roadwidth. The found tracks were scanned, deleting those ambiguous tracks which shared too many common projections or had too many missing hits. Two PC tracks within 6mm were treated as a single track.

Multiple particles could be identified in a single MC counter by pulse height analysis. For a set of events, the average number of prongs in each counter was determined by fitting the summed pulse height disribution with spectra expected for 0,1,2,3,... particle events. To get the

multiplicity in each MC counter on an event-by-event basis, the pulse height cut between n and n+1 particles was chosen such that the number of events with n particles misidentified as n+1 particle events equalled the number of events with n+1 particles misidentified as events with n particles, thereby preserving the average multiplicity for that set of events. In those cases where a single MC counter appeared to have more than three particles detected, it was assumed that a secondary interaction occurred in the lucite counter and the true multiplicity for that counter was set to one. The percentage of good events with more than three particles in a single MC counter was estimated to be appreciably less than 1%.

Wide-angle particles were detected by a coincidence between the inner MT counter and the corresponding MB counter. A coincidence was not required for particles stopping in the inner counter provided there was at least a six times minimum energy deposition in the MT counter.

The overall multiplicity and angular distribution for each event were then determined by combining the results from the three vertex detector systems. Coincidences between the overlapping regions of the individual detectors were checked to prevent double counting. The charged particle distribution was integrated over azimuthal angle and stored in six polar angle bins for each reaction channel and kinematic setting. Empty target subtractions were performed on all distributions at this point.

C. Corrections

For each reaction type, the raw charged prong count N_{oj} was measured. To extract the true charged prong count, N_{Ti}, there is a linear transformation

$$N_{oj} = \sum_i M_{ji} N_{Ti} \qquad (2)$$

where M_{ji} is the probability of an event with i charged prongs being measured as having j charged particles. The elements M_{ji} were determined using a Monte Carlo method which simulated events with both charged and neutral particles, including the vertex detector response.[7,18]

In the Monte Carlo calculation, two related methods were used to generate the outgoing hadron distribution. Reconstructed Fermilab 30" bubble chamber events for 100 GeV pp interactions[19] were used for the charged tracks. Extra neutral tracks were generated using a P_T-limited phase space Monte Carlo method to balance momentum.[20] The number of extra neutrals was generated as a Poisson distribution using the average number of K^o, π^o, and Λ^o measured in bubble chamber data.[21]

The second method involved generating both charged and neutral particles using the p_T-limited phase space Monte Carlo. This method also generated simulated events which were triggered by the detected spectrometer particle. The recoiling hadrons were generated for the appropriate missing mass M_x^2 and recoil momenta. The overall single particle distributions generated were constrained to reproduce the inclusive data measured by the spectrometer. The two methods were found to be in good agreement with each other and with data taken using a total cross section trigger, (see Section D).

The generated events of a given multiplicity j were then propagated through the vertex detector taking the following effects into account: two or more particles in the same MT.MB counter, delta rays, multiple scattering, ionization energy loss, elastic and inelastic scattering, gamma ray conversion, and the decays of neutral particles. The measured detector inefficiencies, misalignments, and responses were also included in the analysis. The distribution in the number of the particles detected by the vertex detector produced the transform matrix

$$M_{ij} = \frac{\text{Number of j prong events detected as i prongs}}{\text{Number of simulated events with j prongs}} \qquad (3)$$

The charged prong distribution N_{Tj} was calculated by least squares minimization of

$$\chi^2 = \sum_i \left\{ \frac{(N_{oj} - \Sigma_j M_{ij} N_{Tj})^2}{\sigma_i^2} \right\} \qquad (4)$$

where σ_i is the statistical error on the number of events, N_{oi}, of apparent multiplicity i. A problem regarding the oscillation of the fitted charged prong coefficients in the high multiplicity tail was solved by smoothing the low statistics bins with the formula

$$N_{Ti} = ae^{-bi} \qquad (5)$$

for i greater than twice the average multiplicity. For rare channels, such as $\bar{p}p \to K^+X$, with less than 100 detected events, a correction ratio of (fitted <n>/raw <n>) was determined for a much higher statistics process measured simultaneously, such as $\pi^-p \to \pi^+X$. A similar least squares matrix approach was used to correct the pseudo-rapidity distributions.

Three data sets were used to calibrate the Monte Carlo and detector models. Non-interacting beam particles produced delta rays in the hydrogen target. By studying the vertex detector response to these beam triggers, the difficult to model major backgrounds due to production, absorbtion, multiple scattering and transport of very low energy electrons through the hydrogen target and detector were determined. Elastic scattering data were used to calibrate the response of the MT and MB counters to slow recoil protons. Finally, as discussed in the next section, good agreement of the corrected multiplicities and charged prong distributions with those observed in previous bubble chamber experiments verified the validity of these calibrations.

D. Correction Procedure Verification

A simple transmission trigger was developed which was sensitive to the total hadronic cross section. This allowed the properties of the particles measured with the vertex detector using a minimal bias trigger to be compared with similar bubble chamber results. A small scintillation counter was placed at the momentum dispersed focus of the spectrometer. The scattering angle was set to zero degrees and the spectrometer was tuned to the beam momentum. Particles that met the criteria for beam particles, but failed to fire this scintillation counter, were candidates for inelastic interactions and produced

a trigger for the vertex detector. The largest loss for such a total cross section measurement was from low t, high x scatters that struck the transmission veto counter. False triggers due to scattering or absorbtion in the spectrometer were removed by subtraction of empty target runs.

There are two sources of systematic error for the total inelastic multiplicities and topological cross sections. Uncertainty in the elastic event subtraction can contaminate the two-prong topology and shift the average multiplicity by about 0.06 charged particle. The other source of systematic error is in the modeling of the detector system and in the parameterization of neutral particle production and background used in the Monte Carlo program. The set of physical effects considered and the detector system modeling are summarized in Table 9, together with the actual corrections applied to the 100 GeV π^-p data. For all reactions, the systematic uncertainty from these effects in the average charged multiplicity is $\leq$3% of the multiplicity. The understanding and treatment of this source of error are directly applicable to the associated multiplicity data.

The total cross sections measured in this experiment are listed in Table 10. These were corrected for elastic events vetoed by the spectrometer[1] ($\sim$20% and 50% at 100 and 175 GeV/c respectively) as well as for the loss of low-t ($|t| \leq 0.04$ GeV^2) inelastic diffractive events.[22] The quoted errors are

statistical only. The systematic error is estimated to be about 3%. The largest source of error is the uncertainty in the spectrometer acceptance for the elastic cross section ($\lesssim 1.5\%$). The excellent agreement with the data of Carroll *et al* [23] indicates that the simple transmission trigger provided a good total cross section trigger.

A comparison of the mean multiplicities of charged particles measured in this experiment using the minimum bias trigger, with those measured with bubble chambers[24,25,26,27,28] appears in Table 11. The quoted errors are only statistical. It is evident that these measurements are in quite good agreement with the bubble chamber measurements. Although intended as a calibration, for some channels these data represent the first multiplicity measurements at these energies.

The charged topological cross sections for $\pi^{\pm}p$, pp and $\bar{p}p$ at 100 GeV/c are listed[24,25,28] in Table 12, also indicating good agreement with bubble chamber measurements. Charged topological cross sections of the remaining channels are given in Table 13. It has been shown that charged topological cross sections obey KNO scaling.[29] As an example of this, the 100 and 175 GeV/c negative beam topological cross sections have been plotted as $\langle n\rangle\sigma_n/\sigma_{inelastic}$ vs. $n/\langle n\rangle$ (Fig. 8). The data are in good agreement with the curve, which represents a KNO fit[30] to pp data over the range 50 to 300 GeV/c.

The excellent agreement with the bubble chamber results both for the average multiplicities and for the charged prong distributions verifies that the detector modeling and correction procedure are capable of producing accurate associated vertex data.

V. SINGLE PARTICLE INCLUSIVE RESULTS

The inclusive data include 36 possible reactions of the type $a + p \rightarrow c + X$, where a and c are any of $\pi^{\pm}$, $K^{\pm}$, p or $\bar{p}$ at beam momenta of both 100 and 175 GeV/c. They span a kinematic range of $0.12 < x < 1.0$ and $p_T < 1.25$ GeV/c. Because of the rather small acceptance of the spectrometer, a grid of independent measurements was made; specifically for each spectrometer momentum (or x) setting data were taken for several values of p_T. In this section, the x and p_T dependences of the data will be presented, and simple fitted parameterizations of the data will be given. For completeness, all the measured points are given in Tables 14 and 15, displayed as a combination of x and p_T sweeps, paralleling in part the data acquisition procedure.

A. Feynman x Dependence

The dependence of the inclusive cross sections on x was investigated[3] for several different values of p_T. In Fig. 9, the x dependence of the data at 100 GeV/c incident momentum is displayed at $p_T = 0.3$ GeV/c, for the various incident particle types. In each case, there is a rather flat cross section with a diffractive peak near x = 1 for the leading particle channel, $a + p \rightarrow a + X$. The five other channels, with the outgoing particle different from the incoming one, show a decrease in

cross section with increasing x. The falloff tends to be steepest for those channels with the greatest change in quantum numbers between incoming and outgoing particles. The solid curves shown for the non-leading channels are fits to a $(1-x)^n$ parameterization which are discussed below.

Figure 10 shows the same reactions, but for a larger value of the transverse momentum, $p_T = 0.75$ GeV/c. The data are very similar in shape to those in Fig. 9, but reduced in magnitude. In fact, separate fits to the form $(1-x)^n$ for the two different values of p_T yield values of n which are consistent within errors. The major difference at larger p_T is a relatively smaller leading particle peak near x = 1.

The 175 GeV/c incident momentum data for $p_T = 0.3$ GeV/c are shown in Fig. 11. Within errors, these data are equivalent to those in Fig. 9 from 100 GeV/c, demonstrating Feynman scaling for all the reaction channels at these energies.

All of the x "sweeps" at constant p_T for non-leading reaction channels have been fitted to the functional form $C(1-x)^n$. Here C is a different parameter for each sweep, but the same parameter n is used for all sweeps for a given reaction at a given beam momentum. The results of these fits are given in Table 16 and are shown as the solid curves in Figs. 9, 10, and 11. In general, this form gives an adequate representation of the data between $0.2 < x < 0.7$. However, in a few cases noted in the Table, the x range of the fit has been limited to avoid

contamination from resonance decay products at large x. The exponents, n, of these fits have been previously related[3] to the quark/parton picture via the quark counting rules of Brodsky and Gunion.[31]

B. Transverse Momentum Dependence

Figures 12 and 13 show the p_T dependence at several different values of x for reactions with incident 100 GeV/c π^+ and π^- respectively. It can be seen that the corresponding π^+ and π^- induced reactions have essentially equal cross sections. Figure 14 displays the p_T dependence of reactions with incoming protons at 100 GeV/c.

The functional form of the p_T dependence could be determined at those values of x where detailed p_T sweeps were taken. In general, the data were sufficiently precise to allow discrimination between exponential and Gaussian behavior. However, in most cases, a generalization to the functional form $\exp(-Bp_T^n)$, where n is variable could not be justified.

Individual fits to the p_T dependence of each reaction at each x value were made. The resulting chi-squared values indicated a clear separation into regions of Gaussian and exponential transverse momentum behavior. The reactions in which both the incoming and outgoing particles are mesons show Gaussian behavior for $x \lesssim 0.4$ and exponential behavior at higher

x. This is also true for $p \to p$ and $\bar{p} \to \bar{p}$ where the transition in functional form is at a slightly higher value of x. Channels with an incoming proton and an outgoing meson show exponential behavior in p_T over the entire x range where fits could be made. The two channels $\pi^+ \to p$ and $\pi^- \to \bar{p}$ show Gaussian transverse momemtum dependence over the entire x range observed. Finally, the two charge exchange channels $\pi^+ \to \bar{p}$ and $\pi^- \to p$ had statistics which were inadequate to allow a determination of the functional form.

The fits also indicated that all channels have an average transverse momentum squared which is typically between 0.25 and 0.30 $(GeV/c)^2$. The only exceptions are the baryon induced leading particle channels at high x, namely $p \to p$ and $\bar{p} \to \bar{p}$. Here the average transverse momentum squared shrinks to about 0.15 $(GeV/c)^2$.

C. p_T Integrated Cross Sections

The determination of the functional form of the transverse momentum dependence of the invariant cross section allows computation of the integrated cross section

$$x \frac{d\sigma}{dx} = E \frac{d\sigma}{dp_L} = 2\pi \int_0^\infty E \frac{d^3\sigma}{dp^3} p_T \, dp_T \quad . \tag{6}$$

In the x region where exponential p_T behavior was observed, the functional form used was

$$E\frac{d^3\sigma}{dp^3} = \frac{A}{2\pi B^2} e^{-Bp_T} \qquad (7)$$

In the x region where behavior was Gaussian in p_T the form used was

$$E\frac{d^3\sigma}{dp^3} = \frac{A}{\pi B} e^{-Bp_T^2} \quad . \qquad (8)$$

The powers of B in the denominators normalize the functional forms of the differential cross sections so that the integrated cross section is A for both functional forms. At each x the fitted parameters A and B were essentially independent because the data is centered around the value $p_T \approx 0.5$ GeV/c.

A global fit was made for each reaction in those regions where the cross section showed a particular functional form. Thus, for reactions with both Gaussian and exponential regions, two fits were made. If, within a given region, there existed two or more values of x at which a detailed p_T sweep was made, the value of B, was allowed to vary linearly with x in that region. Thus, the p_T dependence from the detailed sweep could be used to interpolate the B values at other points. Reactions which supplied enough data to allow a linear variation of B with

x were the leading particle channels and $\pi^+ \rightarrow K^+$ in the higher x region, and proton → meson$^{\pm}$ for all x. For other channels, B was taken to be a constant, independent of x.

The coefficients A were then obtained separately for each value of x. The integrals and their errors are listed in Table 17 and are shown in Figs. 15 and 16 at 100 and 175 GeV/c respectively. The curves shown have the functional form $C(1-x)^n$. The value of n used is that obtained in the global fit of the differential cross sections. The value of C was determined by a one-parameter fit to the integrated cross sections. For a given reaction, the fit was made over the same x range as was the global fit to the differential cross sections. The parameter C for the integrated cross sections is also shown in Table 16 for all cases where the data were sufficiently good to derive such a parameter.

D. Triple-Regge Parameterizations

The cross section for the reaction channel $ap \rightarrow cX$ in the kinematic range $s/M_x^2 \gg 1$ and large M_x^2 can be described by triple Regge phenomenology[32,33] as shown schematically by the Feynman diagram in Fig. 17. The form of the invariant cross section is given by the sum over the exchanged trajectories

$$E\frac{d^3\sigma}{dp^3} = \sum_{ijk} G_{ijk}(t)\ (1-x)^{\alpha_k(0)-\alpha_i(t)-\alpha_j(t)}\ s^{\alpha_k(0)-1} \qquad (9)$$

where $\alpha_i(t)$ is the Regge trajectory of the exchanged particle and where $G_{ijk}(t)$ is the product residue functions at the four vertices. In this simplified formulation G_{ijk} also includes the effect of the signatures of the exchanged trajectories.

In addition to the 100 and 175 GeV/c data, runs were also made at 70 GeV/c with positive beam to cover the kinematic range $0.75 < x < 0.97$ and $0.2 < p_T < 1.25$ GeV/c^2. The data for the reactions $\pi^+p \to \pi^+X$, $\pi^-p \to \pi^-X$ and $pp \to pX$ were further broken down into seven Feynman x bins for each spectrometer setting. The lower statistics data accummulated for the $K^\pm$ and $\bar{p}$ leading particle reactions were left in a single bin per setting.

For these leading particle reactions, the invariant cross section data were fit using a triple Pomeron (PPP) and the leading Reggeon-Reggeon-Pomeron (RRP) terms. The Reggeon form incorporates a linear combination of ρ, f, ω, and A_2 exchanges, which share a common trajectory $\alpha_R(t)=1/2+t$. In addition, for the $pp \to pX$ channel, $\pi\pi P$ and $\pi\pi R$ contributions were added. The strength and form of the $\pi\pi P$ and $\pi\pi R$ terms were taken from the analysis by Field and Fox[33]. The t-slope for the Pomeron was taken as a free parameter, except for the lower statistics $K^\pm p \to K^\pm X$ and $\bar{p}p \to \bar{p}X$ channels where it was constrained to zero. This simplified form of the cross section was thus:

$$E\frac{d^3\sigma}{dp^3}(x,t,s) = G_{ppp}(t)\,(1-x)^{-1-2\alpha_p' t} + G_{RRP}(t)\,(1-x)^{-2t} + (\pi\pi P + \pi\pi R)\ . \tag{10}$$

A single triple Regge fit was made for all x,t, and s values simultaneously for each reaction channel. Residue functions of the form $G(t) = Ae^{bt} + Ce^{dt}$ were used. The leading particle reaction data, along with the triple Regge fits are presented in Fig. 18. The contributions of the PPP and RRP terms are shown for the fine bin data for $\pi^+p \to \pi^+X$ in Fig. 19. The parameters of the fits are summarized in Table 18; complete tables of the parameters and their error matrix can be found in Reference 5.

To permit comparison between reaction channels without the complication of residue functions, the contributions of both the PPP and RRP terms were integrated over the t-range covered by the data. Integration over this t-range is estimated to contain 80-90% of the cross section at a given x. These integrated cross sections are listed in Table 19.

The leading particle cross sections change by less than 12% over the 70-175 GeV/c beam momentum range studied. Good fits are obtained without the use of non-scaling PPR terms. To check the sensitivity of the data to a non-scaling PRR interference term, the leading particle data for particle and anti-particle beams were simultaneously fit to a form PPP + RRP + PRR since only the PRR term changes sign between $a^+p \to a^+X$ and $a^-p \to a^-X$ interactions. The contributions of the t-integrated non-scaling terms for $\pi^\pm$, $K^\pm$, and $p^\pm$ beams at $x = 0.88$ are 3±1%, 10±5%, and 3±2% respectively.

Using this data, two simple tests of factorization may be performed. Neglecting kinematic terms, the cross section for leading particle inelastic reactions $a^\pm p \to a^\pm X$ at high x may be written as a product of vertex functions

$$\left.\frac{d^2\sigma(t)}{dM_X^2 dt}\right|_{\text{inelastic}} \propto \beta^2_{aaP}(t)\ \beta_{PPP}(t)\ \beta_{ppP}(0)\ . \qquad (11)$$

In the same spirit of neglecting all exchanges except for the Pomeron, the coupling for the elastic cross section $a^\pm p \to a^\pm p$ can be expressed at the same t value as

$$\left.\frac{d\sigma(t)}{dt}\right|_{\text{elastic}} \propto \beta^2_{aaP}(t)\ \beta^2_{ppP}(t)\ . \qquad (12)$$

Dividing these terms and cancelling the beam dependent $\beta^2_{aaP}(t)$ coupling, the ratio

$$\frac{\left.\frac{d^2\sigma(t)}{dM_X^2 dt}\right|_{\text{inelastic}}}{\left.\frac{d\sigma(t)}{dt}\right|_{\text{elastic}}} \propto \frac{\beta_{PPP}(t)\ \beta_{ppP}(0)}{\beta^2_{ppP}(t)} \qquad (13)$$

is independent of the beam particle species. The inelastic data for 100 GeV, p_T=0.3 GeV/c, x=0.92, t=-0.098 GeV^2 is divided for each leading particle channel by the corresponding elastic cross section as parameterized in Reference 1. The ratios are presented in Table 20. Although the data still contain substantial non-Pomeron contributions at x=0.92, the constancy of the ratios indicates that factorization holds to better than 10% for this test.

Although the particle changing data are somewhat sparser, a similar factorization test can be demonstrated for the reactions $\pi^+p \to K^+X$ ($\pi^-p \to K^-X$). The cross sections may be expressed as products of the $\pi^+K^+\overline{K^{*o}}$ ($\pi^-K^-K^{*o}$) coupling constants squared times the exchanged $\bar{K}^{*o}p(K^{*o}p)$ total cross section, and thus

$$\frac{\left.\frac{d^2\sigma}{dtdM_X^2}\right|_{(\pi^-p\to K^-X)}}{\left.\frac{d^2\sigma}{dtdM_X^2}\right|_{(\pi^+p\to K^+X)}} \propto \frac{\left|\beta_{\pi^-K^-K^*}(t)\right|^2 \sigma_{tot}^{K^*p}(E_{eff} = (1-x)E_{\pi^-})}{\left|\beta_{\pi^+K^+\overline{K^*}}(t)\right|^2 \sigma_{tot}^{\overline{K^*}p}(E_{eff} = (1-x)E_{\pi^+})}\ . \qquad (14)$$

The coupling constants cancel by charge symmetry and the $K^{*o}p$ to $\overline{K^{*o}}p$ cross section ratio should be the same as the K^+p to K^-p total cross section ratio at equivalent energy. The inelastic $\pi^\pm p \to K^\pm X$ data at 100 GeV, P_t = 0.3 GeV/c, and x = 0.92, 0.88, and 0.80 are used to find the ratio of $\sigma_t(K^{*o}p)/\sigma_t(\overline{K^{*o}}p)$ and compared in Fig. 20 with the ratio of $\sigma_t(K^+p)/\sigma_t(K^-p)$ as measured in Reference (34). The agreement of the cross section ratios again indicates agreement with the factorization

hypothesis.

Because of limited statistics or contamination from forward resonance production[2,35] other particle changing reaction channels at high x in the data set are inadequate for further application of triple Regge phenomenology.

VI. ASSOCIATED MULTIPLICITY RESULTS

In addition to the behavior of single particle inclusive cross sections for the process a+p → c+x, this experiment also studied the charged particle multiplicity and pseudo-rapidity distributions of the charged particle secondaries which comprise the recoil state X. Such additional information can shed new insight into the systematics of multiparticle production by correlating the measured distributions with the identities and kinematics of the trigger particles.

Data for this experiment were taken in sweeps of transverse momenta p_T and Feynman x. The natural variable for the study of multiplicities is the missing mass-squared of the recoiling system $M_X^2 = (1-x)s$. Since the longitudinal phase space available for particle production varies as $\ln M_X^2$, it is to be expected that the produced particle multiplicity should vary as $\langle n(x) \rangle = A + B \ln M_X^2$. Here the coefficient A represents the multiplicity of the two fragmentation regions and B represents the height of the central plateau in rapidity space. In models where the central region is uncorrelated with the fragmentation region production, the coefficient B is expected to be independent of the participating particle identities.

This experiment can also investigate whether the associated multiplicities further depend on the p_T or the invariant momentum transfer t between the particles a and c. It might be expected that as p_T or t increases, the interaction involves scattering at shorter distances. This is possibly associated with an increase in the multiplicities.

The average charged particle multiplicities as a function of Feynman x and p_T are listed in Table 21. Complete tables of the charged prong distributions and pseudo rapidity distributions are available in Reference 7.

A. Associated Charged Particle Multiplicities

The average charged particle multiplicities for the reactions a+p → c+X are shown as a function of x at constant p_T in Figure 21. The multiplicity for each beam species a is nearly independent of the detected spectrometer species c. An exception to this rule is evident in comparing pp → pX and pp → π^+X associated multiplicities. The pion production channel multiplicities are systematically lower than the multiplicities for the leading proton channel. Production of π^+ at high x may be due to decays of forward nucleon resonances. In the decays of charged resonances, often most of the incident momentum is carried away by undetected neutrons, thereby lowering the energy available for charged particle production. Leading protons, on the other hand, are often associated with inelastic target

fragmentation leading to relatively higher charged secondary particle multiplicities.

The dependence of the individual charged prong cross sections as a function of x are displayed in Fig. 22, for the leading particle $\pi^+p \to \pi^+X$ and $pp \to pX$ channels and for the charge changing reactions $\pi^+p \to \pi^-X$ and $pp \to \pi^-X$. The leading particle enhancement at high x is observed to consist almost entirely of 1 and 3 prong contributions suggesting the diffractive nature of these topological cross sections in the low-mass region. The contributions of 5, 7, and 9 prong processes for $pp \to \pi^-X$ and $\pi^+p \to \pi^-X$ are similar, falling steeply with increasing x. The OPE[2] high x shoulder in $\pi^+p \to \pi^-X$ is due predominantly to an x independent associated 3-prong contribution where one associated prong arises from the decay of a forward produced vector meson, and where the low effective energy π^+p vertex produces predominantly two prong states.

The associated charged particle multiplicities for leading particle reactions are displayed in Fig. 23 as a function of invariant momentum transfer

$$t = M_a^2(1-x) + M_c^2(1-\tfrac{1}{x}) - p_T^2/x \qquad (15)$$

at fixed x or M_X^2. Similar multiplicities for high statistics

particle exchange reactions are displayed in Fig. 24 as a function of transverse momentum p_T at fixed x. There is a definite increase of the associated multiplicities with increasing $|t|$ or p_T for $x < 0.8$ for all channels with sufficient statistics.

The leading particle data have been fit to the form

$$\langle n(x,|t|)\rangle = \alpha(x) + \beta(x)|t| \qquad (16)$$

at a constant x or M_X^2. Results of this fit are displayed in Fig. 23. For the high statistics channels, the term $\beta(x)$, shown in Fig. 25, is positive indicating an increase in the average multiplicity with increasing scattering angle. $\beta(x)$ is independent of x except for $x > 0.8$, where it falls to zero as $x \to 1$.

Both bubble chamber[36,37] and counter[38,39] experiments have also studied the M_X^2 and t dependences of associated multiplicities for leading particle reactions. Most of the $pp \to pX$ experiments find very little dependence of the multiplicity on the momentum transfer t. However, the ARGO spectrometer group[39] found a definite increase in the associated multiplicity with increasing t with a form

$$n = \alpha(x) + \beta(M_X - M_p)^2|t|. \qquad (17)$$

This functional form is consistent with the behavior of the presently fitted $\beta(x)$ at comparable M_X^2 for $x > 0.8$. The Fermilab Proportional Hybrid System Consortium[37,40] has also found a form $n = \alpha(x)+\beta|t|$ for the reaction $\pi^-p \to \pi^-X$ with the t coefficient, $\beta = 1.2\pm0.2$, independent of x or M_X^2, over the range $0.5 \leq x \leq 0.93$ ($20 \leq M_X^2 \leq 140$ GeV^2). An average of the present $\pi^-p \to \pi^-X$ data for $x < 0.8$ with a constant β produces a smaller t slope, $\beta = 0.6 \pm 0.1$.

The parameters $\alpha(x)$ in the fit, which represent the average multiplicity at $t = 0$, are plotted for $pp \to pX$, and $\pi^\pm p \to \pi^\pm X$ in Fig. 26. Also plotted are the total cross section multiplicities discussed in Section IV D at common $M_X^2 = s$. Also indicated are fits to the world average[41] total multiplicity data and the associated multiplicities[37] for $pp \to pX$ and $\pi^-p \to \pi^-X$. As has been previously noted[42], the $pp \to pX$ associated multiplicities are systematically higher than the corresponding $pp \to X$ total multiplicities. Comparing the s-dependence of the fits[37] to the associated multiplicities, it appears that the associated multiplicities at a fixed M_X^2 increase with increasing s. In comparison, the $\pi^\pm p \to \pi^\pm X$ multiplicity data are systematically lower than for the total cross section multiplicities at comparable s or M_X^2.

Assuming a single exchange trajectory for hp → hX at high x or low M_X^2, one would expect identical behavior for associated multiplicities for all hadrons h, since all target fragments arise at the pomeron-proton vertex.

The average multiplicities for the reactions $\pi^\pm p \to \pi^\pm X$, $\pi^\pm p \to \pi^\mp X$, $K^\pm p \to K^\pm X$, and $p^\pm p \to p^\pm X$ at $t = 0$ and a common $M_X^2 = 53$ GeV^2 are essentiallyy the same with $\langle\bar{n}\rangle = 4.62 \pm 0.18$. These agree well with the bubble chamber [37] results for $pp \to pX$, $\Lambda^o X$, and $\Delta^{++} X$ at the same M_X^2. This shows that at fairly low M_X^2 the multiplicity is independent of the exchange particle, whether there is a dominant PPP or RRP coupling, and primarily depends on M_X^2.

B. Angular Distributions for the Associated Particles

Besides the associated multiplicities, correlations of the produced multiparticle state with the kinematics and identities of the trigger particles may provide further understanding of production and fragmentation processes. In the absence of momentum analysis, the associated particles are described by the pseudo-rapidity

$$\eta_{lab} = -\ln \tan (\theta/2) \qquad (18)$$

where θ is the production angle relative to the beam

direction[43]. Particles produced at 90° in the center of mass have $\eta_{lab} = 2.7$ and 2.9 for 100 GeV and 175 GeV incident momenta respectively. Due to limited statistics, all angular distributions for this experiment have been integrated over azimuthal angle and topology.

Figure 27 shows a similarity between the total and associated rapidity distributions at a common $s = M_X^2 = 190$ GeV^2. The associated η-distribution for $pp \to pX$ measured in this experiment is compared to the total η-distributions for $pp \to X$ (Reference 44) and $\bar{p}p \to X$ (Reference 45) at 100 GeV. The three data sets are in good agreement indicating that these processes can all be described by a common p_T-limited phase space model.[38]

The pseudo-rapidities of charged particles produced in $\pi^+ p \to h^\pm x$ reactions are shown in Fig. 28. The angular distributions associated with leading $\pi^+ p \to \pi^+ X$ processes as a function of x at $p_T = 0.3$ GeV/c show that the width of the pseudo rapidity distribution increases as ln M_X^2 as expected. For $x \leq 0.4$, a central rapidity plateau appears. This is similar to the $pp \to hX$ data presented by the CHLM group[38] which were consistent with many of the detailed predictions of longitudinal or p_T-limited phase space models.

There is very little dependence of the associated angular distributions on the identity of the particle detected in the single arm spectrometer. The rise in the multiplicity with increasing p_T as seen for example in $\pi^+p \to \pi^+X$ at moderate x is due to an increase in the number of particles produced in the central rapidity region as shown in Fig. 28c. The number of target or beam fragments is independent of p_T.

The process $\pi^+p \to \pi^-X$ at high Feynman x exhibits features not described by phase space. The associated charged particle pseudo-rapidity distributions are shown in Fig. 29. As the spectrometer trigger π^- increases in momentum above x = 0.3, the phase space plateau narrows and a very large positive correlation emerges at η=4. At x = 0.88, the integrated number of associated particles above $\eta \geq 3.5$ is one, representing the π^+ from the decay of the forward produced vector meson[2].

VII. DISCUSSION AND SUMMARY

This experiment provides new data on charged particle production in low p_T hadronic fragmentation for $\pi^\pm$, $K^\pm$, p and $\bar{p}$ beams. Compared to bubble chamber[36,37] and spectrometer[15,46,47] experiments, it extends the kinematic range for complete identification of the charged secondary particles. The major contributions of this experiment to understanding production processes are discussed below.

Over most of the fragmentation range, the inclusive spectra are well represented by a power law dependence such as $(1-x)^n$. This form qualitatively agrees with quark counting model predictions of Brodsky and Gunion[31]. Since the earlier publication of this data[3], this production model has been modified to differentiate between hadronic and gluon bremmsstrahlung spectators in the counting rules to better represent the powers n for the large numbers of observed channels[48]. The modified model yields predictions in yet better agreement with the data.

The pion and kaon data have been analyzed in the recombination[49] and valon[50] models. The meson structure functions may be derived from the data using this formulation[4]. The pion structure function determined in this manner agrees well with that derived from Drell-Yan di-muon production. However, the kaon valence structure function so

derived using the recombination model is steeper[51] than those found from di-muon[52] or high p_T π^o production[53] by kaon beams. This disagreement is most likely due to uncertainties in the exact formulation of the recombination model and large resonance production backgrounds at high x for channels which determine the kaon structure function. Amiri and Williams[54] have studied the relative resonance and direct contributions to these channels and find reasonable agreement with the present data using the kaon structure functions of Reference 52 and the valon phenomonology. The single particle inclusive fragmentation data may also be well represented by the Lund model[55] as discussed in Reference 17.

At high x, the leading particle spectra may be well fitted using only scaling PPP + RRP triple Regge terms. The projectile particle independence of the ratio of inelastic $a + p \to a + X$ to elastic $a + p \to a + p$ interactions at comparable t values is indicative of factorization of the aaP vertex from the ppP and PPP verticies. The agreement of the production cross section ratio for $\pi^- p \to K^- X$ / $\pi^+ p \to K^+ X$ with the total cross section ratio of $K^+ p / K^- p$ gives strong evidence of factorization for K exchange channels.

The average associated charged particle multiplicities increase with $\ln M_X^2$ as the total cross section multiplicities increase with $\ln s$. However, there are absolute differences in comparing the multiplicities for $ap \to aX$ and $ap \to X$ at comparable M_X^2 and s-values. For leading particle channels, the multiplicity increases as $|t|$ increases at constant x, except as $x \to 1$ where there is no t-dependence. For particle changing reactions with sufficient statistics, there is also an increase of associated multiplicities with increasing p_T. The angular distributions of the associated particles indicate that this increase in the multiplicity is due to an increase of production in the central region.

ACKNOWLEDGEMENTS

We would like to express our thanks to the many people at Fermilab who have contributed to the successful operation of the Single Arm Spectrometer and of the accelerator. Special thanks are due to the staffs of the Fermilab Meson Laboratory and Computing Center, MIT Physics Department and Laboratory for Nuclear Science, the Brown University Physics Department and the Istituto Nazionale de Fisica Nucleare. Major credit is due for the technical efforts of Travis Minto from Fermilab and Roger Strong from MIT. This work was supported in part by the U. S. Department of Energy under Contract Numbers EY76-C-02-3000 (Fermilab), EY76-C-02-3069 (MIT), EY76-C-02-3130 (Brown), and the Istituto Nazionale de Fisica Nucleare (Italy).

APPENDIX I

Cerenkov Particle Identification

The properties of the eight Cerenkov counters used in this experiment are given in Table 4. Any event within the spectrometer acceptance which has a valid beam Cerenkov pattern is assumed to be the result of one of the 9 hadronic processes ($\pi Kp \rightarrow \pi Kp$). The beam identification is the easier to deal with because any events with ambiguous beam Cerenkov patterns have been eliminated from both incoming flux and spectrometer rate, incurring no change in the measured cross section and only a small loss in statistics.

A. Beam Identification

Valid beam particles used in the analysis required an unambiguous Cerenkov identification. The Cerenkov assignments used were:

$$\pi = (BGAS+BGAS0).\overline{BDISC}.\overline{BDIFR}$$

$$K = BDISC.(\overline{BGAS+BGAS0}).\overline{BIDFR}$$

$$P = BDIFR.\overline{BDIFA}.(\overline{BGAS+BGAS0}).\overline{BDISC}$$

Events not satisfying these criteria were discarded from further analysis due to ambiguous identification. Usually, the ambiguous signatures were caused by two particles in the same RF bucket or by Cerenkov counter inefficiencies.

Requiring strict beam particle identification and readjusting the measured incident fluxes was more desirable than attempting to use all the flux and later applying corrections. The loss of events from application of this cut was 4% at 100 GeV and 8% at 175 GeV.

B. Spectrometer Identification

Each event with valid beam and spectrometer particles reconstructed within the spectrometer aperture by fitting the multi wire proportional chamber data was assumed to correspond to a valid hadron scattering event regardless of the spectrometer Cerenkov pattern. A preliminary spectrometer identification was made for all possible spectrometer Cerenkov patterns. For each kinematic setting, a fitting program then solves for the efficiency and cross-talk between spectrometer counters and corrects for those spectrometer particles mislabelled in the preliminary assignment.

A total of 32 Cerenkov patterns was available using the five spectrometer signals SDIFR, SDIFA, SGAS1, SGAS2, and SGAS3. The nominal settings of the Cerenkov pressures corresponded to the identification in Table A1. There are four important momentum-dependent efficiency changes. The first is a decrease in efficiency of SGAS1, SGAS2, and SGAS3 at high momentum. The second efficiency change is due to the proximity of the kaon and proton light in SDIF at high

momentum, and the finite acceptance of the spectrometer. These circumstances lead to an overlap of the kaon and proton light at the edge of the SDIF ring. The third effect is caused by the dispersion of Cerenkov light at low momentum. For momenta less than 50 GeV/c, the proton ring of light is larger than the SDIF ring, and protons count on both the ring and anti. Finally, as the momentum becomes small, the light from pions and kaons is emitted at very large angles in the SDIF counter. Therefore, the SDIFA efficiency for pions and kaons becomes quite small for low momenta.

For each spectrometer momentum, a fit was made for the efficiencies of each spectrometer Cerenkov counter for detecting π's, K's, and protons. The fitting program is applied to scattering data, using the identity of the beam particles, determining the reaction probability for a beam particle to produce a π, K, or proton in the spectrometer. Thus, 15 efficiencies E_{ia} and nine reaction probabilities B_{ba} are fit where

i = the spectrometer Cerenkov counter
(SDIFR, SDIFA, SGAS1, SGAS2, SGAS3)
b = the beam particle type (π, K, or p)
a = spectrometer particles (π, K, or p)

The sum of the reaction probabilities for each beam particle is constrained to be 1. That is,

$$\sum_b B_{ab} = 1$$

Thus, there are 15 + 9 - 3 = 21 free parameters.

The input to the fitting program is an array of the number of events recorded for each spectrometer Cerenkov pattern. This is a 3 x 32 array where we have 3 beam particle types and 32 spectrometer patterns. We then minimize χ^2 with respect to the 21 free parameters and calculate a complete set of efficiencies and reaction probabilities. From this we construct the "misidenfication matrix" M_{ab} which gives the fraction of spectrometer particles b that are identified as a. This matrix is applied during the run combination program of the analysis to correct the cross sections. For $\pi p \to \pi X$ and $pp \to pX$ reactions this correction is less than 1%. The correction for the $Kp \to KX$ cross section is typically 9%.

References

(a) Present address: Weizmann Institute, Rehovath, Israel.

(b) Present address: Brookhaven National Laboratory, Upton, NY, 11973.

(c) Present address: U.S. Windpower, Burlington, Mass. 01803.

(d) Present address: Harvard University, Cambridge, Mass. 02138.

(e) Present address: Bell Laboratories, Holmdel, N.J. 07733.

(f) Present address: Bell Laboratories, Denver, Colo. 80234.

(g) Present address: P.O. 796 APO San Francisco, CA 96555.

1. For description and references see D. S. Ayres, et al., Phys. Rev. D15, 3105 (1977).

2. D. Cutts, et al., Phys. Rev. Lett. 40, 141 (1978).

3. D. Cutts, et al., Phys. Rev. Lett. 43, 319 (1979).

4. W. Aitkenhead, et al., Phys. Rev. Lett. 45, 157 (1980)

5. W. Aitkenhead, Ph.D. Thesis, MIT (1979), unpublished.

6. W. Aitkenhead, et al., Fermilab-Conf-80/48-EXP (unpublished).

7. L. G. Votta, Ph.D. Thesis, MIT (1979), unpublished.

8. J. Lach and S. Pruss, Fermilab-TM-298(1971), (unpublished).

9. R. L. Anderson and J. A. Grant, Nucl. Instr. Meth., 135, 267 (1976).

10. M. Benot, J. Litt and R. Meunier, Nucl. Instr. Meth., 105, 431 (1972).

11. D. Ayres, ANL report, 1974 (unpublished).

12. P. H. Garbincius, Nucl. Inhstr. Meth. 131, 273 (1978).

13. E. F. Anelli, Rev. Sci. Instrum. 49, 1054 (1978).

14. D. C. Carey, Nucl. Instr. Meth. 104, 173 (1972); K. L. Brown, F. Rothacker, D. C. Carey and Ch. Iselin, Fermilab Report NAL-91 (1977).

15. J. R. Johnson, et al., Phys. Rev. Lett. 39, 1173 (1977); Phys. Rev. D17, 1292 (1978).

16. F. Sannes, et al., Phys.Rev.Lett. 30, 766 (1973).

17. W. W. Toy, Ph.D. Thesis, MIT (1978), unpublished.

18. B. G. Gibbard, et al., Phys. Rev. D11, 2367 (1975), used a similar matrix unfolding procedure.

19. T. Ferbel, private communication of reconstructed bubble chamber events as described by J. W. Chapman, et al., Phys. Lett. 47B, 465 (1973).

20. D. C. Carey and D. Drijard, Journal of Computational Physics, 28, 327 (1978).

21. S. Kahn, APS/DPF, Seattle, 1975, p 292.

22. R. L. Anderson, et al., Phys. Rev. Lett. 38, 880 (1977).

23. A. Carroll, et al., Phys. Rev. Lett. 33, 928 (1974) and 33, 932 (1974).

24. W. M. Morse, et al., Phys. Rev. D15, 66 (1977).

25. E. L. Berger, et al., Nucl. Phys. B77, 365 (1974).

26. V. E. Barnes, et al., Phys. Rev. Lett. 34, 415 (1975).

27. D. Fong, et al., Nucl. Phys. B102, 386 (1976).

28. R. E. Ansorge, et al., Phys. Lett. 59B, 299 (1975).

29. G. Giacomelli, Proc. 19th Int. Conf. on HEP, Tokyo, Japan, p53 (1978); Z. Koba, et al., Nucl. Phys. B40, 317 (1972).

30. P. Slattery, et al., Phys. Rev. Lett. 29, 1624 (1972).

31. S. J. Brodsky and J. F. Gunion, Phys. Rev. D17, 848 (1978).

32. A. Mueller, Phys. Rev. D2, 2963 (1970).

33. R. D. Field and G. C. Fox, Nucl. Phys. B80, 367 (1974).

34. W. Galbraith, et al., Phys. Rev. 138, 913 (1965).

35. D. Brick, et al., "Inclusive Strange Resonance Production in pp, π^+p Interactions at 147 GeV/c," to be published in Phys. Rev. D.

36. J. Whitmore, Physics Reports, 10C, 273 (1974); Physics Reports, 27C, 187 (1976).

37. D. Brick, et al., Phys. Rev. D19, 743 (1979) and references listed therein.

38. M. G. Albrow, et al., Nucl. Phys. B102, 275 (1976).

39. A. Ramanauskas, Phys. Rev. Lett. 31, 1371 (1973); T. S. Clifford, et al., Phys. Rev. Lett. 33, 1239 (1974); W. N. Schreiner, Ph.D. Thesis, VPI (1973), unpublished.

40. C. deTar, Phys. Rev. D17, 870 (1978).

41. E. Albini, et al., Nuovo Cimento 32A, 101(1976).

42. S. J. Barish, et al., Phys. Rev. Lett. 31, 1080 (1973); J. Whitmore and M. Derrick, Phys. Lett. 50B, 280 (1978).

43. Assuming all particles have p_T = 0.3 GeV, a typical average transverse momentum, the maximum pseudo-rapidity available to an associated particle is:

$$\eta_{max} \simeq \ln \frac{2p_o(1-x)}{\langle p_T \rangle}$$

where p_o is the beam momentum and x is the Feynman-x of the trigger hadron. This estimate works reasonably well to define the η-bin center and bin width corresponding to the MC detector region. Similarly, for backward particles $\eta_{min} \simeq -1.1$, independent of x or p_o.

44. J. E. Elias, et al., Phys. Rev. D22, 13(1980).

45. R. Raja, 100 GeV $\bar{p}p \to X$ data set, private communication.

46. R. T. Edwards, et al., Phys. Rev. D18, 76(1978).

47. J. Singh, et al., Nucl. Phys. B140, 189 (1978).

48. J. F. Gunion, SLAC-PUB-2491(1980); Proceedings of the XVth Recontre de Moriond, Les Arcs, Savoie, France, 1980, p151.

49. K. P. Das and R. C. Hwa, Phys. Lett. 68B, 459(1977); R. C. Hwa and R. G. Roberts, Z. Phys. C1, 81(1979).

50. R. C. Hwa, Phys. Rev. 22, 1593(1980).

51. P. H. Garbincius, et al., AIP Conf. Proc. 68, 74(1981).

52. J. Badier, et al., Phys. Lett. 93B, 354(1980).

53. K. W. Lai and R. L. Thews, Phys. Rev. Lett. 44, 1729(1980).

54. F. Amiri and P. K. Williams, Phys. Rev. D24, 2409(1981).

55. B. Andersson, et al., Phys. Lett. 71B, 337 (1977).

Table 1

M6 Beam Species Ratios for 400 GeV Incident Protons

Beam Momentum	Polarity	π	K	p
100	(+)	.60	.04	.36
100	(-)	.93	.04	.03
175	(+)	.10	.01	.89
175	(-)	.96	.03	.01

Table 2

Hodoscope Properties

Name	z Position	Element Size (mm)	Decode Sense	No. of Elements
BP	1032'	~ 2.5	Horiz.	30
By	1397'	3	Horiz.	8
Bϕ	1398'	3	Vert.	8
Bx	1450'	3	Horiz.	11
By	1450'	3	Vert.	8
Sϕ	1555'	3	Vert.	16

Table 3

Beam Dimensions at the Hydrogen Target

Δp/p	±.5%
Δθ	±.2 mrad
Δϕ	±.2 mrad
Δx	± 5mm
Δy	± 2mm

Table 4

Beam and Spectrometer Cerenkov Counters

Name	Ref.	Effective Length	Cerenkov Mode	Cerenkov Angle (mr)
BGASϕ	(8)	82'	threshold	
BGAS	(11)	59'	threshold	$\leq$10
BDIF	(9)	34'	differential	10
BDISC	(10)	16.4'	differential	24.5 $\pm$.25
SDIF	(9)	34'	differential	10 or 8.5
SGAS1	(11)	103'	threshold	$\leq$8
SGAS2	(11)	46.5'	threshold	$\leq$10
SGAS3	(11)	22.5'	threshold	$\leq$14

Table 5

Spectrometer Wire Chambers

(2mm wire spacing)

Name	z Position	No. of Wires
H11	1639.7	64
H12	1641.1	64
V1	1640.4	32
H21	1733.6	64
H22	1734.3	64
V2	1732.4	32
H3	1845.0	160
V3	1745.7	64
H4	1925.5	160
V4	1926.4	64

Table 6

Spectrometer Aperture and Resolution

	Resolution	Aperture
θ Horizontal Angle	±.09 mrad	±1.3 mrad
ϕ Vertical Angle	±.10 mrad	±0.8 mrad
x Position	±.9 mm	±10 mm
y Position	±.9 mm	±10 mm
(Δp/p) Fractional Momentum	±.12%	±3.25%

Table 7

Multiplicity Detector Characteristics

Counter	z Position*	Type of Light Detected	Element Size
MC1 - 6	67.9"	Cerenkov	2.0" (on a side, equilateral triangle)
MT1 - 6	-5.0"	Scintillation	8.5" x 10."
MT7 - 12	+5.0"	Scintillation	8.5" x 10."
MT13 - 18	+15.0"	Scintillation	8.5" x 10."
MB1 - 6	+5.0"	Scintillation	8.5" x 30."
ITC	68.4"	Scintillation	Hole Trigger Counter

Multiwire Proportional Chambers

Sense Plane	z Position*	Plug Size	Coordinate Measured
PC11	25.1"	1.5" x 1.8"	U_1
PC12	24.5"	1.5" x 1.8"	U_2
PC13	23.9"	1.5" x 1.8"	U_3
PC21	45.8"	1.0" x 1.2"	U_1
PC22	45.2"	1.0" x 1.2"	U_2
PC23	44.6"	1.0" x 1.2"	U_3
PC31	63.6"	3.3" x 3.8"	U_1
PC32	63.0"	3.3" x 3.8"	U_2
PC33	62.4"	3.3" x 3.8"	U_3

*All z positions are given relative to the center of the 20" Hydrogen target.

Table 8

Systematic Uncertainties

Transport and Acceptance	7% Overall
	3% point to point
Transmission and Decay loss	P_{spect} > 50 GeV/c
protons	1%
pions	1%
kaons	2%
Multiple Scattering in Spectrometer at Low Momentum	
≥ 50 GeV	<.5%
30 GeV	3%
20 GeV	4.5%
Particle Misidentification Beam	.1%
Spectrometer ap → aX	.5%
Spectrometer ap → bX	1 - 30%
Spectrometer-Wire Chamber Loss	<.5%
Double Scattering Correction	1.8%
Radiative Corrections	1.3%
Double RF Bunches	.5 - 1%
Electrons in Beam	<.5%
Muons in Beam	<.5%

Table 9

Corrections for Average Inelastic Charged Multiplicity

Uncorrected $\pi^- p \to X$ Average = 7.43 ± .10

Correction Type	Correction	Uncertainty
A) Physics Effects		
Delta Ray Production	-.70	.10
γ Conversions in Target Region	-.29	.03
K_s^0 Decays	-.10	.05
Λ^0 Decays	-.07	.02
Secondary Interactions	-.70	.05
B) Equipment Response Correction		
MC Efficiency* and pulse height errors	.10	.02
Wire Chamber Efficiency and tracking Algorithm Failure	.52	.10
MT and MB Efficiency* and Backward Loss of Solid Angle	.15	.03
C) Other Sources		
Elastic Cross Section Subtraction	.48	.06
Inelastic Two-Prong Loss	-.03	.03
Total Correction	-.64	±.17**

Final Corrected $\pi^- p \to X$ Average = 6.79 ± .11

*Note that these corrections include γ-ray conversions in the counters.

**Total correction uncertainty is the uncertainty in each correction added in quadrature. Note that the final quoted error does not include the .17.

Table 10

Total Cross Sections

Channel	Momentum	This Experiment	Reference 23
$\pi^+ p$	100 GeV	23.4±0.9 mb	23.3±0.1 mb
$\pi^+ p$	175	22.9±1.2	23.6±0.1
$K^+ p$	100	18.4±1.7	18.9±0.1
$K^+ p$	175	18.2±1.8	19.6±0.1
pp	100	38.7±1.3	38.4±0.1
pp	175	39.6±1.1	38.8±0.1
$\pi^- p$	100	23.9±0.7	24.0±0.1
$\pi^- p$	175	23.4±0.8	24.2±0.1
$K^- p$	100	20.8±1.2	20.4±0.1
$K^- p$	175	21.4±1.1	20.7±0.1
$\bar{p}p$	100	40.4±1.2	42.0±0.2
$\bar{p}p$	175	41.2±1.7	41.6±0.5

Table 11

Mean Inelastic Charged Multiplicity

Reaction	Incident Beam Momentum (GeV/c)	This Experiment Mean	This Experiment Dispersion	Other Experiments Mean	Other Experiments Dispersion	Ref
π^+p	100	6.75±.16	3.33±.12	6.62±.07	3.19±.05	24
π^-p	100	6.79±.11	3.15±.08	6.79±.08	3.16±.04	25
π^+p	175	7.55±.21	3.67±.14			
π^-p	175	7.83±.14	3.81±.10			
K^+p	100	6.95±.25	3.33±.18	6.65±.31	3.34±.19	26
K^-p	100	6.76±.18	3.17±.10			
K^+p	175	7.61±.37	3.85±.21			
K^-p	175	7.56±.18	3.63±.11	7.33±.21	3.51±.15	27*
pp	100	6.44±.17	3.24±.13	6.37±.06	3.26±.05	24
$\bar{p}p$	100	6.52±.11	3.13±.09	6.74±.05	3.26±.05	28
pp	175	7.54±.15	3.71±.10			
$\bar{p}p$	175	7.36±.24	3.81±.17			

*Results at 147 GeV/c

Table 12

Inelastic Charged Topology Cross Section Comparisons

Charged Prong	100 π^+p This Exp. (mb)	100 π^+p Ref 24 (mb)	100 pp This Exp. (mb)	100 pp Ref 24 (mb)	100 π^-p This Exp. (mb)	100 π^-p Ref 25 (mb)	100 $\bar{p}p$ This Exp. (mb)	100 $\bar{p}p$ Ref 28 (mb)
2	2.5±.9	2.4±.2	3.7±.9	4.9±.3	1.9±.6	2.0±.3	4.6±.6	3.6±.3
4	4.2±.5	4.7±.2	8.9±.9	7.3±.3	4.8±.4	4.8±.1	8.0±.7	8.1±.2
6	4.4±.6	4.8±.2	7.0±.9	7.0±.3	5.0±.5	5.2±.1	8.3±.9	8.3±.2
8	4.0±.8	3.6±.2	4.3±1.0	5.6±.2	3.9±.6	4.3±.1	4.9±1.1	6.9±.2
10	2.5±.8	2.6±.2	4.4±.8	3.7±.2	2.8±.6	2.5±.1	4.4±1.1	4.1±.1
12	1.6±.5	1.3±.1	1.7±.2	1.7±.1	1.7±.4	1.4±.1	3.0±.7	2.2±.1
14	.5±.1	.5±.1	.7±.2	.8±.1	.5±.1	.6±.04	.8±.4	.9±.1
16	.2±.1	.13±.03	.3±.1	.2±.04	.12±.10	.13±.03	.2±.1	.4±.04
18	.1±.1	.04±.02	.1±.05	.1±.02	.03±.01	.05±.01	.06±.06	.12±.02
20	------	.02±.01	-------	.1±.1	-------	.01±.018	-------	.04±.01
All	20.0±.9	20.2±.2	31.3±1.2	31.4±.2	20.7±.7	21.0±.2	34.2±1.1	35.6 ±.4

Table 13

Inelastic Charged Topology Cross Section

Charged Prong	+100 K^+p (mb)	-100 K^-p (mb)	+175 π^+p (mb)	+175 K^+p (mb)	+175 pp (mb)	-175 π^-p (mb)	-175 K^-p (mb)	-175 $\bar{p}p$ (mb)
2	1.7±.9	2.1±.5	1.9± .8	2.1±1.6	3.7± .8	2.2±.5	1.5±1.0	4.0±2.0
4	3.5±.5	3.8±.5	3.7± .7	2.6± .9	5.4± .8	3.7±.4	3.7± .5	6.8±1.2
6	3.8±.6	4.9±.7	4.2± .9	3.4±1.1	6.5±1.0	3.6±.5	3.4± .7	6.9±1.7
8	3.2±.6	2.9±.7	3.6±1.0	3.6±1.3	5.9±1.0	3.7±.6	3.7± .8	7.0±2.3
10	2.3±.5	2.8±.7	2.5±1.0	2.3±1.2	4.2±1.0	2.9±.4	2.7± .5	3.5±1.5
12	1.1±.5	1.3±.4	2.7± .7	1.5± .7	3.7± .8	1.7±.3	1.5± .3	3.3±1.5
14	.5±.1	.4±.2	1.0± .5	.5± .5	1.5± .2	1.0±.3	.8± .3	1.7± .5
16	.2±.1	.1±.1	.4± .3	-------	.6± .2	.6±.2	.5± .2	.9± .3
18	.1±.1	.05±.05	.1± .1	-------	.3± .1	.4±.1	.2± .1	.5± .3
20	------	-------	-------	-------	.1± .06	.2±.1	.1± .1	.3± .2
22	------	-------	-------	-------	--------	.13±.07	-------	-------
Total Inelastic Cross Section:	16.4±1.6	18.4±1.1	20.2±1.1	17.1±1.7	31.7±1.0	19.9±.7	18.1±1.1	34.9±1.6

Table 14 Complete data set of inclusive cross sections, $E\frac{d^3\sigma}{dp^3}$, in mb/(GeV^2/c^3) at 100 and 175 GeV/c at constant Feynman-x values. The errors shown below each entry include both statistical and estimated systematic errors in quadrature. In addition, there is an overall 7% absolute normalization uncertainty. The notation for reactions is (a,c) ≡ a + p → c + X.

	a. 100 GEV/C X = .200								
PT=	.100	.200	.300	.500	PT=	.100	.200	.300	.500
PI+,PI+	11.37 .68	10.90 .41	9.17 .29	4.92 .43	PI-,PI-	11.25 1.23	8.96 .50	7.58 .29	3.23 .29
PI+,K+	1.22 .38	.98 .23	.66 .17	.49 .36	PI-,K-	1.16 .59	.94 .22	.55 .14	
PI+,P	1.13 .24	.71 .13	.68 .10	.24 .18	PI-,P-	.33 .28	.39 .14	.57 .08	.36 .10
K+,PI+	11.43 2.63	7.04 1.29	5.74 1.06	4.08 2.32	K-,PI-	11.20 5.60	8.65 2.12	5.04 1.06	4.78 1.48
K+,K+	5.24 3.02		2.61 1.55		K-,K-		5.98 2.65	4.47 1.94	
P,PI+	17.88 1.10	12.33 .58	9.37 .39	3.22 .47	P-,PI-	27.80 11.88	9.54 3.58	9.01 1.74	
P,K+	1.11 .44	.73 .26	.76 .24		P-,P-	13.99 10.34			
P,P	3.40 .61	4.06 .35	3.74 .30	2.17 .46					

b. 100 GEV/C X = .300

PT=	.100	.150	.200	.250	.300	.400	.500	.625	.750
PI+,PI+	8.42 .44	8.93 .27	7.71 .24	7.10 .23	6.37 .22	5.17 .18	3.58 .15	2.30 .13	1.18 .11
PI+,K+	.82 .20	.95 .14	.94 .14	.74 .12	.66 .12	.45 .10	.35 .08	.19 .07	.12 .07
PI+,P	.70 .14	.80 .09	.69 .08	.55 .08	.65 .09	.51 .06	.43 .05	.26 .05	.11 .05
K+,PI+	4.20 2.37	4.80 1.17	6.53 1.55	5.43 .71	3.71 .61	2.72 .61	2.88 .57	.84 .46	
K+,K+	5.28 1.71	5.34 1.29	3.56 .80	3.03 .95	2.59 .85	2.59 1.27	1.16 .73	1.29 .81	
P,PI+	12.91 .75	11.69 .41	8.74 .35	6.73 .31	5.50 .27	3.49 .22	2.44 .16	1.69 .15	.80 .13
P,K+	.77 .26	.79 .17	.61 .14	.71 .14	.96 .16	.44 .13	.44 .12	.16 .10	
P,P	7.12 .60	7.37 .36	6.63 .34	6.35 .32	5.62 .29	3.95 .24	2.90 .18	1.77 .16	.82 .14
PI-,PI-	8.38 .27	7.47 .26	7.67 .21	6.85 .15	6.02 .13	4.52 .11	2.98 .13	1.92 .08	.95 .07
PI-,K-	.88 .12	.53 .11	.60 .09	.61 .07	.43 .05	.38 .05	.28 .05	.17 .03	.13 .03
PI-,P-	.61 .07	.47 .07	.45 .05	.48 .04	.42 .04	.35 .03	.22 .04	.14 .03	.07 .03
K-,PI-	4.35 1.92	4.95 1.20	7.59 1.43	3.93 .59	3.99 .51	3.11 .41	2.14 .51	.89 .36	.41 .31
K-,K-	4.28 1.26	4.56 1.21	2.96 .90	4.09 .68	2.92 .61	1.33 .53	.84 .65	1.35 .47	.74 .53
P-,PI-	8.29 1.96	9.59 1.52	9.59 1.38	7.00 .86	5.61 .70	3.47 .61	2.35 .69	1.77 .49	.88 .53
P-,P-	7.84 1.55	4.41 1.43	6.84 1.26	5.51 .87	4.50 .67	3.44 .55	2.78 .73	2.51 .59	1.05 .58
PI+,PI-	5.04 .22	4.61 .16	4.29 .15	3.96 .15	3.52 .14	2.80 .13	1.76 .11	.90 .07	
PI+,K-	.45 .13	.58 .10	.41 .08	.63 .09	.40 .07	.24 .07	.15 .06	.15 .05	
PI+,P-	.40 .06	.34 .05	.30 .04	.27 .05	.26 .04	.21 .04	.16 .04	.06 .03	
K+,PI-	2.69 1.20	3.55 .57	3.08 .52	2.17 .51	2.83 .48	1.99 .53	.96 .50	.61 .40	
P,PI-	4.45 .28	3.90 .20	3.28 .17	3.07 .17	2.71 .16	1.99 .14	1.33 .12	.80 .08	
P,K-	.25 .08	.17 .06	.24 .07	.18 .06	.19 .07	.20 .10			
P,P-	.13 .04	.10 .03	.10 .03	.06 .03	.09 .04				
PI-,PI+	4.37 .31	4.64 .28	3.93 .27	4.10 .23	3.48 .19	2.83 .16	1.77 .12	.77 .06	.38 .04
PI-,K+	.59 .16	.58 .15	.72 .13	.52 .11	.44 .11	.27 .08	.18 .06	.10 .04	.06 .03
PI-,P	.46 .13	.32 .13	.52 .10	.64 .08	.53 .08	.32 .07	.26 .05	.18 .03	.06 .02
K-,PI+		3.99 1.26	8.64 2.24	3.52 1.14	2.01 .81	2.31 .74	1.03 .57	.75 .42	
P-,PI+	6.25 1.63	3.52 1.63	5.13 1.68	3.01 1.45	3.25 1.34	2.39 1.10	2.06 1.02	1.05 .65	.97 .45

c. 100 GEV/C X = .600

PT=	.200	.300	.400	.500	.625	.750	1.000	1.250
PI+,PI+	6.06 .20	4.35 .09	.55 .08	1.58 .04	.95 .03	.55 .02	.18 .01	.06 .01
PI+,K+	.35 .06	.24 .03	.16 .03	.16 .02	.11 .01	.08 .01	.02 .01	
PI+,P	.22 .04	.17 .02	.17 .02	.14 .01	.12 .01	.07 .01	.03 .01	.01 .00
K+,PI+		1.34 .19	.48 .18	.51 .11	.23 .09	.12 .06		
K+,K+	1.67 .65	1.45 .28	1.12 .29	.98 .16	.74 .13	.43 .09		.04 .04
P,PI+	.90 .12	.81 .05	.53 .05	.35 .03	.21 .02	.13 .01	.04 .01	.01 .00
P,K+	.13 .05	.13 .02	.13 .03	.09 .02	.04 .01	.04 .01		
P,P	14.15 .46	10.00 .20	6.67 .18	4.37 .10	2.60 .07	1.50 .05	.37 .02	.14 .01
PI-,PI-	5.79 .14	4.12 .06	2.59 .07	1.52 .05	.91 .03	.53 .02	.18 .01	.05 .00
PI-,K-	.23 .04	.19 .02	.17 .03	.12 .02	.08 .01	.06 .01	.02 .00	.01 .00
PI-,P-	.11 .02	.10 .01	.09 .01	.08 .01	.05 .01	.04 .01	.02 .00	.00 .00
K-,PI-		1.16 .24	.75 .20	.26 .14	.26 .10	.14 .08	.05 .05	
K-,K-	2.72 .55	1.93 .25	1.03 .28	.80 .21	.56 .14	.52 .12	.20 .08	
P-,PI-	.68 .46	1.38 .20	.81 .23	.58 .19		.12 .10		
P-,P-	10.91 1.16	8.05 .52	6.66 .60	3.76 .42	2.69 .31	1.33 .19	.42 .11	

d. 100 GEV/C X = .920

PT=	.300	.400	.500	.625	.750	1.000	1.250
PI+,PI+	6.11 .12	4.33 .11	2.80 .05	1.54 .04	.83 .02	.23 .01	.06 .01
PI+,K+	.23 .02	.13 .02	.07 .01	.04 .01	.02 .00		
K+,K+	3.83 .42	3.35 .40	1.89 .21	1.38 .18	.78 .11	.26 .09	
P,P	15.01 .27	9.19 .23	5.17 .10	2.48 .07	1.15 .04	.25 .02	.03 .01
PI-,PI-	5.77 .09	4.34 .10	2.70 .06	1.44 .04	.76 .03	.20 .01	.05 .00
PI-,K-	.15 .02	.09 .02	.06 .01	.02 .01	.01 .00	.00 .00	
K-,K-	3.73 .35	3.19 .39	2.00 .27	1.18 .17	.38 .10	.20 .05	
P-,P-	13.16 .67	9.88 .59	5.29 .42	2.17 .27	.75 .15	.22 .07	

e. 175 GEV/C X = .300

PT=	.150	.225	.300	.400	.500	.625	.750	.850
PI+,PI+	8.60 .37	7.42 .30	6.22 .29	4.85 .23	3.70 .18	2.10 .12	1.21 .07	.69 .06
PI+,K+	.70 .15	.90 .13	.63 .11	.40 .08	.39 .08	.26 .05	.17 .04	.07 .03
PI+,P	.82 .14	.82 .10	.61 .10	.38 .08	.32 .06	.15 .04	.18 .03	.07 .03
K+,PI+	4.58 1.17	4.10 1.15	3.41 .85	4.14 .78	2.08 .60	1.11 .34	.68 .23	.50 .24
K+,K+	3.70 .80	3.11 .85	4.01 .84	1.87 .77	1.33 .69	1.86 .48	.45 .27	
P,PI+ /	10.39 .21	7.25 .18	5.11 .16	3.91 .17	2.45 .09	1.50 .06	.83 .03	.50 .03
P,K+	.77 .08	.66 .08	.54 .07	.41 .07	.32 .04	.19 .03	.12 .02	.05 .02
P,P	6.81 .17	5.78 .16	5.24 .16	3.97 .17	2.86 .10	1.68 .06	.99 .04	.60 .03
PI-,PI-	7.45 .22	6.75 .21	6.20 .12	4.87 .09	3.45 .07	2.16 .05	1.14 .04	
PI-,K-	.55 .09	.51 .09	.61 .06	.41 .04	.33 .04	.22 .02	.12 .02	
PI-,P-	.41 .06	.43 .06	.42 .03	.34 .03	.29 .02	.17 .01	.12 .01	
K-,PI-	8.84 1.50	5.74 1.37	3.85 .57	2.86 .46	2.21 .40	1.34 .24	.63 .22	
K-,K-	6.28 1.36	3.33 .99	3.00 .62	2.65 .49	1.68 .45	.90 .25	.55 .29	
P-,PI-	12.25 2.37	7.37 2.19	5.12 .95	4.02 .73	3.16 .65	1.72 .44	.69 .51	
P-,P-	5.14 1.95	5.89 1.49	5.17 1.01	3.03 .68	1.46 .70	2.05 .45	.74 .47	
PI+,PI-	4.76 .25	3.61 .22	3.86 .22	2.78 .18	1.85 .15	.78 .08	.43 .05	.24 .06
PI+,K-	.48 .10	.53 .10	.29 .09	.36 .10	.29 .08	.16 .05	.05 .03	
PI+,P-	.46 .08	.52 .08	.25 .07	.31 .07	.18 .08	.08 .03	.08 .03	.08 .06
K+,PI-	3.74 .79	3.59 .63	2.72 .70	1.50 .71	2.05 .79	.87 .48		
P,PI-	3.95 .08	3.08 .10	2.40 .11	1.69 .09	1.28 .08	.81 .04	.41 .03	.27 .03
P,K-	.24 .03	.24 .03	.24 .04	.19 .03	.09 .03	.05 .02	.05 .01	.03 .02
P,P-	.14 .02	.11 .02	.10 .02	.05 .02	.04 .02	.03 .01	.02 .01	
PI-,PI+	4.01 .12		3.21 .10	2.73 .08	1.77 .06	.88 .03	.42 .02	
	**		.54 .06	.42 .04	.35 .03	.15 .02	.10 .01	

f. 175 GEV/C X = .600

PT=	.200	.300	.400	.500	.625	.750	.850	1.000	1.250
PI+,PI+		3.86 .13	2.60 .08	1.53 .07	.82 .04	.55 .02	.27 .02	.13 .01	.01 .00
PI+,K+		.28 .04	.20 .03	.19 .03	.11 .02	.08 .01	.04 .01	.02 .01	
PI+,P		.28 .03	.20 .02	.18 .02	.11 .01	.09 .01	.03 .01	.02 .01	
K+,PI+		1.60 .41	.66 .17	.45 .12	.27 .07	.17 .04	.10 .05	.05 .04	
K+,K+		1.97 .31	1.26 .23	1.14 .18	.70 .11	.30 .06	.27 .06	.11 .05	
P,PI+		.96 .06	.54 .02	.35 .02	.21 .01	.13 .00	.06 .00	.03 .00	
P,K+		.10 .03	.09 .01	.08 .01	.05 .01	.03 .00	.01 .00	.01 .00	
P,P		9.39 .16	6.29 .06	4.26 .07	2.58 .03	1.50 .01	.71 .01	.32 .01	.02 .00
PI-,PI-		3.89 .07	2.49 .05	1.41 .04	.85 .03	.43 .03		.15 .02	.06 .01
PI-,K-		.28 .02	.22 .02	.14 .02	.08 .01	.07 .01		.01 .01	.01 .00
PI-,P-		.11 .01	.09 .01	.08 .01	.05 .01	.03 .01		.02 .01	
K-,PI-		1.45 .31	.77 .14	.45 .13	.37 .10	.25 .13			
K-,K-		1.98 .24	1.27 .18	.95 .17	.27 .17	.48 .17		.18 .11	
P-,PI-		.68 .25	.71 .21	.39 .21					
P-,P-		9.44 .80	6.84 .64	4.05 .54	1.73 .44	1.08 .51		.86 .29	
PI+,PI-	1.47 .08	.83 .05	.54 .05	.41 .04	.26 .03	.12 .01	.06 .01		.01 .00
PI+,K-	.12 .03	.10 .02	.14 .02	.09 .02	.05 .01	.02 .01	.01 .00		
PI+,P-	.08 .02	.04 .01	.03 .01	.02 .01	.02 .01	.02 .01	.01 .00		
K+,PI-	1.19 .23	.46 .13	.34 .08	.12 .09	.08 .05	.13 .06	.03 .02		.02 .01
P,PI-	.31 .02	.26 .01	.17 .01	.12 .01	.08 .01	.04 .01	.02 .00		
P,K-	.02 .00	.01 .00	.01 .00	.01 .00					

g. 175 GEV/C X = .920

PT=	.500	.625	.750	1.000	1.250
PI-,PI-	2.59 .04	1.40 .03	.73 .02	.20 .01	.06 .00
PI-,K-	.06 .01	.03 .01	.02 .00		
K-,K-	1.88 .16	1.03 .14	.34 .08	.14 .04	.08 .04
P-,P-	5.02 .37	2.27 .30	1.05 .18	.17 .07	

h. 175 GEV/C X = .940

PT=	.500	.625	.750	1.000	1.250
PI+,PI+	3.70 .04	2.34 .08	1.27 .03	.35 .01	.10 .01
PI+,K+	.09 .01	.05 .02	.02 .01		
K+,K+	2.97 .19	2.49 .32	1.26 .14	.33 .06	.09 .03
P,P	7.46 .08	3.67 .08	1.67 .03	.30 .01	.06 .00

Table 15 Complete data set of inclusive cross sections, $E\frac{d^3\sigma}{dp^3}$, in mb/(GeV^2/c^3) at 100 and 175 GeV/c at constant p_T values. The errors shown below each entry include both statistical and estimated systematic errors in quadrature. In addition, there is an overall 7% absolute normalization uncertainty. The notation for reactions is (a,c) ≡ a + p → c + X.

a. 100 GEV/C PT = .200

X =	.300	.400	.500	.600	.700	.800	.840
PI+,PI-	4.29 .15	2.62 .22	1.98 .15	1.54 .11	1.47 .13	1.28 .07	1.15 .07
PI+,K-	.41 .08	.32 .10	.17 .06	.15 .04		.05 .02	.04 .01
PI+,P--	.30 .04	.11 .06	.10 .03	.06 .02	.03 .02	.01 .00	
K+,PI-	3.08 .52	3.88 .88	2.11 .55	1.29 .38	.70 .25		
P,PI-	3.28 .17	2.43 .23	1.21 .13	.33 .06	.12 .04		
P,K-	.24 .07	.21 .09	.07 .06				
P,P-	.10 .03						

b. 100 GEV/C PT = .300

X =	.200	.300	.400	.500	.600	.700	.800	.840	.880	.920	.940	.960
PI+,PI+	9.17 .29	6.37 .22	5.15 .19	4.50 .18	4.34 .09	4.29 .09	4.35 .07	4.78 .10	4.94 .11	6.11 .12		13.14 .24
PI+,K+	.66 .17	.66 .12	.49 .08	.38 .07	.24 .03	.22 .03	.19 .02	.19 .02	.19 .02	.23 .02		.15 .03
PI+,P	.68 .10	.65 .08	.45 .06	.33 .05	.17 .02	.11 .02	.04 .01	.05 .01	.03 .01			
K+,PI+	5.74 1.06	3.71 .61	2.91 .62	2.44 .52	1.34 .19	.62 .19	.27 .13					
K+,K+	2.61 1.55	2.59 .85	2.21 .69	2.05 .62	1.45 .28	1.74 .27	2.52 .23	2.87 .30	2.98 .36	3.83 .42		7.83 .97
P,PI+	9.37 .39	5.50 .27	2.34 .19	1.78 .17	.81 .05	.37 .03	.06 .01	.06 .02	.02 .02			
P,K+	.76 .24	.96 .16	.38 .09	.16 .07	.13 .02	.05 .02	.02 .01					
P,P	3.74 .30	5.62 .29	6.41 .33	8.51 .39	10.00 .20	10.72 .21	11.75 .17	12.54 .24	13.61 .28	15.01 .27		29.34 .47
PI-,PI-	7.50 .29	6.02 .13	4.64 .13	4.18 .07	4.12 .06	4.26 .05	4.25 .08		4.86 .08	5.77 .09		
PI-,K-	.55 .14	.43 .05	.35 .05	.26 .03	.19 .02	.20 .02	.15 .02		.12 .02	.15 .02		
PI-,P-	.57 .08	.42 .04	.30 .03	.17 .02	.10 .01	.05 .01	.02 .01					
K-,PI-	5.04 1.06	3.99 .51	3.06 .45	1.70 .27	1.16 .24	.89 .13	.81 .17					
K-,K-	4.47 1.94	2.92 .61	2.08 .55	2.34 .29	1.93 .25	1.97 .18	2.20 .29		2.99 .28	3.73 .35		
P-,PI-	9.01 1.74	5.61 .70	4.35 .65	2.00 .29	1.38 .20	.48 .11						
P-,P-		4.50 .67	5.45 .86	7.75 .53	8.05 .52	9.83 .40	10.79 .73		10.71 .54	13.16 .67		
PI+,PI-		3.52 .14	2.02 .07	1.11 .04	.97 .04	.83 .03	.65 .03	.52 .03	.46 .02		.20 .02	
PI+,K-		.40 .07	.33 .04	.16 .02	.10 .01	.07 .01	.03 .01	.01 .01	.01 .00			
PI+,P-		.26 .04	.16 .02	.09 .01	.04 .01	.03 .00	.01 .00					
K+,PI-		2.83 .48	1.11 .21	.66 .16	.57 .11	.25 .08	.16 .06					
P,PI-		2.71 .16	1.31 .07	.48 .04	.25 .02	.08 .01	.02 .01					
P,K-		.19 .07	.10 .03	.03 .01	.02 .01							
P,P-		.09 .04	.03 .01									
PI-,PI+	5.35 .31	3.48 .19	1.82 .10	1.27 .04	1.05 .03	.83 .02	.70 .03		.52 .02			
PI-,K+	.65 .16	.44 .11	.32 .05	.20 .02	.13 .01	.08 .01	.05 .01		.02 .01			
PI-,P	.68 .12	.53 .08	.29 .04	.16 .02	.09 .01	.04 .01	.02 .00					
K-,PI+	2.82 1.27	2.01 .81	1.20 .42	1.26 .20	.58 .09	.35 .06	.17 .06					
P-,PI+	8.71 2.47	3.25 1.34	.98 .41	1.02 .19	.40 .09	.18 .05						

c. 100 GEV/C PT = .400

X =	.200	.300	.500	.600	.700	.880	.920
PI-,PI-		4.52 .11	2.62 .14	2.59 .07			4.34 .10
PI-,K-		.38 .05	.18 .04	.17 .03			.09 .02
PI-,P-		.35 .03	.16 .04	.09 .01			
K-,PI-		3.11 .41	1.04 .48	.75 .20			
K-,K-		1.33 .53	1.23 .70	1.03 .28			3.19 .39
P-,PI-		3.47 .61	.78 .64	.81 .23			
P-,P-		3.44 .55	6.03 1.14	6.66 .60			9.88 .59
PI+,PI-	5.69 .26	2.80 .13	.84 .05		.43 .02	.19 .02	
PI+,K-	.71 .18	.24 .07	.15 .02		.04 .01	.01 .00	
PI+,P-	.29 .10	.21 .04	.06 .01		.01 .00		
K+,PI-	3.70 .92	1.99 .53	.49 .18		.21 .05		
P,PI-	4.65 .32	1.99 .14	.42 .04		.05 .01		
P,K-	.42 .22	.20 .10	.04 .03				
P,P-	.11 .10						
PI-,PI+		2.83 .16			.43 .02	.19 .02	
PI-,K+		.27 .08			.07 .01	.02 .01	
PI-,P		.32 .07			.07 .01		
K-,PI+		2.31 .74			.10 .06		
P-,PI+		2.39 1.10					

d. 100 GEV/C PT = .500

X =	.200	.300	.400	.500	.600	.700	.800	.840	.880	.920	.940	.960
PI+,PI+	4.92 .43	3.58 .15	2.66 .10	1.91 .06	1.58 .04	1.44 .04	1.60 .03	1.85 .04	2.08 .04	2.80 .05		6.04 .09
PI+,K+	.49 .36	.35 .08	.30 .05	.20 .03	.16 .02	.14 .02	.07 .01	.10 .01	.08 .01	.07 .01		.07 .01
PI+,P	.24 .18	.43 .05	.33 .03	.19 .02	.14 .01	.07 .01	.05 .01	.03 .01	.02 .01			
K+,PI+	4.08 2.32	2.88 .57	.92 .29	.76 .17	.51 .11	.20 .11	.21 .06					
K+,K+		1.16 .73	1.79 .49	1.13 .23	.98 .16	1.03 .15	.85 .10	1.24 .14	1.61 .18	1.89 .21		4.70 .43
P,PI+	3.22 .47	2.44 .16	1.27 .09	.65 .04	.35 .03	.14 .02	.04 .01	.01 .01	.01 .01			
P,K+		.44 .12	.22 .06	.09 .03	.09 .02	.04 .01	.03 .01					
P,P	2.17 .46	2.90 .18	3.90 .17	3.79 .12	4.37 .10	4.14 .10	4.13 .06	4.34 .08	4.49 .10	5.17 .10		10.38 .17
PI-,PI-	3.23 .29	2.90 .13	2.27 .06	1.66 .06	1.52 .05		1.66 .04		2.04 .05	2.70 .06		
PI-,K-		.28 .05	.20 .02	.15 .02	.12 .02		.08 .01		.06 .02	.06 .01		
PI-,P-	.36 .10	.22 .04	.20 .02	.13 .02	.09 .01		.02 .00					
K-,PI-	4.78 1.48	2.14 .51	1.17 .24	.83 .19	.26 .14		.23 .11					
K-,K-		.84 .65	1.77 .34	.97 .25	.80 .21		1.34 .19		1.50 .32	2.00 .27		
P-,PI-		2.35 .69	1.59 .32	.41 .22	.58 .19							
P-,P-		2.78 .73	3.17 .42	3.48 .49	3.76 .42		3.36 .33		3.54 .39	5.29 .42		
PI+,PI-	2.97 .58	1.76 .11	1.41 .18	.68 .04	.35 .05	.24 .02	.14 .02	.10 .02	.08 .01		.03 .00	
PI+,K-		.15 .06		.10 .02		.04 .01	.01 .01					
PI+,P-		.16 .04	.26 .12	.05 .01		.01 .01	.01 .01					
K+,PI-	6.90 4.13	.96 .50		.32 .12		.09 .08	.19 .13					
P,PI-	2.95 .83	1.33 .12	.57 .21	.23 .03	.12 .05	.03 .01	.01 .01					
PI-,PI+	1.60 .15	1.77 .12	1.03 .06	.66 .04	.36 .02	.22 .02	.18 .01		.10 .01			
PI-,K+	.30 .09	.18 .06	.18 .03	.12 .02	.08 .01	.06 .01	.02 .01					
PI-,P	.20 .08	.26 .05	.14 .03	.09 .02	.06 .01	.03 .01	.01 .00					
K-,PI+	1.68 .74	1.03 .57	1.09 .29	.34 .15	.29 .08	.13 .06						
P-,PI+	3.02 1.10	2.06 1.02	.80 .48		.18 .11							

e. 100 GEV/C PT = .625

X =	.300	.500	.700
PI+,PI-	.90 .07	.38 .03	.12 .02
PI+,K-	.15 .05	.07 .02	.01 .01
PI+,P-	.06 .03	.04 .01	.01 .01
K+,PI-	.61 .40	.17 .12	
P,PI-	.80 .09	.14 .03	.03 .01
PI-,PI+	.77 .06	.42 .04	.16 .01
PI-,K+	.10 .04	.07 .02	.02 .01
PI-,P	.18 .03	.05 .02	.02 .01
K-,PI+	.75 .42		
P-,PI+	1.05 .65		

g. 100 GEV/C PT = 1.000

X =	.600	.800	.840	.880	.920	.960
PI+,PI+	.18 .01	.11 .01	.14 .01	.16 .01	.23 .01	.46 .01
PI+,K+	.02 .01	.01 .00	.01 .00	.00 .00		
PI+,P	.03 .01	.01 .00	.00 .00	.00 .00		
K+,K+		.12 .03	.20 .09	.16 .06	.26 .09	.47 .05
P,PI+	.04 .01	.00 .00				
P,P	.37 .02	.23 .01	.23 .01	.21 .01	.25 .02	.33 .01

f. 100 GEV/C PT = .750

X =	.300	.400	.500	.600	.700	.800	.840	.880	.920	.960
PI+,PI+	1.18 .11	.96 .05	.73 .03	.55 .02	.45 .02	.48 .02	.54 .02	.61 .02	.83 .02	1.90 .03
PI+,K+	.12 .07	.11 .03	.06 .02	.08 .01	.04 .01	.04 .01	.03 .01	.02 .01	.02 .00	.01 .00
PI+,P	.11 .05	.13 .02	.08 .01	.07 .01	.05 .01	.02 .00	.02 .00	.01 .00		
K+,PI+		.40 .21	.19 .12	.12 .06	.09 .06					
K+,K+		.40 .30	.37 .17	.43 .09	.43 .10	.52 .07	.37 .07	.63 .12	.78 .11	1.65 .16
P,PI+	.80 .13	.48 .04	.29 .03	.13 .01	.05 .01	.02 .00	.01 .01			
P,K+		.06 .04	.04 .02	.04 .01	.02 .01					
P,P	.82 .14	1.29 .07	1.47 .07	1.50 .05	1.35 .06	1.01 .03	1.06 .03	1.00 .03	1.15 .04	2.02 .05
PI-,PI-	.95 .07	.88 .03	.63 .02	.53 .02	.44 .02	.47 .01			.76 .03	
PI-,K-	.13 .03	.08 .01	.05 .01	.06 .01	.05 .01	.03 .01			.01 .00	
PI-,P-	.07 .03	.06 .01	.05 .01	.04 .01	.02 .00	.01 .00				
K-,PI-	.41 .31	.39 .12	.21 .08	.14 .08	.12 .06					
K-,K-	.74 .53	.46 .16	.41 .10	.52 .12	.26 .09	.35 .08			.38 .10	
P-,PI-	.88 .53	.61 .19	.45 .12	.12 .10	.13 .13					
P-,P-	1.05 .58	1.07 .22	1.28 .20	1.33 .19	1.46 .18	.68 .13			.75 .15	

h. 175 GEV/C PT = .150

X =	.120	.200	.300
PI+,PI+	15.08 1.85	11.77 .85	8.60 .37
PI+,K+	2.10 1.05	1.02 .33	.70 .15
PI+,P	1.81 .54	1.12 .29	.82 .14
K+,PI+	16.19 5.35	4.89 3.56	4.58 1.17
K+,K+	10.87 9.69	3.49 2.28	3.70 .80
P,PI+	22.69 1.32	17.02 .81	10.39 .21
P,K+	1.22 .53	1.45 .36	.77 .08
P,P	2.97 .51	4.34 .42	6.81 .17
PI-,PI-	16.14 1.35	11.50 .55	7.45 .22
PI-,K-	1.02 .53	.99 .21	.55 .09
PI-,P-	.81 .33	.60 .14	.41 .06
K-,PI-		6.52 3.69	8.84 1.50
K-,K-		3.18 2.03	6.28 1.36
P-,PI-	64.96 23.04	32.35 7.69	12.25 2.37
P-,P-		6.68 3.88	5.14 1.95

i. 175 GEV/C PT = .200

X =	.400	.500	.600	.700
PI+,PI-	2.55 .17	1.83 .13	1.47 .08	1.37 .07
PI+,K-	.29 .07		.12 .03	.10 .02
PI+,P-	.15 .05	.11 .03	.08 .02	.02 .01
K+,PI-	1.28 .66	1.13 .45	1.19 .23	.58 .16
P,PI-	1.76 .08	.91 .05	.31 .02	.09 .01
P,K-	.10 .02		.02 .00	
P,P-		.01 .01		

j. 175 GEV/C PT = .300

X =	.120	.200	.300	.400	.500	.600
PI+,PI+	13.00 1.15	9.68 .47	6.22 .29	4.96 .16	4.54 .16	3.86 .13
PI+,K+	1.05 .82	.98 .24	.63 .11	.49 .06	.27 .05	.28 .04
PI+,P	.74 .44	.85 .17	.61 .10	.42 .05	.34 .04	.28 .03
K+,PI+	8.31 4.23	4.42 1.29	3.41 .85	2.33 .38	2.25 .44	1.60 .41
K+,K+		3.38 1.76	4.01 .84	2.44 .38	1.81 .36	1.97 .31
P,PI+	13.33 .75	9.94 .35	5.11 .16	2.91 .06	1.65 .05	.96 .06
P,K+	1.24 .50	1.33 .21	.54 .07	.39 .03	.23 .03	.10 .03
P,P	2.15 .32	3.19 .21	5.24 .16	6.66 .09	7.77 .10	9.39 .18
PI-,PI-	11.80 .69	9.63 .27	6.20 .12	4.69 .10	4.09 .09	3.89 .07
PI-,K-	.55 .21	.72 .10	.61 .06	.43 .04	.29 .03	.28 .02
PI-,P-	.65 .20	.48 .07	.42 .03	.33 .03	.17 .02	.11 .01
K-,PI-	11.35 3.51	7.61 1.26	3.85 .57	3.30 .48	1.25 .39	1.45 .31
K-,K-		3.27 1.22	3.00 .62	2.62 .46	1.50 .32	1.98 .24
P-,PI-		10.85 2.56	5.12 .95	2.19 .69	1.78 .37	.68 .25
P-,P-			5.17 1.01	6.04 .99	6.21 .76	9.44 .80
PI+,PI-	9.80 .76	7.02 .43	3.86 .22	1.87 .11	1.17 .08	.83 .05
PI+,K-	1.06 .57	.66 .23	.29 .09	.17 .05	.13 .03	.10 .02
PI+,P-	.59 .22	.39 .13	.25 .07	.17 .04	.10 .02	.04 .01
K+,PI-	7.63 2.48	2.83 1.27	2.72 .70	1.52 .27	.74 .19	.46 .13
P,PI-	10.79 .55	5.29 .24	2.40 .11	1.22 .03	.63 .02	.26 .01
P,K-	1.28 .36	.48 .11	.24 .04	.09 .01	.04 .01	.01 .00
P,P-	.36 .10	.19 .06	.10 .02	.02 .01	.00 .00	
PI-,PI+	8.25 .59	6.44 .25	3.21 .10	1.93 .07	1.09 .06	.91 .03
PI-,K+	.73 .25	.78 .13	.54 .06	.36 .04	.18 .03	.10 .01
PI-,P	.57 .22	.57 .09	.37 .04	.24 .02	.15 .02	.07 .01
K-,PI+	11.24 3.46	4.54 1.20	2.62 .60	1.00 .33	.61 .22	.43 .15
P-,PI+		5.45 2.62	3.17 .95	1.54 .48	.47 .35	.47 .15

k. 175 GEV/C PT = .400

X =	.300	.500	.600	X =	.300	.500	.600
PI+,PI-	2.78 .18	.89 .06	.54 .05	P,PI-	1.69 .09	.42 .01	.17 .01
PI+,K-	.36 .10	.14 .03	.14 .02	P,K-	.19 .03	.03 .00	.01 .00
PI+,P-	.31 .07	.08 .02	.03 .01	P,P-	.05 .02	.00 .00	
K+,PI-	1.50 .71	.70 .15	.34 .08				

l. 175 GEV/C PT = .500

X =	.200	.300	.400	.500	.600	.700	.800	.880	.895	.920	.940
PI+,PI+	5.44 .37	3.70 .18	2.50 .11	1.81 .07	1.53 .07	1.41 .04	1.54 .05		2.10 .03		3.70 .04
PI+,K+	.38 .22	.39 .08	.30 .04	.18 .03	.19 .03	.14 .01	.10 .02		.08 .01		.09 .01
PI+,P	.30 .14	.32 .06	.34 .04	.25 .03	.18 .02	.11 .01	.08 .01				
K+,PI+	2.74 1.41	2.08 .60	1.23 .22	.63 .16	.45 .12	.23 .08	.28 .08				
K+,K+		1.33 .69	1.39 .26	1.18 .21	1.14 .18	.92 .12	.91 .17		1.49 .11		2.97 .19
P,PI+	4.44 .22	2.45 .09	1.40 .04	.72 .02	.35 .02	.14 .01	.03 .01				
P,K+	.72 .14	.32 .04	.26 .02	.15 .02	.08 .01	.03 .01	.01 .00				
P,P	1.58 .15	2.86 .10	3.79 .06	4.21 .05	4.26 .07	4.16 .04	3.93 .05		4.55 .05		7.46 .08
PI-,PI-	5.10 .29	3.45 .07	2.59 .07	1.60 .06	1.41 .04	1.42 .02	1.48 .02	1.99 .03		2.59 .04	
PI-,K-	.43 .13	.33 .04	.18 .02	.13 .02	.14 .02	.11 .01	.08 .01	.07 .01		.06 .01	
PI-,P-	.22 .08	.29 .02	.22 .02	.12 .02	.08 .01	.06 .00	.01 .00				
K-,PI-	3.90 1.72	2.21 .40	1.71 .36	.67 .22	.45 .13	.38 .06	.18 .06				
K-,K-	.	1.68 .45	2.09 .38	1.26 .32	.95 .17	.97 .08	1.02 .09	1.15 .14		1.83 .16	
P-,PI-	5.20 3.89	3.16 .65	1.14 .48	.72 .37	.39 .21	.12 .07	.09 .05				
P-,P-		1.46 .70	3.56 .71	4.03 .87	4.05 .54	3.51 .23	3.72 .22	4.41 .34		5.02 .37	
PI+,PI-	2.70 .21	1.85 .15	1.12 .10	.57 .07	.41 .04	.24 .02					
PI+,K-	.39 .12	.29 .08	.18 .04	.12 .03	.09 .02	.04 .01					
PI+,P-	.28 .08	.18 .08	.14 .04	.06 .02	.02 .01	.01 .01					
K+,PI-	2.07 .67	2.05 .79	.85 .22	.42 .16	.12 .09	.10 .04					
P,PI-	2.72 .12	1.28 .08	.67 .02	.29 .02	.12 .01	.03 .01					
P,K-	.21 .05	.09 .03	.04 .01	.02 .01	.01 .00						
P,P-	.13 .03	.04 .02	.01 .00	.01 .00							

m. 175 GEV/C PT = .625

X =	.300	.400	.500	.600	.700
PI+,PI-	.78 .08	.58 .07	.37 .05	.26 .03	.13 .02
PI+,K-	.16 .05	.11 .04	.07 .03	.05 .01	.03 .01
PI+,P-	.08 .03	.07 .05	.05 .02	.02 .01	.01 .01
K+,PI-	.87 .48	.45 .30	.25 .14	.08 .05	.14 .09
P,PI-	.81 .04	.43 .03	.19 .01	.08 .01	.02 .01
P,K-	.05 .02	.05 .01	.01 .00	.00 .00	
P,P-	.03 .01		.01 .00		

o. 175 GEV/C PT = 1.000

X =	.600	.895	.940
PI+,PI+	.13 .01	.16 .01	.35 .01
PI+,K+	.02 .01	.01 .00	.00 .00
PI+,P	.02 .01		
K+,PI+	.05 .04		
K+,K+	.11 .05	.19 .07	.33 .06
P,PI+	.03 .00		
P,K+	.01 .00		
P,P	.32 .01	.21 .00	.30 .01

n. 175 GEV/C PT = .750

X =	.300	.400	.500	.600	.700	.800	.895	.920	.940
PI+,PI+	1.21 .07	.93 .06	.73 .04	.55 .02	.46 .02	.43 .02	.58 .02		1.27 .03
PI+,K+	.17 .04	.08 .03	.11 .02	.08 .01	.05 .01	.03 .01	.63 .00		.02 .01
PI+,P	.18 .03	.15 .03	.08 .01	.09 .01	.05 .01	.02 .00			
K+,PI+	.68 .23	.59 .17	.32 .09	.17 .04	.09 .04	.05 .03			
K+,K+	.45 .27	.61 .20	.47 .10	.30 .06	.31 .07	.27 .05	.60 .06		1.26 .14
P,PI+	.03 .03	.52 .02	.29 .01	.13 .00	.04 .00	.01 .00			
P,K+	.12 .02	.08 .01	.05 .01	.03 .00	.01 .00	.01 .00			
P,P	.99 .04	1.36 .03	1.59 .02	1.50 .01	1.29 .02	1.00 .02	1.01 .01		1.67 .03
PI-,PI-	1.14 .04	.98 .04	.66 .03	.43 .03	.42 .02	.40 .01		.73 .02	
PI-,K-	.12 .02	.10 .02	.06 .01	.07 .01	.03 .01	.02 .00		.02 .00	
PI-,P-	.12 .01	.10 .01	.05 .01	.03 .01	.02 .00	.01 .00			
K-,PI-	.63 .22		.13 .12	.25 .13	.08 .05	.05 .05			
K-,K-	.55 .29	.54 .23	.43 .18	.48 .17	.25 .09	.46 .08		.34 .08	
P-,PI-	.68 .51	.57 .43	.72 .30						
P-,P-	.74 .47	1.36 .47	1.86 .40	1.08 .51	1.19 .26	.90 .18		1.05 .18	

Table 16A

100 GeV/c Coefficients For $C(1-x)^n$ Fits

The differential cross section at several values of p_t and the integrated cross section are fit to the functional form $C(1-x)^n$. The coefficient C is a function of p_t, while the exponent n is constrained to be independent of p_t. The full x range at which data were taken is used for all reactions except those indicated by an asterisk. In those cases, values of x only up to .5 are used. Units for $C(p_t)$ are $mb/(GeV^2/c^3)$, while units for C_{int} are mb.

	n	C(.3)	C(.5)	C(.625)	C(.75)	C_{int}
$\pi^+ \to K^+$	1.55±.40*	1.07±.10	.62±.06		.20±.03	1.49±.06
$\pi^+ \to p_-$	1.73±.06	.94±.05	.71±.03		.33±.02	1.69±.04
$\pi^+ \to \pi^-$	3.37±.09*	11.47±.25	6.45±.25			12.80±.14
$\pi^+ \to \bar{K}^-$	2.10±.12	.78±.05	.40±.06			1.12±.04
$\pi^+ \to \bar{p}_+$	2.98±.18	.74±.05	.44±.07			
$K^+ \to \pi^-$	2.16±.19	9.03±.69	3.82±,41		.97±.28	9.73±.44
$K^+ \to \pi_+$	2.29±.25*	4.17±.39	1.74±.47			4.91±.26
$p \to \pi^+$	3.39±.05	18.09±.44	7.52±.23		2.91±.14	23.18±.28
$p \to K^+$	2.56±.20	1.41±.14	.82±.09		.32±.06	2.56±.14
$p \to \pi^-$	4.39±.10	12.17±.40	5.98±.40	3.59±.33		18.57±.32
$p_- \to K_+$	4.59±.92	.92±.16				
$\pi^- \to \pi^+$	2.65±.11*	8.08±.19	3.90±.13	2.18±.14		8.87±.13
$\pi^- \to K^+$	1.76±.10	.72±.04	.41±.03	.21±.04		1.08±.04
$\pi^- \to p_-$	2.43±.11	.89±.04	.52±.04	.36±.05		
$\pi^- \to \bar{K}^-$	1.84±.30*	.88±.06	.53±.04		.19±.02	1.26±.04
$\pi^- \to \bar{p}_+$	2.29±.08	.86±.03	.62±.03		.25±.02	1.34±.03
$K^- \to \pi^-$	2.31±.25	5.27±.45	2.39±.37			6.19±.41
$\bar{K}^- \to \pi_+$	2.58±.37*	10.19±.78	4.97±.59		1.32±.30	11.27±.50
$\bar{p} \to \pi^-$	3.56±.43	10.72±1.22	5.84±1.43			18.0±1.8
$p \to \pi^-$	3.00±.19	17.7 ±1.1	6.3 ±.9		2.95±.50	21.81±.93

Table 16B

175 GeV/c Coefficients For $C(1-x)^n$ Fits

	n	C(.3)	C(.5)	C(.625)	C(.75)	C_{int}
$\pi^+ \to K^+$	2.11±.38*	1.37±.11	.83±.07		.37±.05	2.01±.08
$\pi^+ \to p_-$	1.36±.09	.92±.06	.62±.03		.26±.02	1.33±.04
$\pi^+ \to \pi^-$	3.56±.12*	13.48±.38	6.44±.28	3.17±.22		13.88±.22
$\pi^+ \to K^-$	2.07±.20	.61±.07	.53±.05	.32±.05		1.04±.05
$\pi^+ \to \bar{p}_+$	3.28±.25	.87±.10	.57±.09	.33±.08		
$K^+ \to \pi^-$	2.37±.25	8.77±.85	4.02±.43		1.65±.22	11.06±.53
$K^+ \to \pi_+$	2.84±.31*	6.34±.69	3.23±.50	1.64±.49		8.21±.46
$p \to \pi^+$	3.50±.03	18.49±.25	8.54±.14		3.15±.05	24.7 ±.2
$p \to K^-$	2.77±.10	1.59±.09	1.00±.05		.33±.02	2.38±.06
$p \to \pi^-$	4.36±.05	12.50±.18	6.36±.14	3.96±.13		16.77±.14
$p \to \bar{K}^-$	5.48±.24	1.60±.10	.67±.08	.43±.07		2.21±.09
$p_- \to \bar{p}_+$	8.03±.44	1.19±.14	.71±.12	.58±.21		1.70±.12
$\pi^- \to \pi^+$	3.75±.13*	13.25±.24				
$\pi^- \to K^+$	2.85±.22	1.44±.08				
$\pi^- \to p_-$	2.87±.22	1.04±.05				
$\pi^- \to \bar{K}^-$	2.06±.25*	1.20±.06	.58±.04		.26±.03	1.52±.04
$\pi^- \to p_+$	2.21±.07	.88±.04	.64±.02		.27±.02	1.37±.03
$K^- \to \pi^-$	4.33±.77	12.3 ±1.5				
$\bar{K}^- \to \pi_+$	3.32±.45*	14.7 ±1.2	7.7 ±.9		1.85±.62	16.96±.86
$\bar{p} \to \pi^+$	3.72±.87	10.9 ±1.8				
$p \to \pi^-$	3.59±.37	18.9 ±2.0	9.8 ±1.5		3.7 ±1.4	28.8 ±1.9

Table 17A Cross sections, $x\frac{d\sigma}{dx}$, in millibarns integrated over p_T at 100 GeV/c. The errors shown below each entry include both statistical and estimated systematic errors in quadrature. In addition, there is an overall 7% absolute normalization uncertainty. The notation for reactions is (a,c) ≡ a + p → c + X.

X =	.200	.300	.400	.500	.600	.700	.800	.840	.880	.920	.940	.960
PI+,PI+	10.91 .24	7.91 .10	6.56 .11-	5.71 .12	4.89 .05	4.64 .08	4.79 .05	5.39 .07	5.92 .08	7.87 .08		16.97 .15
PI+,K+	.89 .13	.79 .05	.80 .06	.58 .06	.42 .02	.33 .03	.23 .01	.26 .02	.22 .02	.23 .02		.17 .02
PI+,P	1.11 .12	.99 .05	.74 .05	.46 .03	.34 .01	.19 .01	.11 .01	.08 .01	.04 .01			
K+,PI+	6.38 .72	4.40 .33	2.87 .35	2.48 .38	1.37 .15	.69 .17	.45 .11					
K+,K+	3.44 1.45	3.49 .41	3.65 .53	3.29 .52	2.61 .22	2.82 .27	3.00 .19	3.14 .25	4.29 .32	5.73 .30		11.73 .62
P,PI+	10.83 .30	7.32 .13	3.42 .16	2.06 .10	.98 .03	.44 .03	.11 .01	.06 .02	.03 .02			
P,K+	1.37 .28	1.20 .11	.68 .12	.29 .07	.26 .02	.12 .02	.05 .02					
P,P	4.09 .22	6.56 .13	8.20 .23	11.15 .26	12.23 .13	12.47 .18	12.86 .13	13.87 .17	14.66 .20	17.18 .18		32.93 .32
PI-,PI-	8.46 .25	7.00 .07	5.82 .07	5.09 .07	4.72 .05	4.94 .05	4.87 .06		5.73 .08	7.26 .07		
PI-,K-	.84 .14	.63 .03	.50 .03	.38 .03	.31 .02	.30 .02	.22 .02		.17 .02	.12 .01		
PI-,P-	.73 .09	.60 .02	.43 .03	.27 .02	.17 .01	.08 .01	.03 .01					
K-,PI-	6.35 .89	4.19 .27	3.26 .26	2.08 .25	1.26 .18	1.05 .15	.88 .17					
K-,K-	5.65 1.76	3.46 .34	3.47 .36	3.18 .32	2.63 .22	2.44 .23	3.10 .28		3.83 .33	5.02 .29		
P-,PI-	11.60 1.88	7.39 .43	5.17 .59	2.37 .31	1.49 .18	.65 .14						
P-,P-		6.16 .42	6.84 .62	10.77 .59	10.73 .42	11.69 .46	10.85 .58		11.52 .53	15.49 .51		
PI+,PI-	8.11 .36	3.77 .06	2.14 .05	1.37 .03	1.02 .03	.85 .02	.69 .02	.57 .02	.40 .02		.14 .01	
PI+,K-		.43 .03	.43 .04	.29 .02	.19 .02	.10 .01	.05 .01	.03 .01	.02 .00			
K+,PI-	5.44 1.29	2.45 .20	1.31 .14	.86 .13	.62 .10	.34 .06	.18 .07					
P,PI-	11.53 .78	4.06 .09	1.97 .09	.72 .03	.29 .02	.09 .01	.02 .01					
P,K-		1.54 .22	.29 .07	.06 .02								
P,P-		.06 .01										
PI-,PI+	4.52 .23	3.52 .08	2.16 .06	1.50 .04	1.15 .03	.86 .02	.70 .02		.47 .02			
PI-,K+	.66 .12	.46 .04	.45 .04	.35 .03	.24 .02	.15 .01	.07 .01		.03 .01			
K-,PI+	3.29 1.04	3.09 .44	1.78 .28	1.38 .21	.72 .10	.35 .06						
P-,PI+	11.24 2.57	5.27 .72	1.88 .65		.74 .16							

Table 17B Cross sections, $x\frac{d\sigma}{dx}$, in millibarns integrated over p_T at 175 GeV/c. The errors shown below each entry include both statistical and estimated systematic errors in quadrature. In addition, there is an overall 7% absolute normalization uncertainty. The notation for reactions is (a,c) ≡ a + p → c + X.

X =	.120	.200	.300	.400	.500	.600	.700	.800	.895	.920	.940
PI+,PI+	15.21 1.09	11.58 .40	7.79 .14	6.01 .10	5.56 .13	4.47 .08	4.53 .11	4.66 .12	6.21 .08		11.64 .11
PI+,K+	1.72 .74	1.09 .20	.82 .06	.76 .05	.57 .06	.47 .03	.40 .03	.25 .03	.27 .02		.25 .02
PI+,P	1.09 .44	1.07 .16	.80 .05	.67 .05	.51 .04	.39 .02	.26 .02	.15 .02			
K+,PI+	13.26 3.76	5.52 1.32	4.66 .45	3.08 .24	2.29 .32	1.40 .16	.65 .20	.57 .16			
K+,K+		4.04 1.68	3.96 .44	3.60 .29	3.10 .36	2.75 .20	2.57 .29	2.35 .30	4.53 .27		9.18 .45
P,PI+	17.48 .71	12.87 .32	7.00 .08	3.90 .06	2.18 .04	1.04 .02	.39 .02	.11 .01			
P,K+	1.77 .54	2.04 .23	.80 .04	.62 .03	.37 .02	.18 .01	.08 .01	.05 .01			
P,P	2.77 .31	3.86 .18	6.35 .08	8.32 .08	11.29 .09	12.81 .07	15.18 .12	14.58 .15	17.64 .12		29.35 .23
PI-,PI-	15.00 .72	11.64 .26	7.53 .07	6.30 .07	5.04 .09	4.51 .05	4.21 .05	4.45 .05		8.39 .08	
PI-,K-	.82 .26	1.00 .11	.71 .03	.54 .03	.40 .03	.40 .02	.32 .02	.21 .02		.14 .01	
PI-,P-	1.02 .25	.70 .08	.61 .02	.51 .03	.27 .02	.17 .01	.13 .01	.03 .00			
K-,PI-		7.89 1.19	4.75 .34	3.96 .34	1.62 .36	1.57 .17	1.06 .17	.51 .15			
K-,K-		3.49 1.13	3.78 .36	4.30 .38	2.67 .41	2.60 .21	2.75 .23	3.18 .25		5.77 .39	
P-,PI-		13.98 2.32	7.58 .65	3.48 .83	3.78 .67	3.02 .65					
P-,P-			5.46 .57	7.73 .92	10.72 1.03	12.07 .66	10.66 .67	12.27 .68		19.90 1.18	
PI+,PI-		6.58 .32	3.66 .09	2.17 .06	1.49 .05	1.06 .03	.86 .04				
PI+,K-		.86 .20	.52 .05	.31 .03	.25 .03	.16 .02	.11 .01				
K+,PI-		3.96 1.05	3.43 .38	1.74 .18	1.06 .15	.64 .08	.38 .08				
P,PI-		8.11 .26	3.41 .05	1.76 .03	.84 .02	.32 .01	.08 .01				
P,K-		.92 .16	.32 .02	.13 .01	.05 .00	.01 .00					
P,P-		.25 .05	.11 .01	.02 .00	.83 .15						
PI-,PI+			3.56 .05								
PI-,K+			.63 .03								
K-,PI+			2.93 .25								
P-,PI+			4.54 .60								

Table 18

Triple Regge Fits to ap→aX

$$\frac{Ed^3\sigma}{dp^3} = \left\{ \begin{array}{l} (C_2 e^{C_3 t} + C_4 e^{C_5 t})\ (1-x)^{-1-2\alpha'_P t} \\ + \\ (C_6 e^{C_7 t} + C_8 e^{C_9 t})\ (1-x)^{-2t} \\ + \\ \text{(Field \& Fox } \pi\pi P \text{ and } \pi\pi R\text{) for pp→px only} \end{array} \right\} = \left\{ \begin{array}{l} PPP \\ + \\ RRP \\ + \\ (\pi\pi P + \pi\pi R) \end{array} \right\}$$

Parameter	Unit	π^+	K^+	p	π^-	K^-	$\bar{p}$
α'_P	GeV^{-2}	0.01± .03	-0-	0.14± .03	0.40± .04	-0-	-0-
C_2	mb/GeV^2	0.36± .04	0.32± .02	1.00± .04	0.32± .08	0.42± .05	1.11± .14
C_3	GeV^{-2}	4.52± .67	2.57± .11	4.53 ± .40	2.26±1.10	4.47± .38	4.77± .34
C_4	mb/GeV^2	0.10± .05	-	0.10 ± .05	0.11± .09	-	-
C_5	GeV^{-2}	1.73± .40	-	1.29 ± .35	-0.03± .57	-	-
C_6	mb/GeV^2	4.93± .67	1.41± .41	7.46 ±6.38	5.37± .52	0.84± .28	2.87±1.05
C_7	GeV^{-2}	7.16±1.94	1.50±1.01	12.44 ±6.75	3.65± .44	1.95± .60	-0.61± .76
C_8	mb/GeV^2	1.62± .35	-	2.83 ± .26	-	-	-
C_9	GeV^{-2}	-0.54± .26	-	-1.02 ± .10	-	-	-

Table 19 - Integrated Cross Sections

$d\sigma/dM^2$ (10^{-2} mb/GeV^2)

(t integrated from -.1 to -1.0 GeV/c^2)

Reaction	Term	x = .8	.84	.88	.92	.96
p → p	PPP	1.191±.08	1.485±.11	1.970±.16	2.920±.25	5.618±.50
	RRP	1.804±.18	1.524±.10	1.246±.05	.961±.02	.652±.004
$\pi^+ \to \pi^+$	PPP	.721±.05	.901±.07	1.199±.09	1.796±.13	3.580±.26
	RRP	.984±.05	.853±.03	.718±.02	.574±.006	.409±.001
$K^+ \to K^+$	PPP	.717±.03	.896±.04	1.195±.05	1.792±.07	
	RRP	.312±.06	.273±.06	.232±.05	.188±.04	
$\bar{p} \to \bar{p}$	PPP	1.188±.08	1.486±.11	1.981±.14	2.971±.21	
	RRP	1.284±.22	1.085±.18	.886±.15	.682±.12	
$\pi^- \to \pi^-$	PPP	.962±.06	1.120±.07	1.367±.08	1.818±.11	2.944±.18
	RRP	.658±.04	.591±.04	.517±.03	.433±.03	.325±.02
$K^- \to K^-$	PPP	.491±.04	.614±.05	.819±.06	1.228±.10	
	RRP	.666±.27	.544±.20	.427±.11	.312±.05	

Table 20

Ratio of inelastic cross section for a+p → a+x at x = 0.92 and elastic cross section (Reference 1) for a+p → a+p for a common beam momentum of 100 GeV/c and t = -0.098 GeV^2.

a	$\frac{d^2\sigma/dM_x^2\, dt\|_{inelastic}}{d\sigma/dt\|_{elastic}}$
p	0.57 ± 0.02
$\bar{p}$	0.46 ± 0.03
K^+	0.45 ± 0.05
K^-	0.42 ± 0.04
π^+	0.52 ± 0.02
π^-	0.49 ± 0.02
Weighted Average	0.51 ± 0.01

Table 21 Average associated multiplicity as a function of Feynman X and p_T for all reaction channels. The errors shown below each entry are statistical only. There is an overall systematic error estimated to be ±0.17 not included in the listed errors. The notation for reactions is (ac) ≡ a + p → c + X.

a. 100 GeV/c $a^- + p \rightarrow c^- + X$

X	P_T	$\pi\pi$	πK	πp	$K\pi$	KK	Kp	$p\pi$	pp
.920	.300	3.21 .05	3.11 .41			3.05 .23			3.40 .27
.920	.400	3.22 .06	3.22 .29		2.81 .46	3.44 .20			3.39 .13
.920	.500	3.23 .08	3.38 .34			3.87 .26			3.67 .20
.920	.625	3.22 .05	2.25 .74			3.76 .28			3.38 .24
920	.750	3.23 .10	3.19 .53			3.66 .42	3.72 .36		3.24 .30
.920	1.000	3.24 .12				3.31 .36			4.04 .43
.920	1.250	2.96 .20							
.880	.300	3.67 .08	3.20 .44		3.41 .50	4.50 .24			3.93 .19
.800	.500	4.52 .10		3.78 .42			5.10 .55		5.21 .33
800	.750	4.56 .10		4.15 .33			4.35 .63		4.89 .62
.700	.300	4.33 .05	4.55 .28	3.33 .36	3.83 .41	4.57 .30		5.40 1.21	4.38 .15
.700	.500	4.76 .10	4.62 .52	4.00 .28	3.87 .54	5.21 .68			4.90 .20
.700	.750	5.10 .13	5.34 .50	4.49 .42	4.66 .88	4.70 .57			5.08 .28
.600	.200	4.47 .09	5.31 .34	4.98 .49		5.97 83		4.82 .59	4.38 .26
.600	.300	4.67 .07	5.28 .22	4.57 .23	4.89 .42	4.07 .28		4.55 .59	5.08 .20
.600	.400	4.70 .08	5.20 .31	4.96 .39	3.84 .58	4.70 .52		4.39 .9[illegible]	5.59 .31
.600	.500	5.09 .14	5.25 .41	5.20 .42	4.52 1.17	5.21 .66		3.39 1.04	5.44 .36
.600	.625	5.28 .14	5.81 .47	3.94 .50	4.81 .74	4.76 .71			4.41 .31
.600	.750	5.21 .15	5.10 .42	4.79 .37	6.38 1.66	4.83 .47			5.77 .42
.600	1.000	5.48 .22	6.32 .75	5.94 .71		5.80 .84			5.45 .58
.600	1.200	5.38 .23	6.03 1.52						

X	P_T	$\pi\pi$	πK	πp	$K\pi$	KK	Kp	$p\pi$	pp
.500	.300	4.92 .07	4.98 .18	5.44 .27	3.60 .28	5.85 .45		4.08 .77	5.69 .24
.500	.400	5.17 .20	4.92 .85	4.67 .69					4.92 .51
.500	.500	5.46 .14	5.25 .48	4.69 .28	4.84 .91	6.90 .94		3.55 2.34	5.47 .13
.500	.750	5.48 .18	5.68 .45	5.67 .38	4.93 .72	7.35 .86		4.38 .58	6.46 .39
.400	.300	5.20 .08	5.39 .28	5.52 .26	4.56 .50	6.11 .73	6.34 .82	6.20 .53	5.94 .33
.400	.500	5.76 .11	6.31 .40	5.46 .26	5.67 .59	7.04 .69		4.43 .53	6.91 .51
.400	.750	5.94 .15	6.91 .55	5.87 .89	8.18 2.27			3.75 1.58	5.48 .59
.300	.100	5.46 .22	6.84 .83	6.37 .56	5.73 2.35	4.16 1.00		5.19 .84	6.44 .93
.300	.150	5.46 .11	6.16 .58	5.27 .30	4.36 .44	4.69 .83		4.69 .33	6.85 .89
.300	.200	5.57 .10	6.37 .43	5.96 .32	4.32 .44	7.62 1.42		5.20 .32	5.97 .51
.300	.250	5.74 .14	6.14 .35	5.32 .23	4.47 .67	5.71 .51		5.75 .45	6.68 .52
.300	.300	5.61 .10	6.34 .34	6.66 .41	5.22 .46	7.06 .86		5.71 .62	6.36 .59
.300	.400	5.82 .10	5.74 .44	6.23 .35	6.52 .51	5.70 .62		6.12 .82	7.10 .66
.300	.500	5.79 .19	5.48 .81	6.82 .50	5.86 .70			5.66 1.21	6.50 .69
.300	.625	6.23 .17	5.41 1.12	6.66 .78	5.75 1.23	7.00 .93		6.71 1.13	8.19 1.24
.300	.750	6.28 .24	5.95 .57	6.88 1.69					
.200	.100	6.77 .91							
.200	.200	6.28 .22	8.83 1.50	6.75 1.17	4.31 1.98				
.200	.300	6.36 .15	8.72 1.00	7.05 .55	7.66 .94			5.99 .99	
.200	.500	7.32 .39							

b. 100 GeV/c $a^- + p \rightarrow c^+ + X$

X	P_T	$\pi\pi$	πK	πp	$K\pi$	$p\pi$
.880	.300	3.05 .06	3.55 .35	3.24 .40		
.880	.400	2.96 .17		3.68 .39		
.880	.500	2.64 .22				
.800	.300	3.92 .10	3.98 .32	4.67 .32	1.96 .29	
.800	.500	3.71 .13	4.00 .39	4.45 .59		
.700	.300	4.21 .10	4.46 .17	5.01 .25	3.89 .38	4.15 .52
.700	.400	4.22 .13	4.60 .52	4.93 .29		
.700	.500	4.07 .18	4.83 .43	5.54 .61		
.700	.625	4.22 .22	5.06 .56	5.21 .84		
.600	.300	4.72 .09	4.99 .20	5.52 .21	4.38 .40	5.21 .55
.600	.500	4.62 .14	4.98 .38	5.55 .42	4.09 .55	
.500	.300	5.29 .11	5.58 .35	6.33 .32	4.53 .30	5.67 .70
.500	.500	5.40 .21	6.18 .51	4.78 .93	3.97 .65	
.500	.625	4.87 .28				
.400	.300	5.51 .11	5.09 .24	6.39 .29	4.93 .54	6.81 1.20
.400	.500	5.10 .16	5.97 .55	5.21 .87	4.81 .51	
.300	.100	5.28 .24	8.06 1.51	7.86 1.31		
.300	.150	6.01 .25	5.96 1.23	6.54 1.34	5.05 1.93	4.71 .92
.300	.200	6.11 .26	5.56 .65	7.87 .92	3.89 1.67	
.300	.250	6.22 .20	7.10 1.18	6.88 .49	4.71 2.49	
.300	.300	5.92 .17	6.72 .67	7.58 .55		6.47 1.13
.300	.400	5.92 .17	7.28 .83	6.63 .77	6.39 1.08	
.300	.500	6.19 .21	6.79 1.16	7.21 .64		
.300	.625	6.32 .23	6.58 1.68	7.70 .68		
.300	.750	9.08 .47				
.200	.300	6.60 .19	7.04 .90	7.15 .86	4.33 2.56	
.200	.500	6.66		5.84		

c. 100 GeV/c $a^+ + p \rightarrow c^- + X$

X	P_T	$\pi\pi$	πK	πp	$K\pi$	$p\pi$	pK	pp
.880	.300	3.82 .09	3.97 .75					
.880	.400	3.38 .14						
.880	.500	4.20 .26						
.840	.300	3.93 .10	4.40 .58		3.89 .48			
.800	.300	3.88 .13	4.70 .81		2.23 .43			
.700	.300	4.51 .12	4.56 .53	4.76 .48	3.91 .56	4.65 .55		
.700	.400	4.44 .12	4.64 .34		3.98 .40	4.55 .40		
.700	.500	4.66 .25	4.63 .38					
.700	.625	4.45 .24				4.41 .47		
.600	.300	5.01 .11	4.90 .39	5.29 .37	5.05 .51	4.59 .20		
.600	.500	5.05 .47						
.500	.300	5.36 .11	4.65 .27	5.23 .35	4.51 .34	5.46 .22	6.36 .86	
.500	.400	5.30 .19	6.20 .52	6.07 .78	4.86 1.50	4.71 .24		
.500	.500	5.31 .16	6.18 .49	4.40 .33		4.82 .33		
.500	.625	4.91 .23	4.92 .59	4.06 .36		4.92 .71		
.400	.300	5.68 .13	5.55 .34	6.12 .42	4.58 .50	5.64 .19	4.79 .46	
.400	.500	5.59 .46						
.300	.100	6.35 .28	6.27 1.18	6.25 .73	8.75 3.62	5.64 .32	6.12 .62	
.300	.150	6.06 .15	7.82 .91	6.92 .43	5.21 .56	6.26 .67		
.300	.200	6.45 .14	6.09 .42	5.53 .32	6.57 .76	5.67 .17	6.77 1.34	6.87 1.14
.300	.250	6.06 .15	5.96 .41	6.24 .47	6.01 .72	5.90 .21		
.300	.300	6.23 .15	7.21 .43	6.44 .45	5.55 .52	6.01 .21		
.300	.400	6.15 .17	8.29 1.11	7.44 .64	6.09 .62	5.71 .15		
.300	.625	6.69 .28	5.60 .68	6.71 .72		6.32 .37		
.200	.400	7.00 .20	6.94 .55	6.92 .66	8.62 1.74	6.81 .34	8.37 1.12	

d. 100 GeV/c $a^+ + p \rightarrow c^+ + X$

X	P_T	$\pi\pi$	πK	πp	$K\pi$	KK	$p\pi$	pK	pp
.960	.300	2.24 .08	2.61 .24			2.12 .21	2.18 .31		2.27 .06
.960	.500	2.18 .09	2.15 .46			2.52 .29			2.21 .11
.960	.750	2.15 .06				2.20 .17			2.20 .06
.960	1.000	2.10 .08				2.19 .32			2.21 .16
.920	.300	3.23 .07	3.24 .33			3.08 .48		3.58 .42	3.17 .05
.920	.400	3.23 .11	3.45 .44			3.01 .34			3.18 .07
.920	.500	3.18 .06	3.72 .33			3.34 .29			3.24 .05
.920	.625	3.23 .07	3.85 .69			3.48 .30			3.22 .07
.920	.750	3.11 .10	3.61 .80			2.53 .30			3.25 .10
.920	1.000	3.35 .15				2.82 .35			3.18 .21
.920	1.250	3.20 .27				0.00 0.00			2.80 .33
.880	.300	3.43 .10	3.03 .30			3.91 .32			3.52 .09
.880	.500	3.54 .11	3.24 .30			3.83 .32			3.54 .12
.880	.750	3.47 .10	2.79 .30			2.52 .54			3.51 .11
.880	1.000	3.82 .22				3.37 .47			3.76 .22
.840	.300	3.89 .11	4.01 .34		4.48 .64	3.74 .49	3.12 .76	3.24 .87	3.93 .15
.840	.500	4.30 .08	4.06 .37	5.29 .62		4.38 .43	3.07 53	4.47 1.02	4.11 .07
.840	.750	4.43 .16	3.67 .30	4.42 .56		4.58 .39			4.41 .10
.840	1.000	4.72 .19	5.19 .75			4.51 .82			4.32 .19
.800	.300	4.14 .11	4.52 .37	4.63 1.15	0.00 0.00	5.02 .48			4.38 .09
.800	.500	4.49 .07	4.74 .21	4.80 .32	3.67 .45	4.46 .25	3.91 .40	4.28 .80	4.47 .06
.800	.750	4.52 .08	5.42 .25	4.33 .35	4.43 .58	5.39 .27	3.26 .47		4.55 .10
.800	1.000	4.72 .13	4.68 .41	4.30 .53		5.73 .49			4.63 .11
.700	.300	4.38 .10	4.32 .34	5.02 .74	4.71 1.12	4.22 1.10	3.58 .32		4.64 .09
.700	.500	4.60 .08	4.87 .21	5.04 .35	4.56 1.21	4.14 .37	4.00 .30	4.47 .41	4.75 .07
.700	.750	4.79 .20	4.86 .40	5.20 .56	0.00 0.00	0.00 0.00	4.37 .53		4.74 .10

X	P_T	$\pi\pi$	πK	πp	$K\pi$	KK	$p\pi$	pK	pp
.600	.200	4.59 .10	5.26 .38	5.94 .51		5.53 .90	3.27 .27	6.46 1.06	4.86 .12
.600	.300	4.69 .14	4.94 .21	5.04 .22	3.50 .30	5.36 .77	3.66 .15	4.87 1.14	5.15 .10
.600	.400	4.97 .10	4.90 .28	5.05 .41	5.87 1.00	6.09 .88	3.67 .22	5.72 .64	5.17 .09
.600	.500	5.09 .11	4.65 .23	4.75 .21	5.50 .64	4.71 .64	4.27 .19	4.88 .51	5.42 .09
.600	.625	5.34 .12	5.43 .44	5.11 .27	5.12 .86	5.70 .60	3.67 .25	5.94 .50	5.48 .10
.600	.750	5.22 .18	5.36 .36	4.63 .29	4.91 .71	6.28 .67	4.49 .30	5.19 .52	5.33 .11
.600	1.000	5.26 .15	5.44 .71	5.53 .75			4.25 .59		5.29 .19
.600	1.200	5.42 .28	0.00 0.00	6.44 1.20			5.06 .54		6.11 .23
.500	.300	4.98 .14	6.12 .53	6.11 .40	4.14 .52	5.15 1.09	4.07 .32		5.88 .15
.500	.500	5.45 .15	5.70 .38	5.89 .37	6.34 .68	5.31 .59	4.66 .24	6.62 1.01	6.00 .11
.500	.750	5.59 .16	5.38 .50	6.45 .55		5.56 .85	5.55 .54		5.97 .15
.400	.300	5.29 .16	5.28 .60	5.49 .57	4.23 .48	6.19 1.30	4.60 .25	5.43 .67	6.29 .17
.400	.500	5.62 .13	6.14 .52	6.20 .34	5.40 .74	5.95 .82	5.18 .29	5.02 .66	6.20 .16
.400	.750	6.09 .16	5.61 .64	6.62 .52			4.58 .24		6.35 .17
.300	.100	5.74 .30	5.27 1.13	5.96 .99	4.89 1.40		4.79 .25		8.16 .68
.300	.150	5.91 .19	5.68 .72	7.06 .52	6.22 1.28	6.25 97	4.93 .19	3.85 .72	7.02 .20
.300	.200	5.59 .18	5.69 .46	6.58 .45	7.68 3.23	4.26 .51	5.04 .19	6.78 .93	6.71 .19
.300	.250	5.81 .13	7.26 .72	6.60 .68	4.59 .42		5.13 .18	7.12 1.03	7.23 .22
.300	.300	5.99 .14	6.95 .62	6.63 .45	6.68 1.09	5.27 1.04	5.69 .19	7.61 .71	7.47 .20
.300	.400	5.94 .20	6.66 .86	7.39 .54	5.99 .86		5.57 .22	7.89 1.07	7.33 .30
.300	.500	6.23 .18	6.59 .63	7.27 .41	6.16 .91		5.84 .29	7.40 .89	7.11 .22
.300	.625	6.03 .20		5.77 .64			5.34 .25		6.86 .29
.300	.750	6.36 .33					5.41 .46		6.84 .61
.200	.100	6.16 .30		9.73 3.20	7.44 2.67		5.24 .31		8.88 1.43
.200	.200	6.66 .20	6.38 .66	8.62 .83	5.62 .84		5.83 .17		7.03 .32
.200	.300	6.19 .16	6.48 .55	6.37 .77	6.78 .70		6.16 .18	6.65 .99	7.67 .24
.200	.500	9.64 .42					8.07 .70		10.58 .74

e. 175 GeV/c $a^- + p \rightarrow c^- + X$

X	P_T	$\pi\pi$	πK	πp	$K\pi$	KK	Kp	$p\pi$	pp
.920	.500	3.86 .12				3.74 .31			3.86 .30
.920	.625	3.87 .11				3.85 .38			4.41 .32
.800	.500	4.88 .10	4.78 .18	4.12 .46	4.64 .55	4.98 .34			4.91 .32
.800	.750	4.60 .09	4.48 .29	3.27 .67	0.00 0.00	5.15 .40			0.00 0.00
.700	.500	5.50 .10	5.26 .26	3.55 .65	4.52 .59	5.28 .36			5.35 .48
.600	.300	5.26 .12	5.54 .22	4.99 .43	5.35 1.19	5.26 .42			5.85 .52
.600	.400	5.26 .11	5.93 .31	5.84 .39	6.85 .80	5.56 .44			6.71 .34
.300	.150	6.10 .14	6.97 .56	6.63 .46	4.72 .72	7.33 1.08		5.49 .56	7.89 .92
.300	.225	6.28 .14	6.19 .57	6.66 .45	6.61 .91	7.88 1.25		4.68 1.06	6.79 1.00
.300	.300	6.44 .10	6.05 .22	6.89 .33	5.82 .53	6.91 .75		7.50 .85	9.07 .52
.300	.400	6.41 .12	7.22 .32	6.94 .26	6.26 .47	7.75 1.03		5.23 .67	8.64 .84
.300	.500	6.70 .11	6.87 .32	7.23 .24	6.98 .66	6.54 .98		7.32 .89	6.24 2.42
.300	.625	7.11 .11	7.22 .41	6.69 .23	7.06 .82	6.22 1.19	7.87 1.13	6.18 .63	7.63 .81
.300	.750	7.45 .15	7.55 .81	8.40 .52	8.27 .94				
.200	.150	6.87 .21	6.66 .84	7.35 1.15	4.10 1.11			6.93 .92	
.200	.300	6.99 .20	7.79 .41	9.00 .48	6.60 .89	7.16 1.01		6.85 1.09	
.200	.500	7.13 .15	5.22 1.10	9.01 1.36					

f. 175 GeV/c $a^- + p \rightarrow c^+ + X$

X	P_T	$\pi\pi$	πK	πp	$K\pi$	$p\pi$
.300	.150	6.59 .16	6.35 .62	8.35 .69	6.77 .99	7.98 1.24
.300	.225	6.62 .17	6.59 .43	8.03 .63	7.23 1.50	
.300	.400	6.48 .11	6.95 .37	8.35 .36	6.14 .59	6.24 .98
.300	.500	6.71 .12	6.81 .44	7.53 .32	6.67 .65	
.300	.625	7.28 .15	6.35 .49	7.54 .35	6.49 .81	5.52 .62
.300	.750	7.63 .20	7.58 .46	8.44 .49	7.94 .91	7.62 1.30
.200	.300	7.75	9.50	8.92	7.67	

g. 175 GeV/c $a^+ + p \rightarrow c^- + X$

X	P_T	$\pi\pi$	πK	πp	$K\pi$	$p\pi$	Kp	pp
.700	.500	4.89 .20	4.51 .42	4.62 .95		5.14 .37		
.600	.300	5.21 .17	5.24 .52	5.36 .79	4.91 .72	5.07 .14	4.13 .38	
.600	.400	5.37 .25	6.30 .55	5.88 .92	5.09 .68	5.24 .13	4.50 .49	
.600	.400	5.00 .20	6.02 .54		5.35 .67	5.24 .16	4.07 .62	
.600	.500	5.06 .27	5.42 .65			5.51 .20		
.600	.625	5.75 .41				5.77 .31		
.500	.300	5.85 .15	6.01 .48		5.38 .74	5.69 .12	5.51 .29	
.500	.400	6.01 .22	6.55 .52		5.16 .45	6.02 .12	6.05 .40	
.500	.500	5.19 .25	7.26 1.02		5.74 .93	5.64 .16	6.29 .58	
.500	.625	6.04 .42				6.21 .25		
.400	.300	6.38 .19	6.67 .47	6.40 .50	6.86 .83	6.57 .10	6.27 .26	6.54 .81
.400	.500	6.40 .28	7.39 .69	4.71 1.20	5.66 .58	6.69 .14	8.05 .58	
.300	.150	6.67 .22	7.73 1.08		6.71 .70	6.38 .12	7.00 .42	
.300	.225	6.52 .15	6.96 .78		7.50 .65	6.64 .13	6.94 .41	
.300	.300	6.60 .15	6.28 1.13		6.62 .96	6.87 .15	5.50 .95	
.300	.400	6.15 .19	7.13 .71		6.11 1.66	6.90 .19	7.56 .50	
.300	.500	6.69 .37	5.14 .83			6.36 .18	6.91 .95	
.300	.625	6.64 .39				7.82 .29	5.35 .92	
.300	.750	8.52 .50				8.37 .40		
.300	.850	8.71 .49				9.63 .58		
.200	.300	7.51 .27	7.72 .85	8.65 1.36	10.73 2.43	7.83 .20	4.41 1.99	8.17 1.26
200	.500	7.83 .32	10.80 1.23	8.72 .83	6.24 .74	7.85 .23	8.43 .94	6.32 .64
120	.300	8.03 .35	9.18 1.52		8.94 .91	8.73 .30	9.75 1.38	7.23 1.92

h. 175 GeV/c $a^+ + p \rightarrow c^+ + X$

X	P_T	$\pi\pi$	πK	πp	$K\pi$	KK	Kp	$p\pi$	Kp	pp
.940	.500	3.53 .05	3.32 .38	3.70 .31	3.43 .48	3.70 .18	3.49 .48		4.48 .79	3.61 .09
.940	.625	3.42 .06	3.63 .34	2.99 .28		3.79 .24			3.38 .34	3.58 .04
.940	.750	3.46 .06	3.38 .57	3.60 .37		3.48 .19			3.30 .32	3.57 .07
.940	1.000	3.53 .10				3.71 .24				3.65 .09
.940	1.250	3.48 .20				5.07 .67				3.90 .17
.895	.500	4.44 .06	4.98 .30	5.33 .41	3.86 .52	4.66 .16			5.51 .88	4.63 .07
.895	.750	4.49 .05	4.59 .28	4.92 .62	5.39 .76	4.28 .20		1.70 .70	4.30 .46	4.66 .04
.895	1.000	4.68 .11	4.51 .43			5.08 .31				4.74 .08
.800	.500	5.36 .06	5.78 .36	5.39 .31	4.49 .52	5.81 .28		4.74 .24	6.09 .61	5.41 .07
.800	.750	5.23 .13	5.20 .31	5.12 .40	5.18 .55	5.06 .31		4.04 .55	4.25 .40	5.28 .07
.700	.500	5.61 .16	5.25 .50	6.23 .54	5.71 .63	6.50 .63		4.55 .18	6.46 .57	5.80 .09
.700	.750	5.91 .14	6.34 .58	5.99 .71	5.39 .78	5.75 .45		4.96 .24	4.96 .95	5.94 .08
.600	.300	5.21 .13	5.65 .34	6.21 .41	5.14 1.02	4.83 .36	4.87 1.19	4.54 .27	6.27 .60	5.76 .11
.600	.400	5.46 .12	6.03 .43	5.56 .34	6.24 .74	6.48 .52		4.84 .14	5.91 .25	5.96 .07
.600	.500	5.67 .13	5.61 .39	6.19 .49	5.88 .79	5.75 .38		5.00 .21	5.79 .33	6.12 .07
.600	.625	5.88 .14	6.70 .51	6.54 .47	6.85 .68	5.47 .50	7.62 .89	5.23 .14	6.03 .28	6.17 .06
.600	.750	5.98 .19	5.53 .62	5.83 .33	6.91 .68	5.20 .57		5.28 .14	6.30 .24	6.26 .05
.600	.900	6.38 .28	5.84 .59	4.94 1.16	6.15 .88	7.20 .82		5.16 .16	5.96 .59	6.50 .06
.600	1.050	6.75 .40	6.40 .86	5.54 .80				5.67 .23	6.76 .89	6.81 .11
.600	1.200	6.50 .49						5.48 .48	6.85 .60	6.84 .12

X	P_T	$\pi\pi$	πK	πp	$K\pi$	KK	Kp	$p\pi$	Kp	pp
.500	.300	5.46 .16	6.29 .44	7.26 .41	5.55 .71	5.25 .54	4.63 .83	5.12 .20	6.20 .18	6.53 .09
.500	.500	6.20 .14	6.49 .46	5.89 .40	6.08 .77	5.73 .47		5.78 .17	6.26 .28	6.76 .09
.500	.750	6.64 .25	5.99 .47	6.15 .52	8.77 1.89	6.61 .73		5.62 .16	6.92 .25	6.96 .08
.400	.300	6.14 .12	7.01 .45	7.35 .40	6.12 .60	5.43 .37	9.63 1.93	6.06 .21	6.63 .21	7.30 .10
.400	.500	6.43 .17	7.71 .64	8.04 .43	6.87 .69	6.90 .64		6.23 .12	6.86 .25	7.44 .09
.400	.750	7.04 .34						5.90 .20	7.59 .70	7.73 .13
.300	.150	6.34 .21	6.04 .82	7.72 .57	6.55 1.25	6.30 .87		5.56 .14	7.03 .38	7.46 .14
.300	.225	6.27 .21	7.69 .60	6.94 .45	6.14 1.12	5.44 .76		5.68 .13	6.69 .29	7.84 .11
.300	.300	6.21 .18	6.94 .55	7.32 .63	5.66 .61	7.12 1.20		6.14 .19	6.67 .39	7.69 .13
.300	.400	6.46 .23	6.49 .63	7.19 .91	6.27 .62			6.59 .21	7.76 .81	8.09 .19
.300	.500	6.88 .19	8.41 .87	6.43 .61	6.78 1.02			6.75 .17	6.54 .65	8.06 .15
.300	.625	6.42 .22	7.17 .64	7.88 1.41	7.54 .78	5.12 .67		6.82 .18	7.13 .55	8.43 .16
.300	.750	6.59 .21	11.28 1.37	11.19 1.01	10.71 1.27			6.78 .20	7.97 .83	10.48 .21
.300	.850	6.97 .42		7.25 .84				7.05 .26	8.31 2.13	8.46 .26
.200	.150	6.65 .28	8.17 .88	11.94 3.04	7.47 1.87			6.79 .23	8.18 1.07	8.33 .46
.200	.300	7.09 .18	8.81 .82	7.81 .66	5.68 .68			7.14 .17	8.21 .55	8.46 .32
.200	.500	7.73 .33	7.40 1.27	7.75 .89				7.07 .19	7.66 .76	9.82 .44
.120	.150	7.24 .60						6.94 .32	0.00 0.00	9.36 1.25
.120	.300	8.06 .51						7.23 .25	8.03 1.19	7.95 .58

Table A1

	>100 GeV/c	≤100 GeV/c
SGAS1	π	π
SGAS2	π	π + K
SGAS3	π	π
SDIFR	p	p
SDIFA	π + K	π + K

Figure Captions

Figure 1: The three stages of the Fermilab Meson Laboratory M6 beam line.

Figure 2: The angle the spectrometer subtended relative to the incident beam direction was adjusted using an angle varying bend (AVB) magnetic system bending in the vertical plane of the incident beam. The three magnets of the AVB are shown here in relation to the target and the spectrometer.

Figure 3: Plan view of the target turntable assembly. The turntable contained 10 and 20 inch long targets each of hydrogen, deuterium and empty target cells.

Figure 4: The Single Arm Spectrometer instrumentation. The quadrupole polarities are indicated for the non-bend, vertical plane.

Figure 5: The arrangement of the apparatus in the target region showing the target hodoscope and the downstream vertex detector.

Figure 6: The acceptance of the spectrometer for the two analyses performed on the data.

Figure 7: The spectrometer transmission for π, K and protons as a function of spectrometer momentum. These curves include the effects of nuclear and multiple scattering as well as decays.

Figure 8: KNO scaling data for negative beam, total cross section trigger. The curve is the KNO fit (Reference 30) for pp → X reactions.

Figure 9: The invariant differential cross section is shown as a function of x, for an incident energy of 100 GeV and a transverse momentum P_T of 0.3 GeV/c. There is one subfigure for each incident particle type. Only those data are plotted for which the error was smaller than the value of the cross section. Comparisons to a functional form $C(1-x)^n$ are shown.

Figure 10: The invariant differential cross section is shown as a function of x, for an incident energy of 100 GeV and a transverse momentum p_T of 0.75 GeV/c. There is one subfigure for each incident particle type. Comparisons to a functional form $C(1-x)^n$ are shown.

Figure 11: The invariant differential cross section is shown as a function of x, for an incident energy of 175 GeV and a transverse momentum p_T of 0.3 GeV/c. There is one subfigure for each incident particle type. Comparisons to a functional form $C(1-x)^n$ are shown.

Figure 12: The invariant differential cross section for π^+ induced reactions is shown as a function of transverse momentum p_T. The incident energy is 100 GeV. The values of x for which the transverse momentum dependence is shown are those at which the most thorough p_T sweeps were made.

Figure 13: The invariant differential cross section for π^- induced reactions is shown as a function of transverse momentum p_T. The incident energy is 100 GeV.

Figure 14: The invariant differential cross section for proton induced reactions is shown as a function of transverse momentum p_T. The incident energy is 100 GeV.

Figure 15: The single differential cross section $x\frac{d\sigma}{dx}$ is shown as a function of x. It is obtained by integrating the invariant cross section over transverse momentum. The incident energy is 100 GeV. There is one subfigure for each incident particle type.

Figure 16: The integrated cross section $X\frac{d\sigma}{dx}$ as a function of x for incident energy of 175 GeV.

Figure 17: Triple Regge exchange diagram for the process $a + p \to c + X$ for $s/M_X^2 \gg 1$ and $s \to \infty$.

Figure 18: Data and triple Regge fits to $\pi^+p \to \pi^+X$, $K^+p \to K^+X$, and $pp \to pX$ at 70, 100 and 175 GeV.

Figure 19: Fine binned data for $\pi^+p \to \pi^+X$ at 100 GeV/c and Pt = 0.5 GeV/c with PPP and RRP contributions to the triple Regge fit.

Figure 20: The ratio, R, of $\sigma_{tot}(K^{*o}p)/\sigma_{tot}$ $(\bar{K}^{*o}p)$ as calculated from $\pi^{\pm}p \to K^{\pm}X$ inclusive scattering. The curve is the $\sigma_{tot}(K^+p)/\sigma_{tot}(K^-p)$ ratio from data of Reference 34.

Figure 21: Average associated charged particle multiplicities for $a + p \to c + X$ as a function of x for fixed p_T.

Figure 22: Feynman x dependence of contribution of n-prong cross sections $E\left.\frac{d^3\sigma}{dp^3}\right|_n$ for $\pi^+p \to \pi^{\pm}X$, $pp \to pX$, and $pp \to \pi^-X$ at fixed p_T.

Figure 23: Dependence of the associated charged particle multiplicity for $pp \to pX$ and $\pi^-p \to \pi^-X$ on the invariant momentum transfer t at fixed x. Linear fit parameters are displayed in Figs. 25 and 26.

Figure 24: Dependence of the associated charged particle multiplicity for particle changing reactions $a+p \to c+X$ on the transverse momentum of particle c at fixed x.

Figure 25: Parameter $\beta(x)$ for fits of the form $\langle n(x,t)\rangle = \alpha(x)-\beta(x)t$ for leading particle $a+p \to a+X$ channels.

Figure 26: Parameter $\alpha(x)$ for fits of the form $\langle n(x,t)\rangle = \alpha(x)-\beta(x)t$ for leading particle $\pi^{\pm}p \to \pi^{\pm}X$ and $pp \to pX$ channels. Also plotted are the multiplicities for the $\pi^{\pm}p \to X$, and $pp \to X$ total cross section trigger of Table 11 at a common $s = M_X^2$. The solid curve is a parameterization of Reference 41, for $ap \to X$ total multiplicities. The dashed curve represents fits of Reference 37 for $ap \to aX$ associated multiplicities as observed in bubble chamber experiments.

Figure 27: Pseudo-rapidity distributions for associated particles in $pp \to pX$ compared with pseudo-rapidities for $pp \to X$ (Reference 44), and $\bar{p}p \to X$ (Reference 45) at a common $s = M_X^2 = 190\ GeV^2$.

Figure 28: Pseudo-rapidity distributions.

a. x dependence for $\pi^+p \to \pi^+x$ at $p_T = 0.3$ GeV/c. Curves are drawn to guide the eye.

b. Trigger particle dependence for $\pi^+p \to h^\pm X$ for 100 GeV/c incident π^+ at $x = 0.6$ and $p_T = 0.3$ GeV/c.

c. p_T dependence for $\pi^+p \to \pi^+X$ at $x = 0.4$ for 100 GeV/c π^+.

Figure 29: x-dependence of the associated pseudo-rapidity distribution for $\pi^+p \to \pi^-X$ at 100 GeV/c and a $p_T = 0.3$ GeV/c.

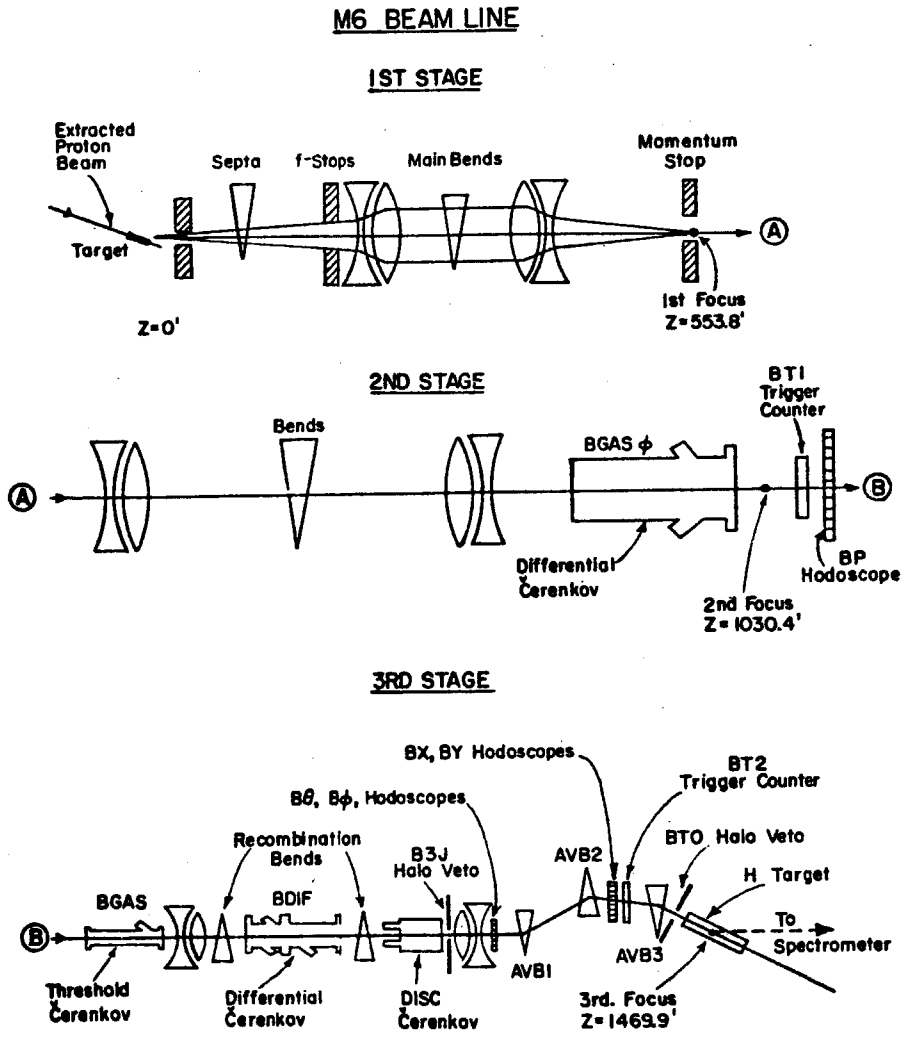

Fig. 1

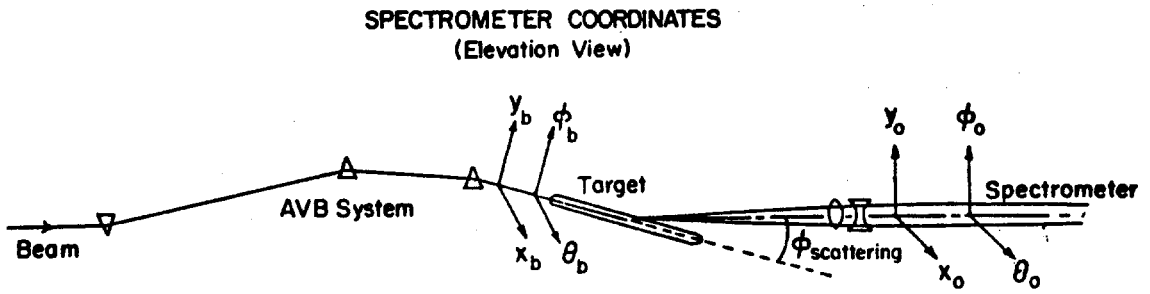
SPECTROMETER COORDINATES
(Elevation View)
y_b
ϕ_b
y_o
ϕ_o
Target
Spectrometer
AVB System
Beam
x_b
θ_b
$\phi_{scattering}$
x_o
θ_o

Fig. 2

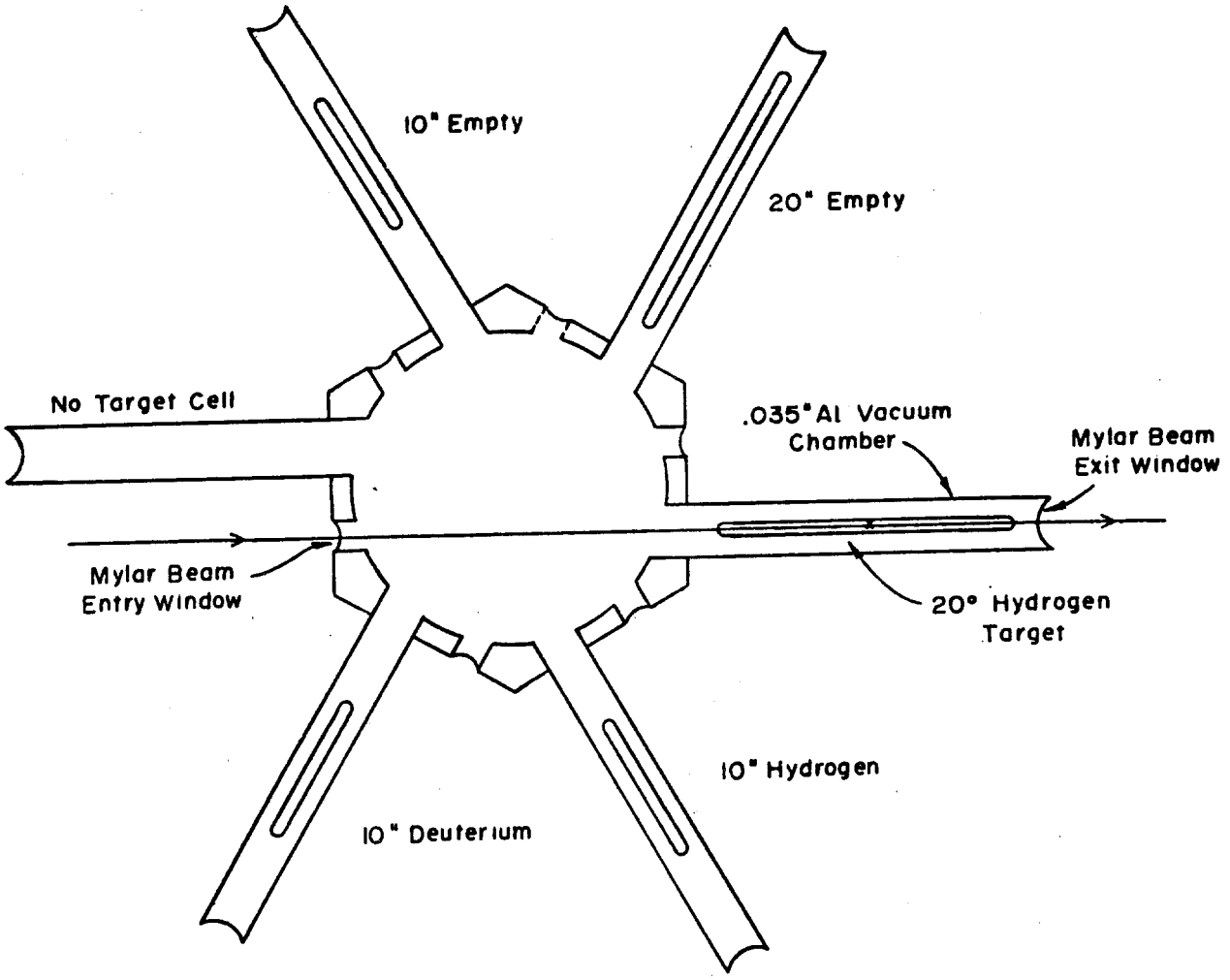
10" Empty
20" Empty
No Target Cell
.035"Al Vacuum Chamber
Mylar Beam Exit Window
Mylar Beam Entry Window
20° Hydrogen Target
10" Hydrogen
10" Deuterium

Fig. 3

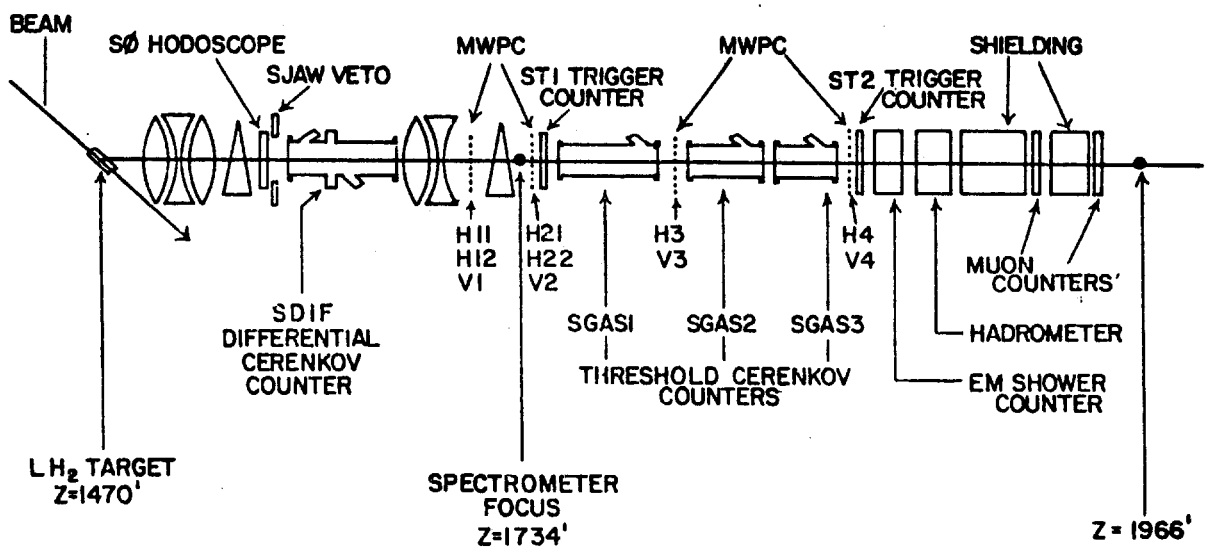
BEAM
SØ HODOSCOPE
SJAW VETO
MWPC
ST1 TRIGGER COUNTER
MWPC
ST2 TRIGGER COUNTER
SHIELDING
H11
H12
V1
H21
H22
V2
H3
V3
H4
V4
MUON COUNTERS'
SDIF DIFFERENTIAL CERENKOV COUNTER
SGAS1
SGAS2
SGAS3
HADROMETER
THRESHOLD CERENKOV COUNTERS
EM SHOWER COUNTER
L H2 TARGET Z=1470'
SPECTROMETER FOCUS Z=1734'
Z = 1966'

Fig. 4

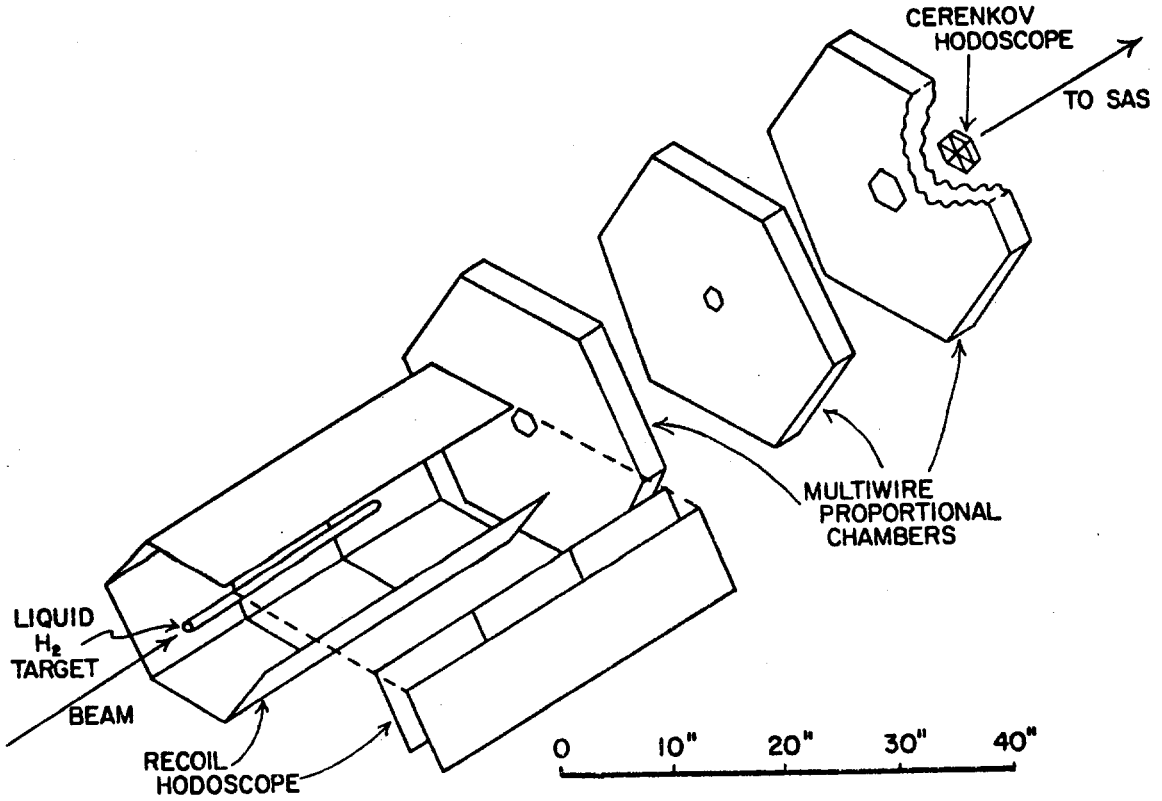
CERENKOV HODOSCOPE
TO SAS
MULTIWIRE PROPORTIONAL CHAMBERS
LIQUID H2 TARGET
BEAM
RECOIL HODOSCOPE
0
10"
20"
30"
40"

Fig. 5

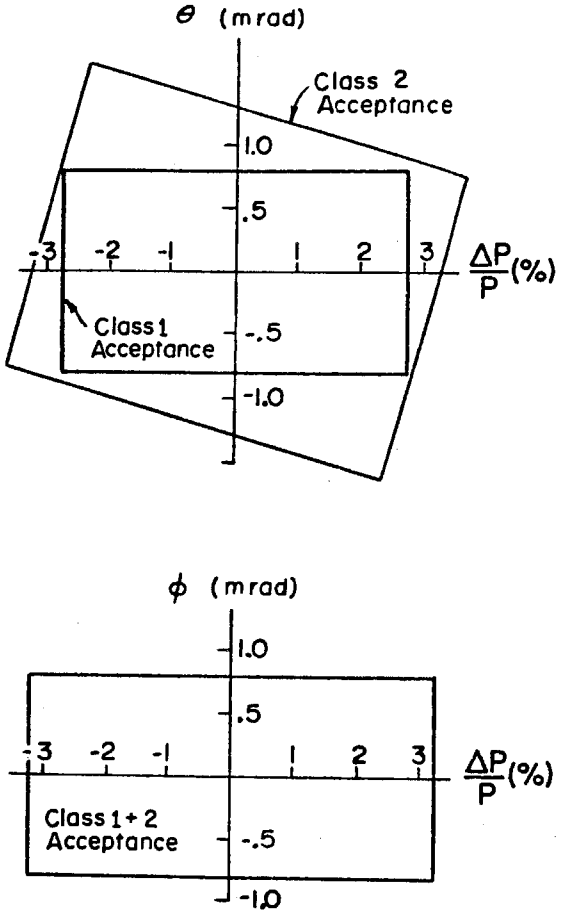
θ (mrad)
Class 2
Acceptance
1.0
.5
-3
-2
-1
1
2
3
ΔP/P(%)
Class 1
Acceptance
-.5
-1.0
φ (mrad)
1.0
.5
-3
-2
-1
1
2
3
ΔP/P(%)
Class 1+2
Acceptance
-.5
-1.0

Fig. 6

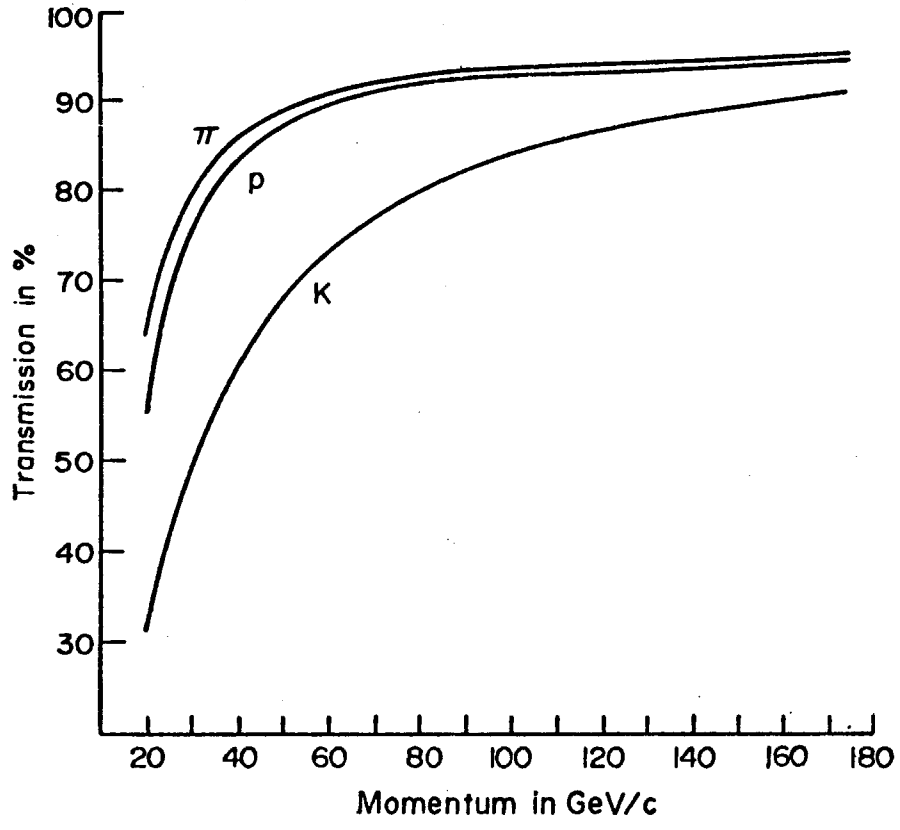
100
90
80
70
60
50
40
30
Transmission in %
π
p
K
20
40
60
80
100
120
140
160
180
Momentum in GeV/c

Fig. 7

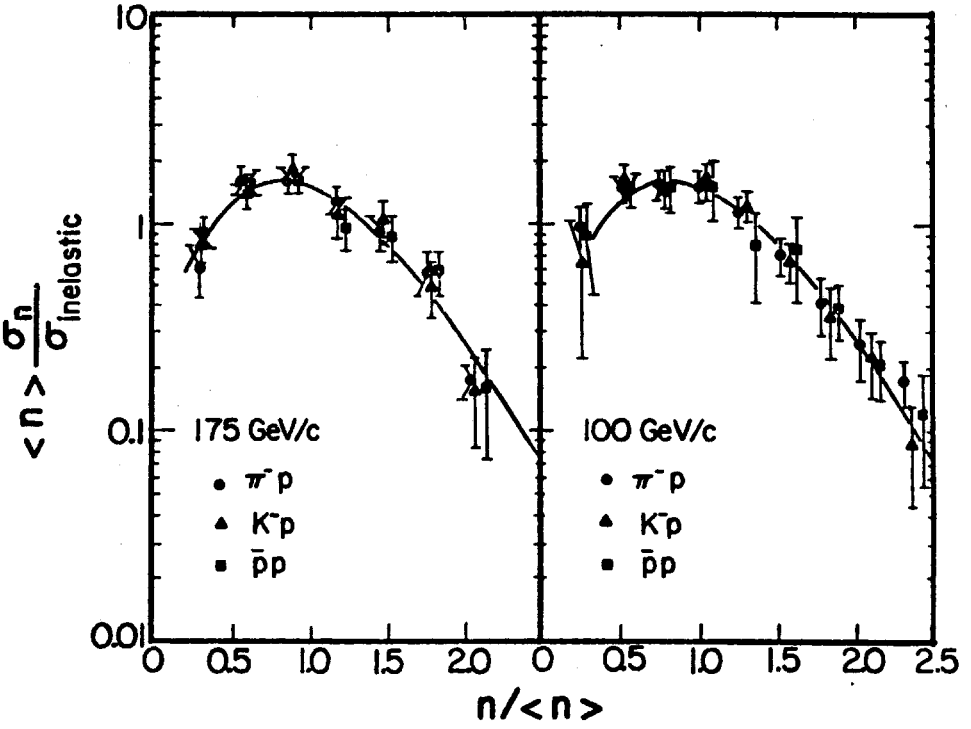
10
1
0.1
0.01
$\frac{\sigma_n}{\sigma_{inelastic}} < n >$
175 GeV/c
$\pi^- p$
$K^- p$
$\bar{p} p$
100 GeV/c
$\pi^- p$
$K^- p$
$\bar{p} p$
0 0.5 1.0 1.5 2.0
0 0.5 1.0 1.5 2.0 2.5
$n/<n>$

Fig. 8

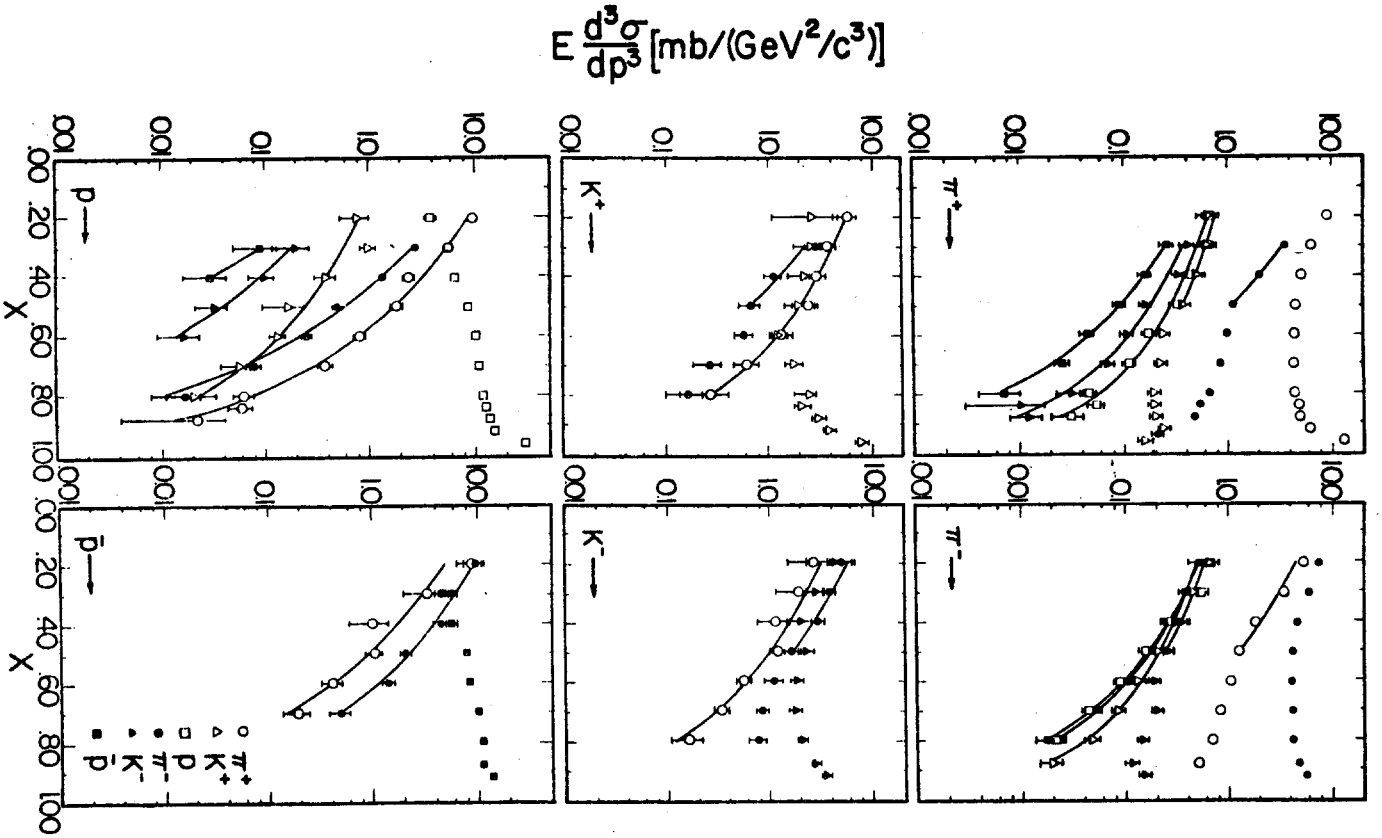
$E\frac{d^3\sigma}{dp^3}[mb/(GeV^2/c^3)]$
p
K^+
π^+
$\bar{p}$
K^-
π^-
X
.00 .20 .40 .60 .80 1.00
.001 .01 .1 1. 10. 100.
$\bar{p}$ p K^+ K^- π^+ π^-

Fig. 9

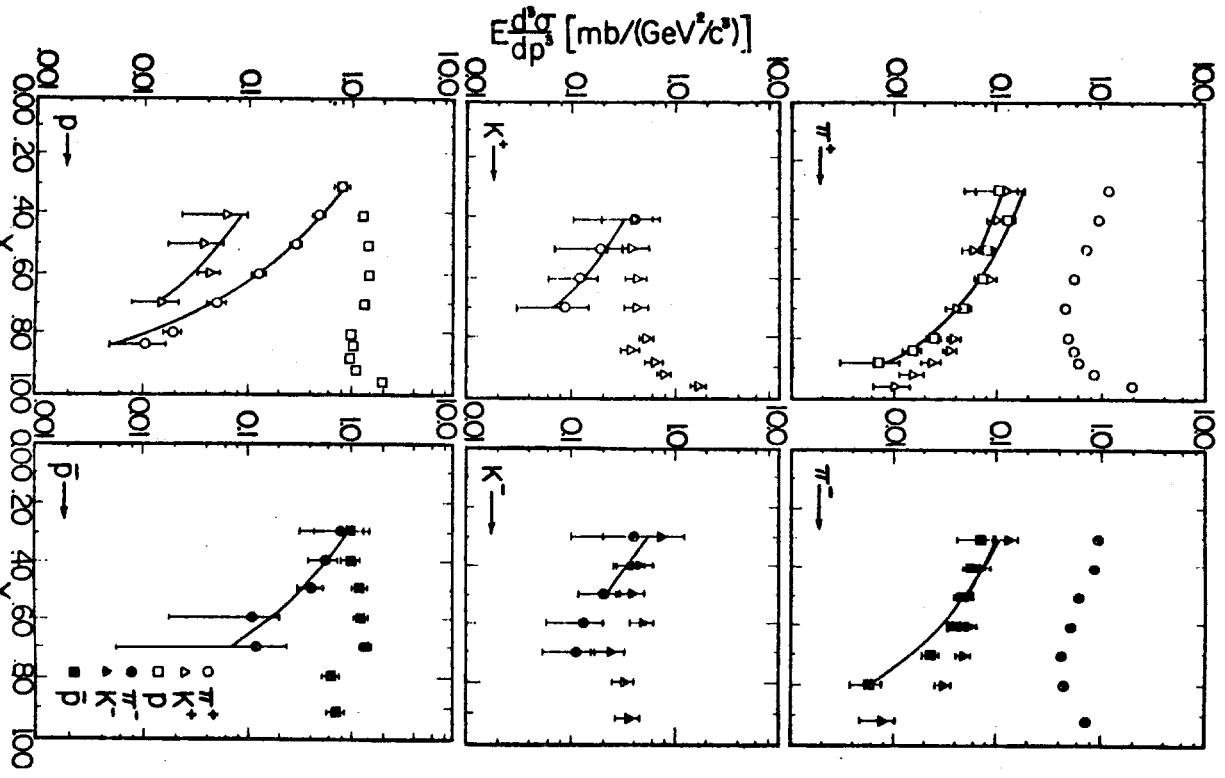
$E\frac{d^3\sigma}{dp^3}$ [mb/(GeV²/c³)]
X
π^+
K^+
p
π^-
K^-
$\bar{p}$
π^+
K^+
p
π^-
K^-
$\bar{p}$

Fig. 10

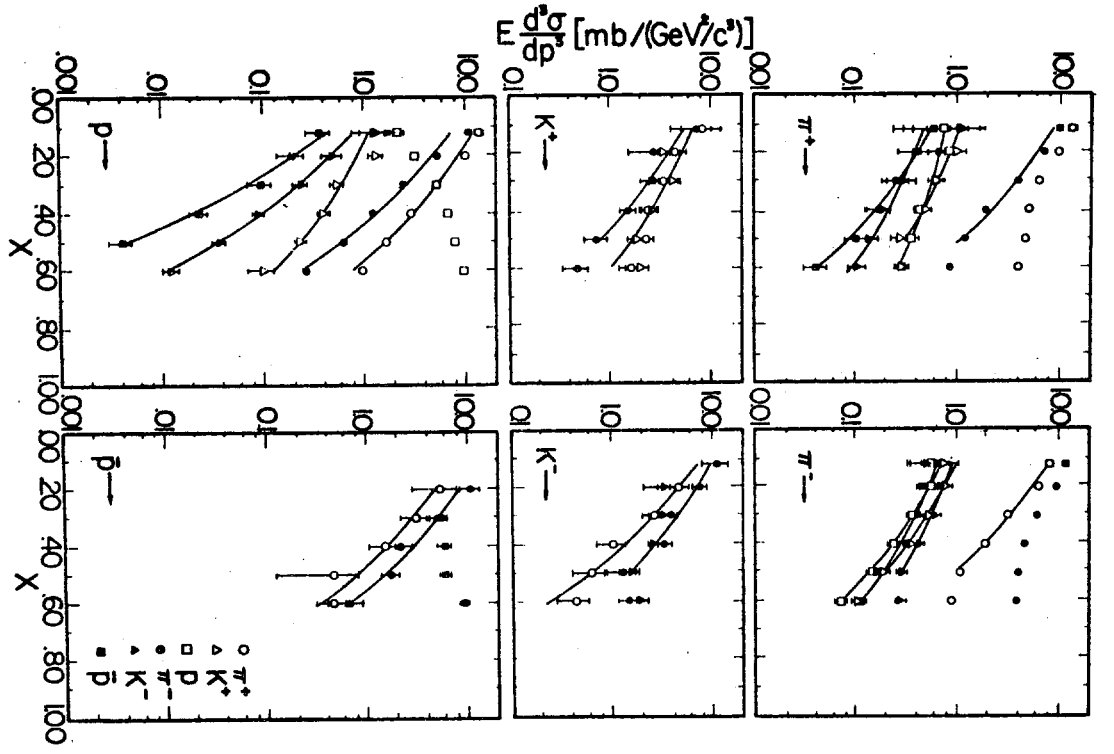
$E\frac{d^3\sigma}{dp^3}$ [mb/(GeV²/c³)]
X
π^+
K^+
p
π^-
K^-
$\bar{p}$
π^+
K^+
p
π^-
K^-
$\bar{p}$

Fig. 11

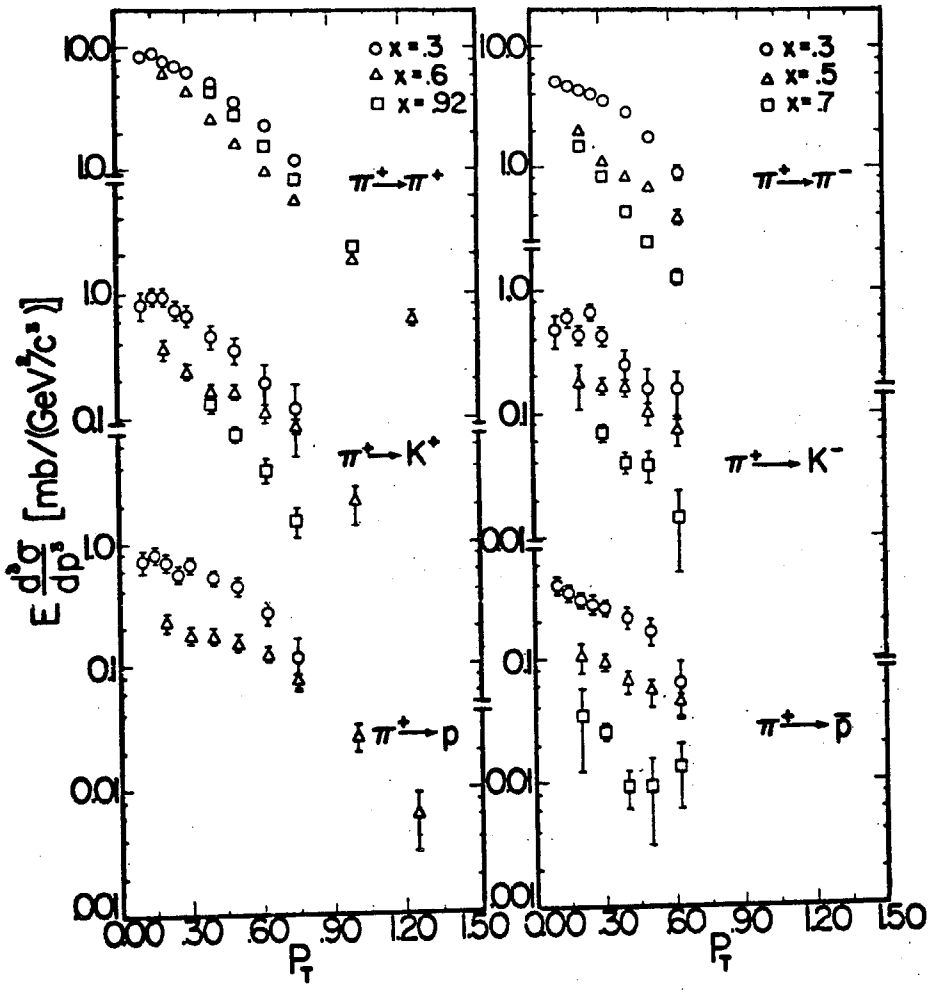
E d³σ/dp³ [mb/(GeV²/c³)]
x=.3
x=.6
x=.92
x=.5
x=.7
π⁺→π⁺
π⁺→K⁺
π⁺→p
π⁺→π⁻
π⁺→K⁻
π⁺→p̄
P_T

Fig. 12

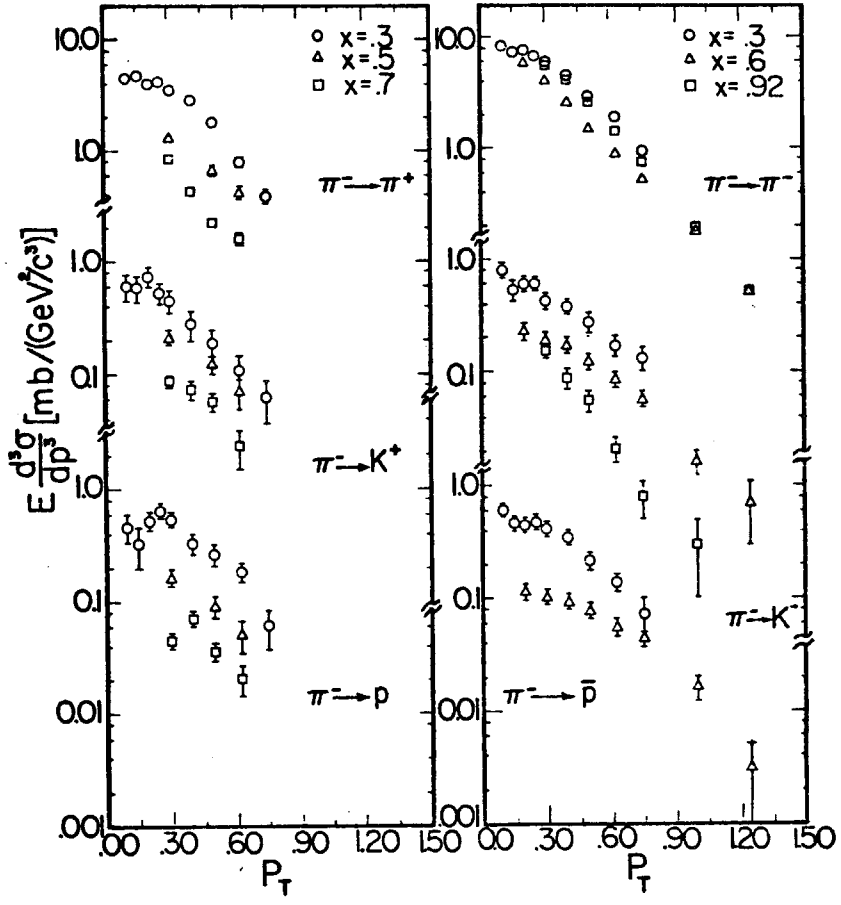
E d³σ/dp³ [mb/(GeV²/c³)]
x=.3
x=.5
x=.7
x=.6
x=.92
π⁻→π⁺
π⁻→K⁺
π⁻→p
π⁻→π⁻
π⁻→K⁻
π⁻→p̄
P_T

Fig. 13

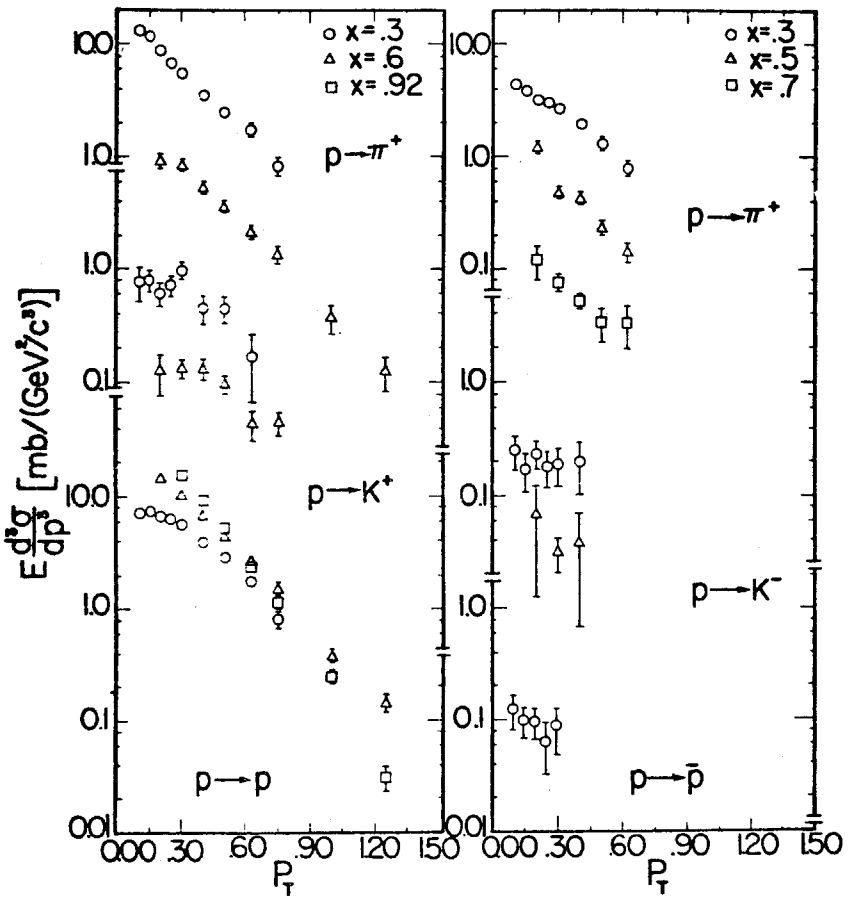
$E\frac{d^3\sigma}{dp^3}$ [mb/(GeV²/c³)]
x=.3
x=.6
x=.92
p→π⁺
p→K⁺
p→p
x=.3
x=.5
x=.7
p→π⁺
p→K⁻
p→p̄
P_T
P_T

Fig. 14

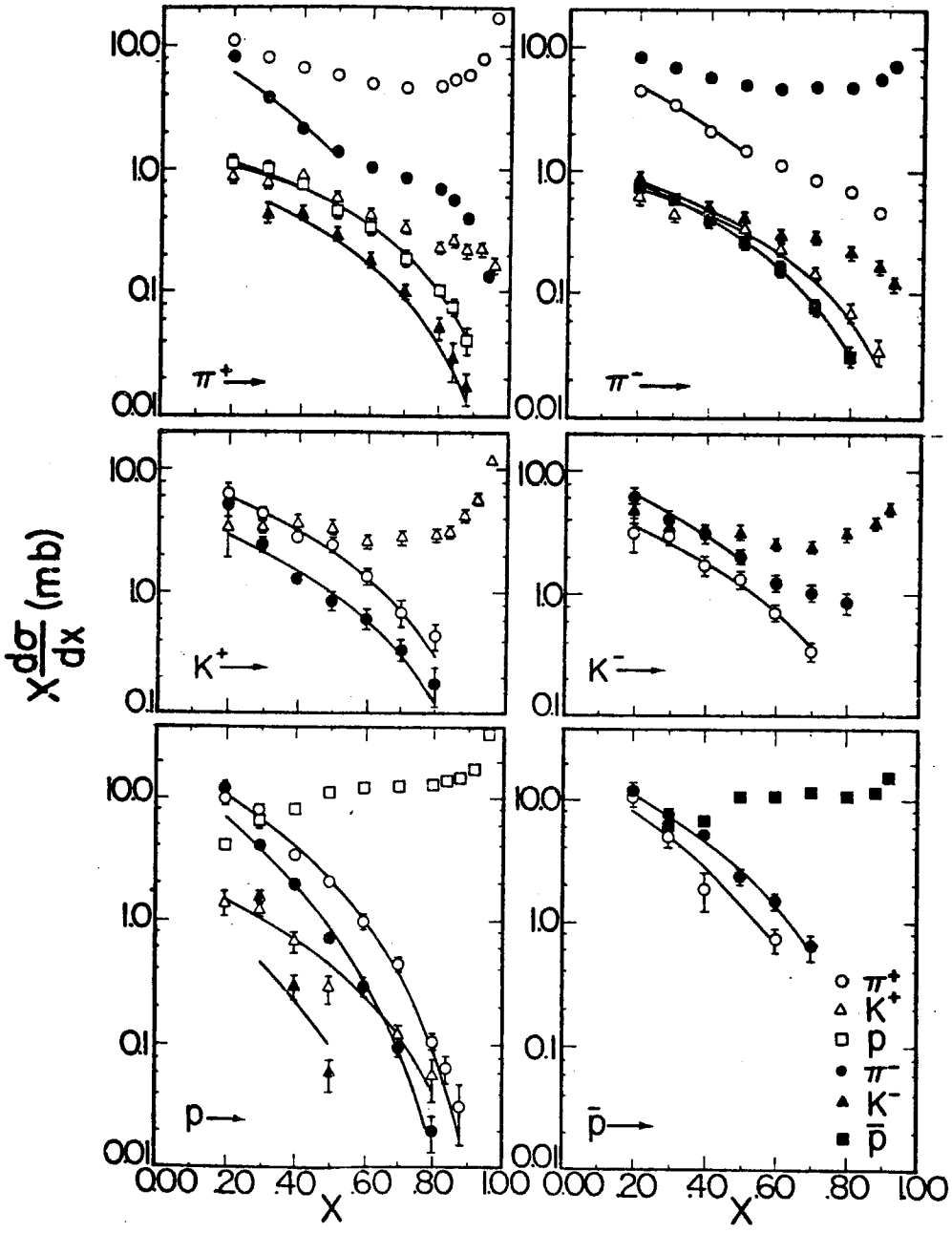
$x\frac{d\sigma}{dx}$ (mb)
π⁺→
π⁻→
K⁺→
K⁻→
p→
p̄→
X
X
π⁺
K⁺
p
π⁻
K⁻
p̄

Fig. 15

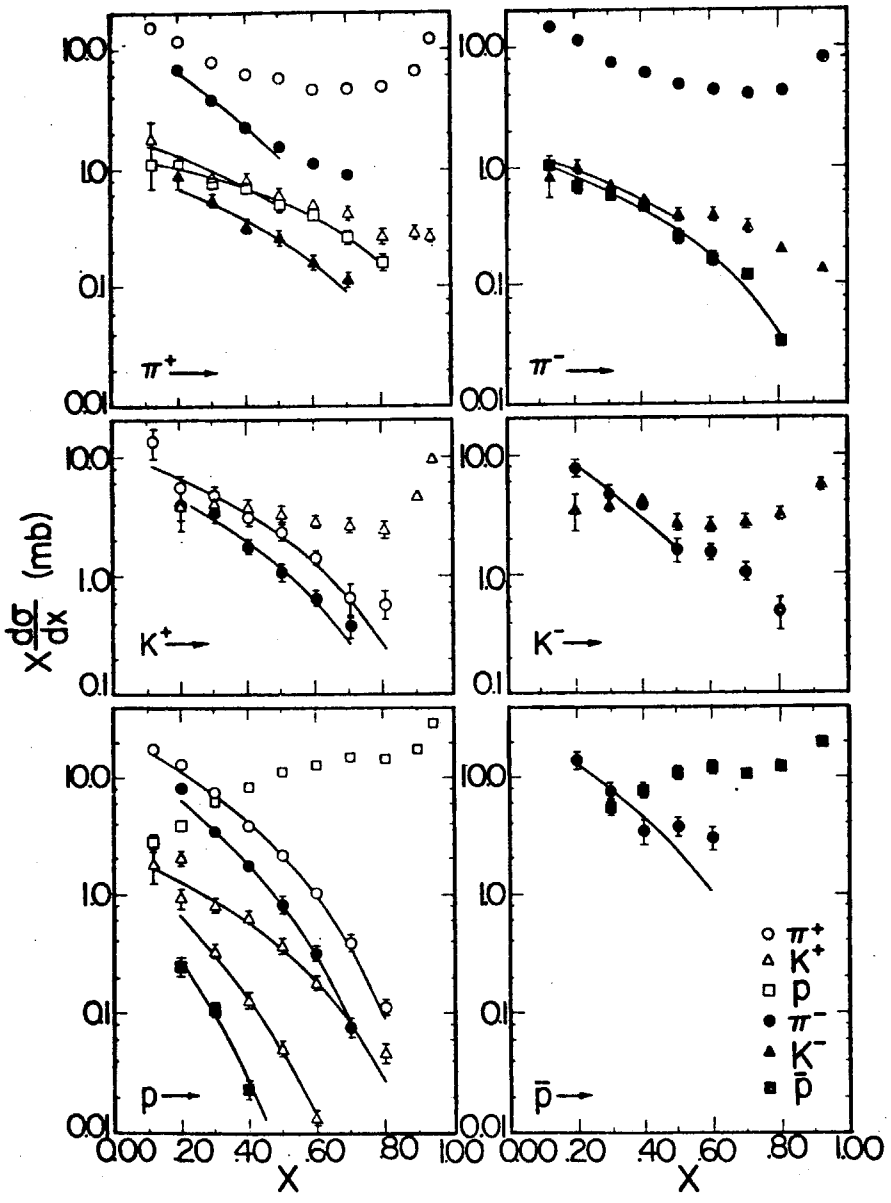
100
10
1.0
0.1
0.01
π^+
π^-
K^+
K^-
p
$\bar{p}$
$X\frac{d\sigma}{dx}$ (mb)
0.00 .20 .40 .60 .80 1.00
X
π^+
K^+
p
π^-
K^-
$\bar{p}$

Fig. 16

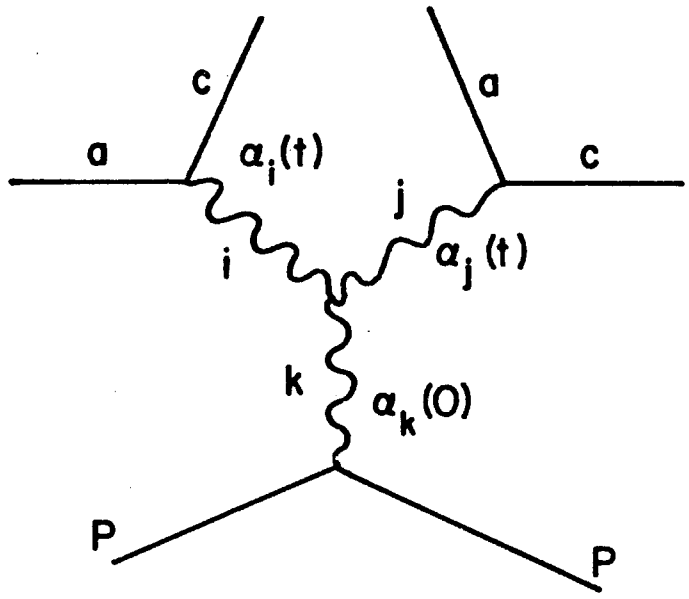
a
c
$\alpha_i(t)$
i
j
a
c
$\alpha_j(t)$
k
$\alpha_k(0)$
P
P

Fig. 17

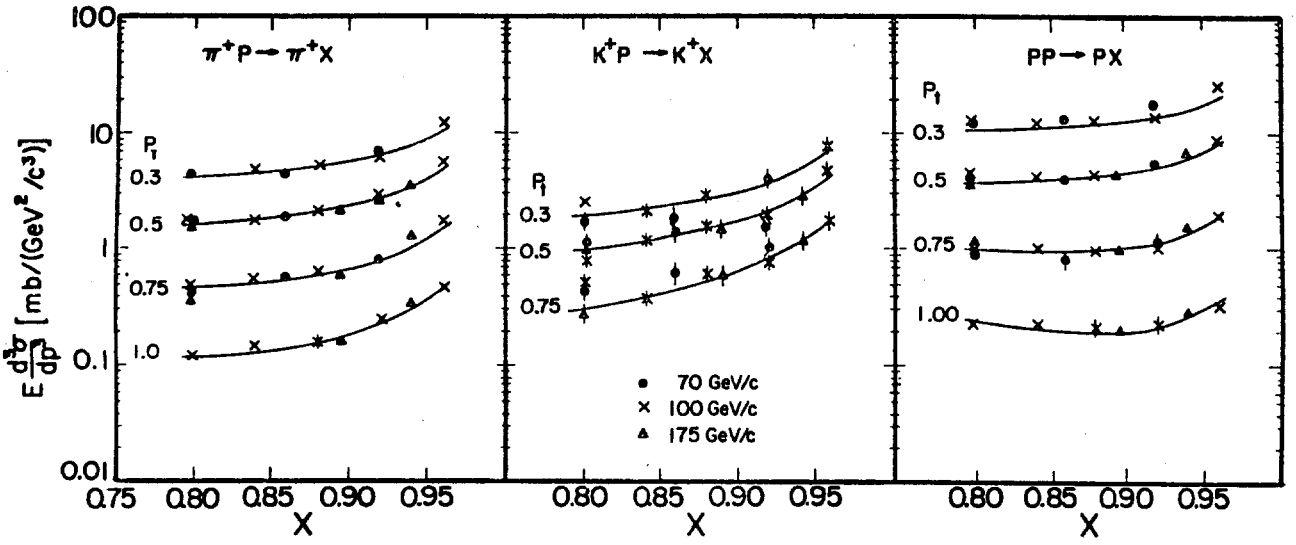
$\pi^+P \to \pi^+X$
$K^+P \to K^+X$
$PP \to PX$
P_t
0.3
0.5
0.75
1.0
1.00
70 GeV/c
100 GeV/c
175 GeV/c
$E\frac{d^3\sigma}{dp^3}$ [mb/(GeV^2/c^3)]
X
100
10
1
0.1
0.01
0.75 0.80 0.85 0.90 0.95

Fig. 18

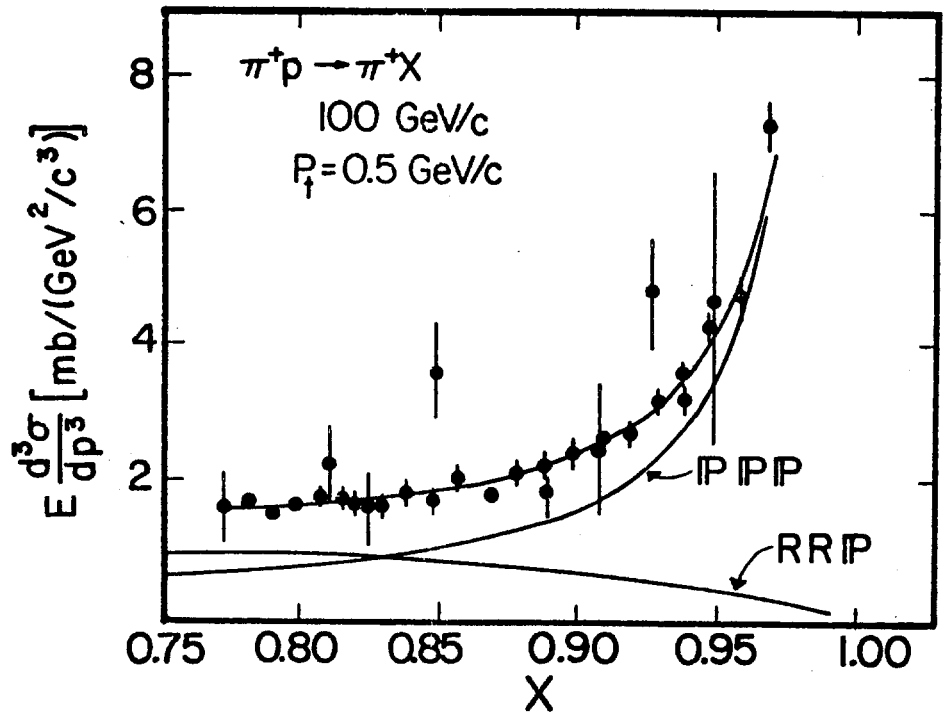
$\pi^+p \to \pi^+X$
100 GeV/c
P_t=0.5 GeV/c
$E\frac{d^3\sigma}{dp^3}$ [mb/(GeV^2/c^3)]
IP IP IP
RR IP
X
8
6
4
2
0.75 0.80 0.85 0.90 0.95 1.00

Fig. 19

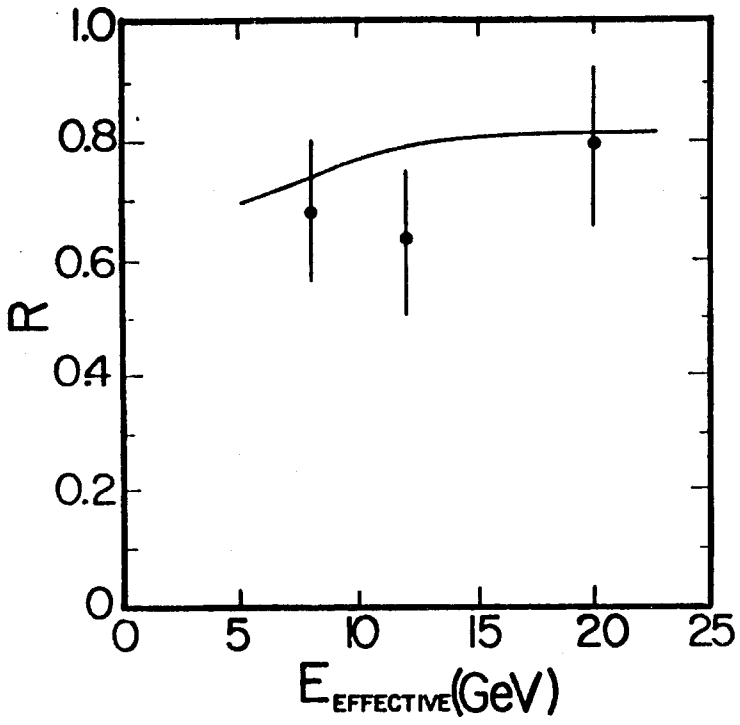
R
E EFFECTIVE (GeV)

Fig. 20

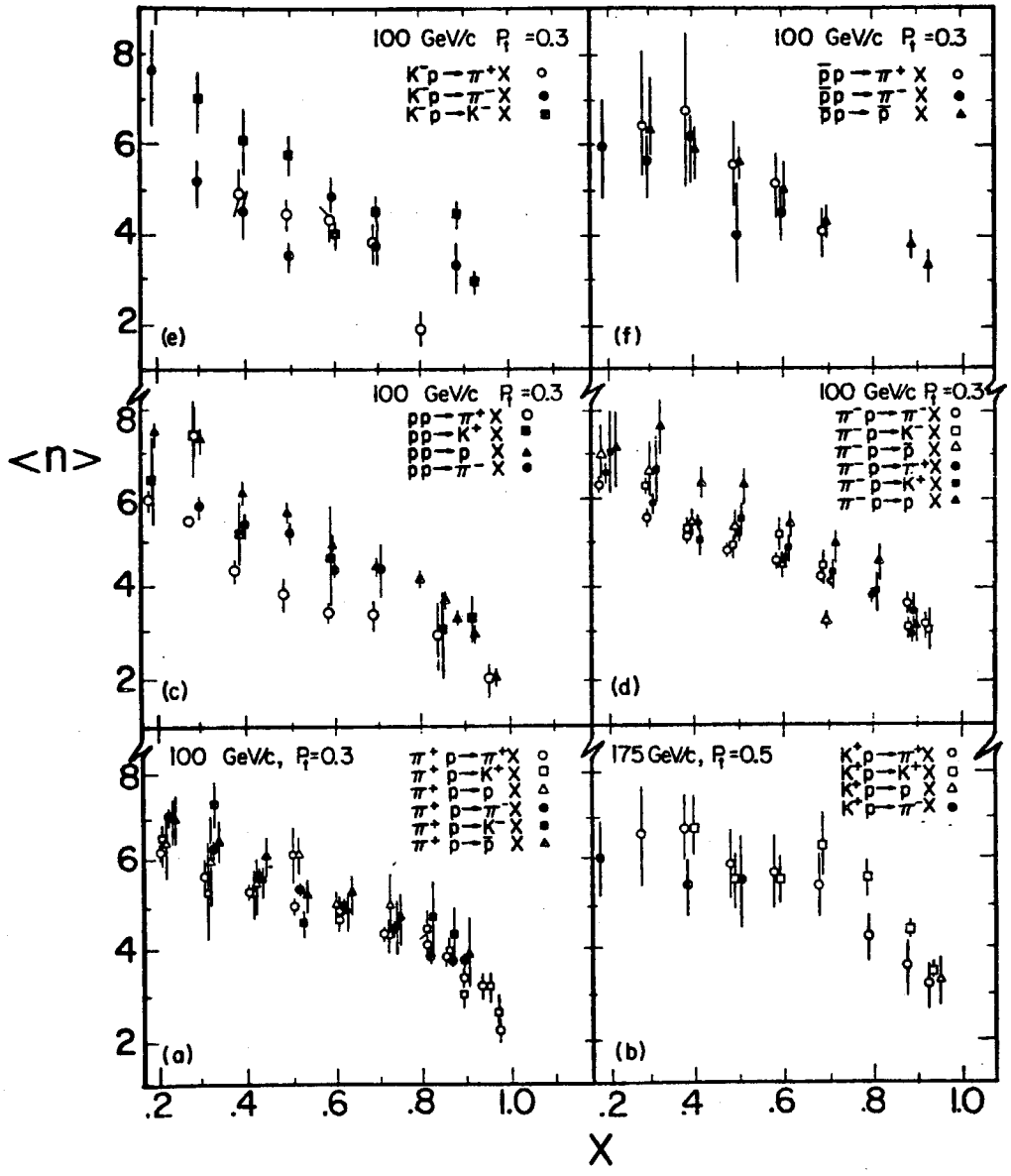
<n>
X
100 GeV/c P_t =0.3
100 GeV/c, P_t=0.3
175 GeV/c, P_t=0.5
(a)
(b)
(c)
(d)
(e)
(f)

Fig. 21

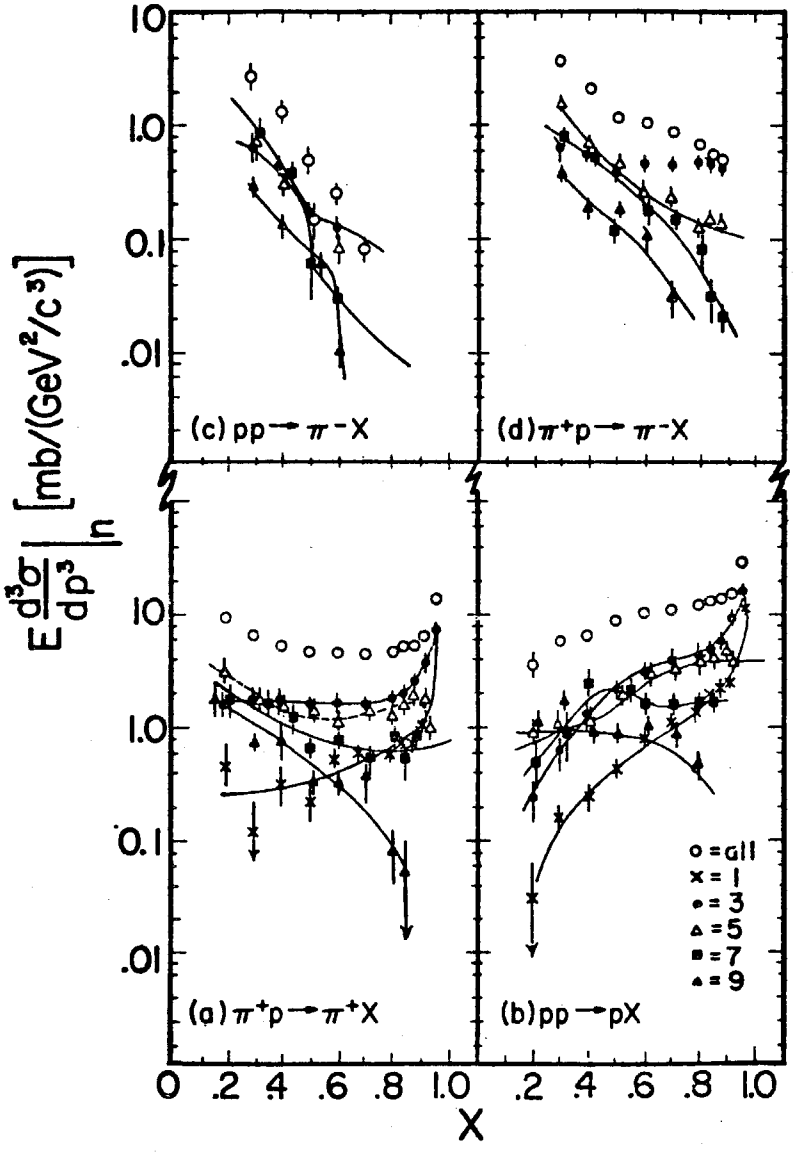
(c) pp → π⁻X
(d) π⁺p → π⁻X
(a) π⁺p → π⁺X
(b) pp → pX
o = all
x = 1
• = 3
△ = 5
■ = 7
▲ = 9
X
E d³σ/dp³ |n [mb/(GeV²/c³)]

Fig. 22

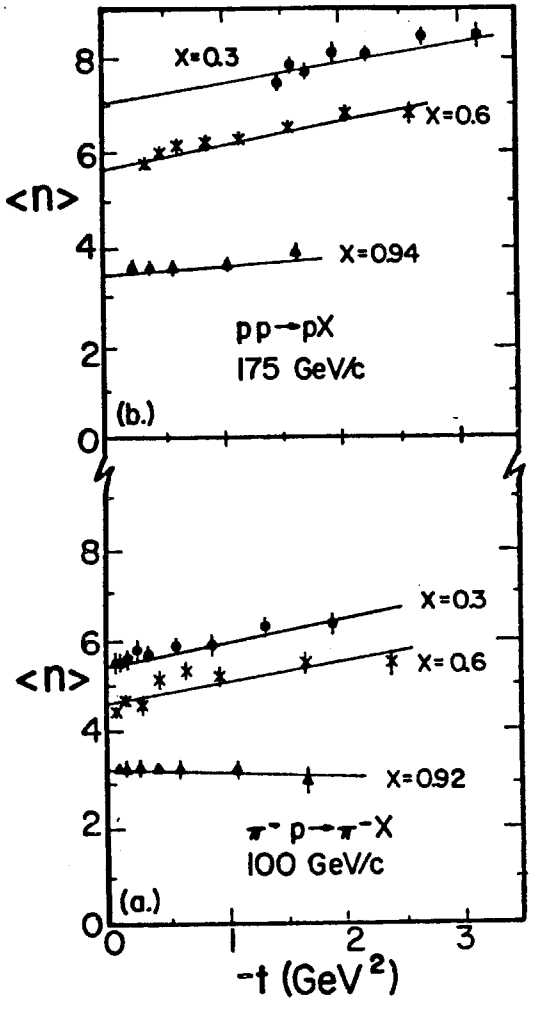
X=0.3
X=0.6
X=0.94
pp → pX
175 GeV/c
(b.)
X=0.3
X=0.6
X=0.92
π⁻ p → π⁻X
100 GeV/c
(a.)
<n>
-t (GeV²)

Fig. 23

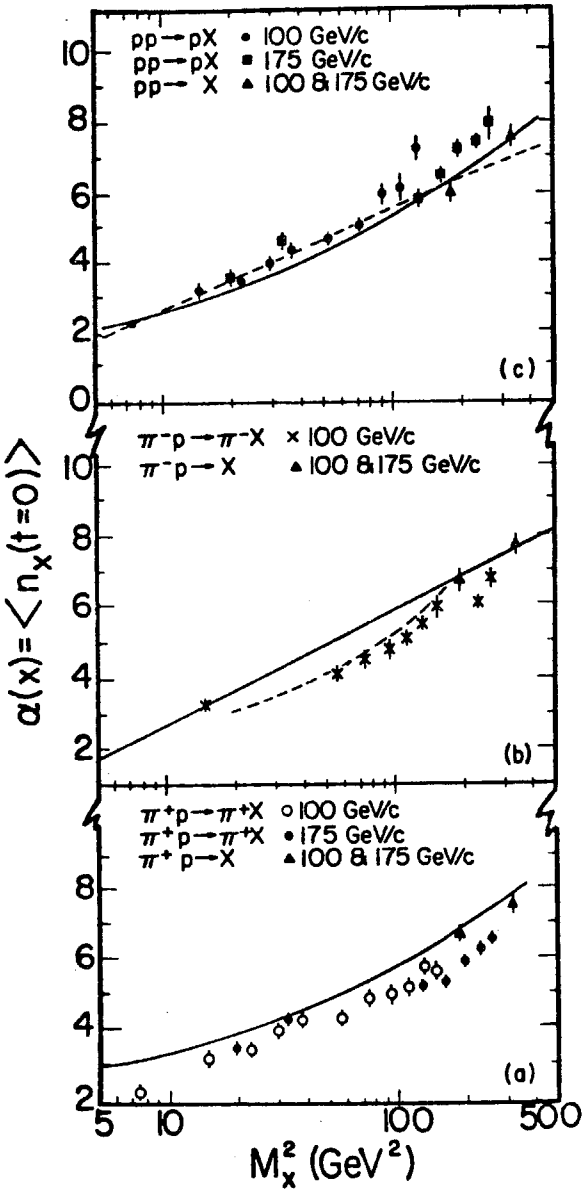
pp→pX • 100 GeV/c
pp→pX ■ 175 GeV/c
pp→ X ▲ 100 & 175 GeV/c
(c)
π⁻p→π⁻X × 100 GeV/c
π⁻p→X ▲ 100 & 175 GeV/c
(b)
π⁺p→π⁺X ○ 100 GeV/c
π⁺p→π⁺X • 175 GeV/c
π⁺p→X ▲ 100 & 175 GeV/c
(a)
α(x)=<n_x(t=0)>
M_x² (GeV²)

Fig. 26

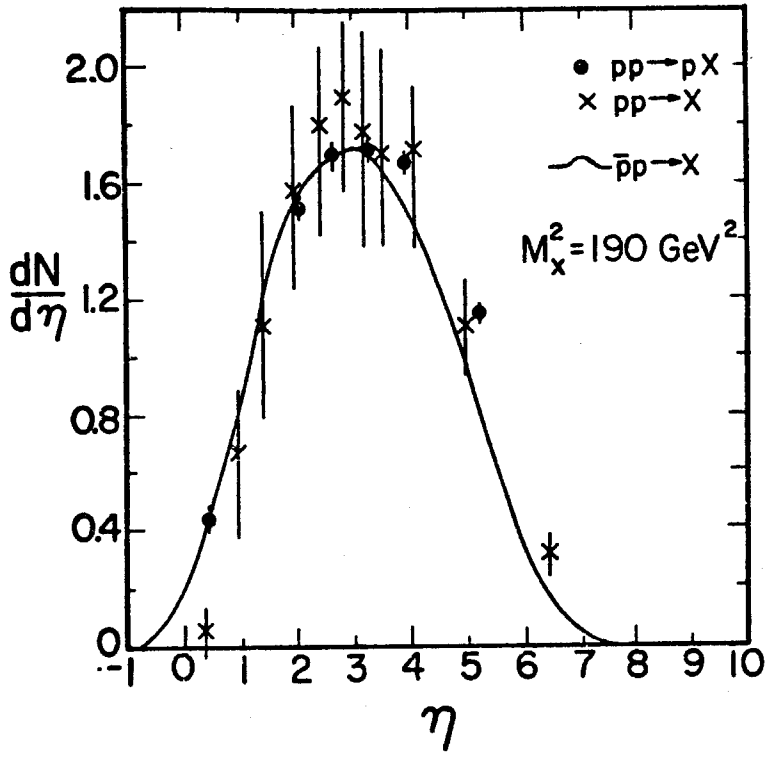
pp→pX
pp→X
p̄p→X
M_x²=190 GeV²
dN/dη
η

Fig. 27

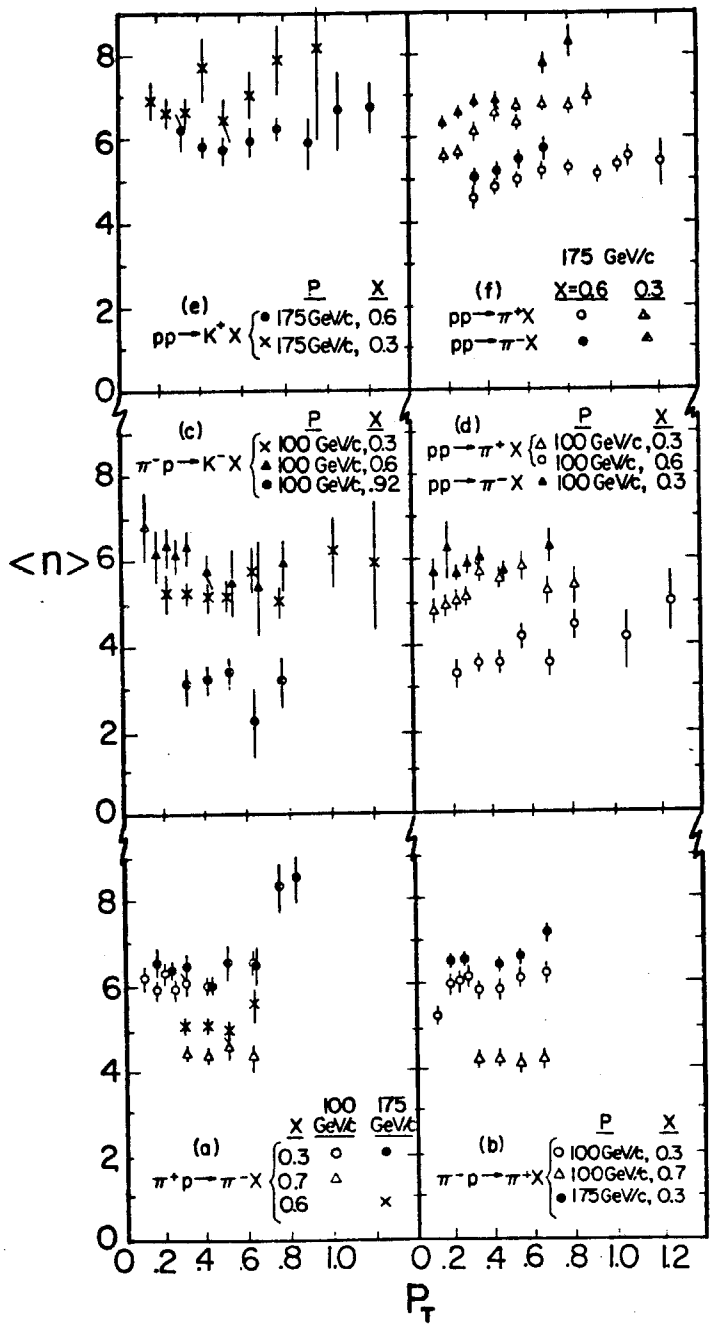
<n>
P_T
(e) $pp \to K^+X$ P X • 175 GeV/c, 0.6 × 175 GeV/c, 0.3
(f) 175 GeV/c X=0.6 0.3 $pp \to \pi^+X$ $pp \to \pi^-X$
(c) $\pi^-p \to K^-X$ × 100 GeV/c, 0.3 ▲ 100 GeV/c, 0.6 • 100 GeV/c, .92
(d) $pp \to \pi^+X$ △ 100 GeV/c, 0.3 ○ 100 GeV/c, 0.6 $pp \to \pi^-X$ ▲ 100 GeV/c, 0.3
(a) $\pi^+p \to \pi^-X$ X 100 GeV/c 175 GeV/c 0.3 ○ • 0.7 △ 0.6 ×
(b) $\pi^-p \to \pi^+X$ ○ 100 GeV/c, 0.3 △ 100 GeV/c, 0.7 • 175 GeV/c, 0.3

Fig. 24

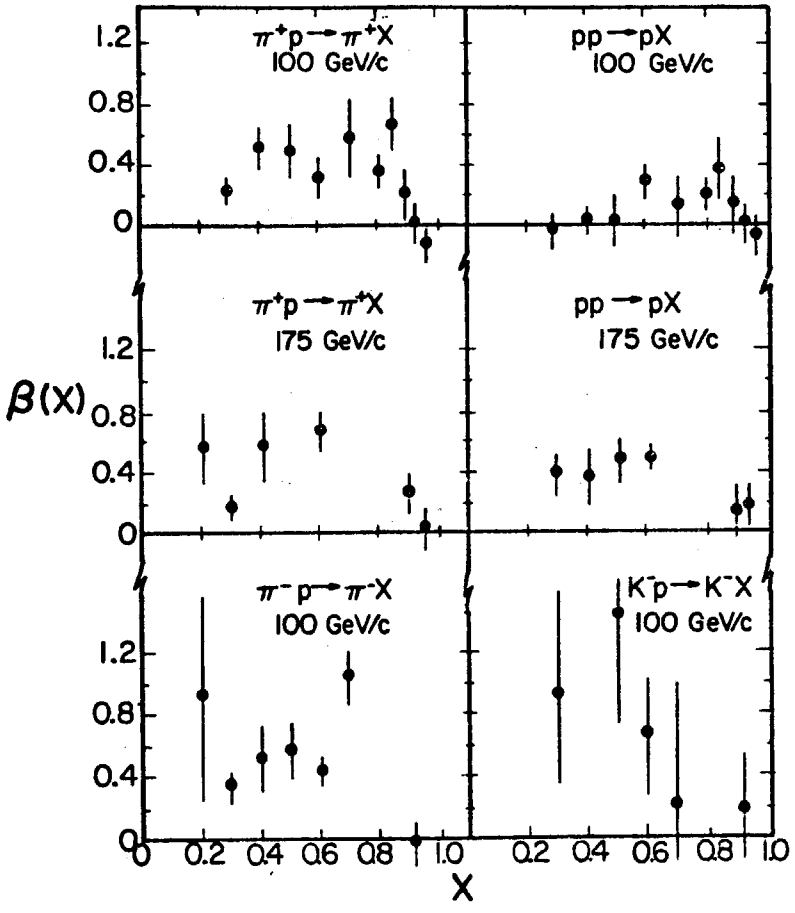
β(X)
X
$\pi^+p \to \pi^+X$ 100 GeV/c
$pp \to pX$ 100 GeV/c
$\pi^+p \to \pi^+X$ 175 GeV/c
$pp \to pX$ 175 GeV/c
$\pi^-p \to \pi^-X$ 100 GeV/c
$K^-p \to K^-X$ 100 GeV/c

Fig. 25

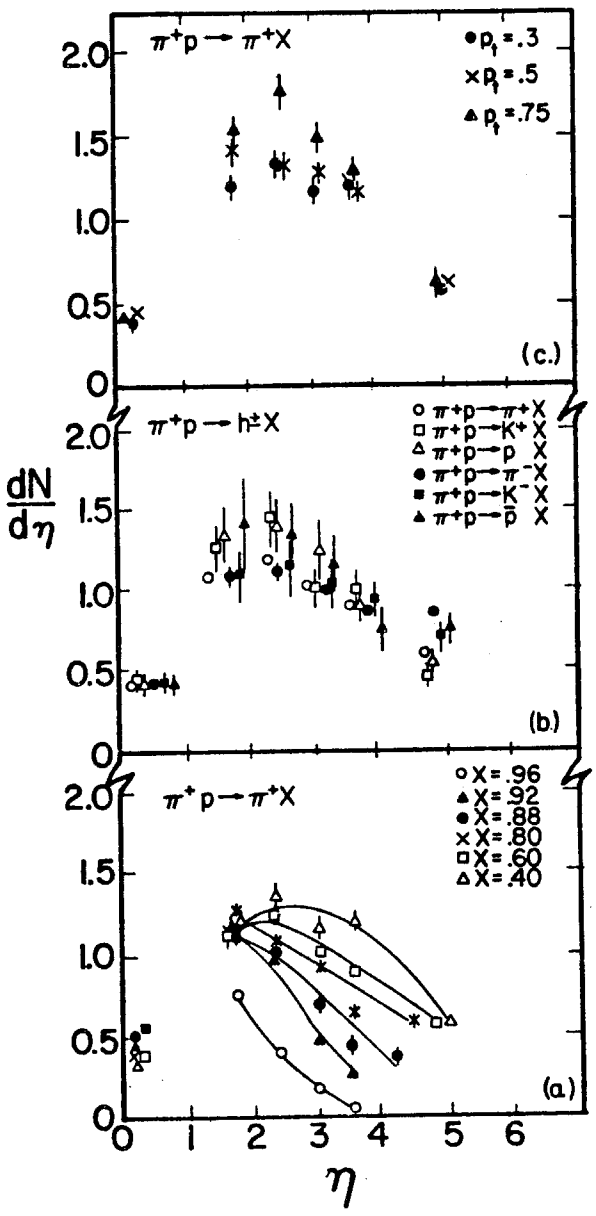
$\pi^+p \to \pi^+X$
p_t=.3
p_t=.5
p_t=.75
(c.)
$\pi^+p \to h^\pm X$
$\pi^+p \to \pi^+X$
$\pi^+p \to K^+X$
$\pi^+p \to pX$
$\pi^+p \to \pi^-X$
$\pi^+p \to K^-X$
$\pi^+p \to \bar{p}X$
(b.)
$\pi^+p \to \pi^+X$
X=.96
X=.92
X=.88
X=.80
X=.60
X=.40
(a.)
$\frac{dN}{d\eta}$
η

Fig. 28

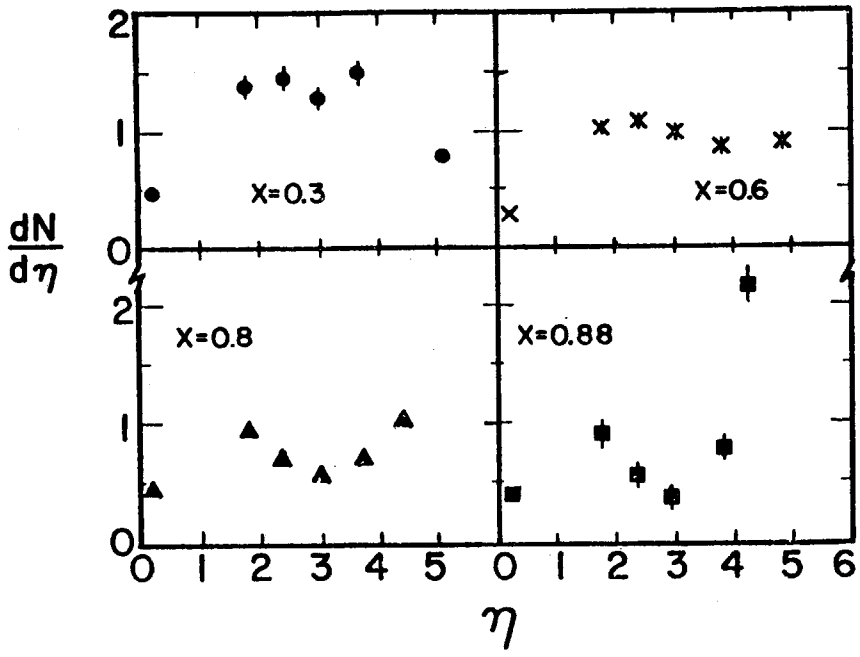
X=0.3
X=0.6
X=0.8
X=0.88
$\frac{dN}{d\eta}$
η

Fig. 29